Developing Ohmic Contacts to Gallium Nitride for High Temperature Applications

by

Shirong Zhao

A Dissertation Presented in Partial Fulfillment
of the Requirements for the Degree
Doctor of Philosophy

Approved July 2016 by the
Graduate Supervisory Committee:

Srabanti Chowdhury, Chair
Stephen Goodnick
Yuji Zhao
Robert Nemanich

ARIZONA STATE UNIVERSITY

August 2016

ABSTRACT

Gallium Nitride (GaN), being a wide-bandgap semiconductor, shows its advantage over the conventional semiconductors like Silicon and Gallium Arsenide for high temperature applications, especially in the temperature range from 300°C to 600°C. Development of stable ohmic contacts to GaN with low contact resistivity has been identified as a prerequisite to the success of GaN high temperature electronics. The focus of this work was primarily derived from the requirement of an appropriate metal contacts to work with GaN-based hybrid solar cell operating at high temperature.

Alloyed Ti/Al/Ni/Au contact and non-alloyed Al/Au contact were developed to form low-resistivity contacts to n-GaN and their stability at high temperature were studied. The alloyed Ti/Al/Ni/Au contact offered a specific contact resistivity (ρ_c) of 6×10^{-6} $\Omega\cdot cm^2$ at room temperature measured the same as the temperature increased to 400°C. No significant change in ρ_c was observed after the contacts being subjected to 400°C, 450°C, 500°C, 550°C, and 600°C, respectively, for at least 4 hours in air. Since several device technology prefer non-alloyed contacts Al/Au metal stack was applied to form the contacts to n-type GaN. An initial ρ_c of 3×10^{-4} $\Omega\cdot cm^2$, measured after deposition, was observed to continuously reduce under thermal stress at 400°C, 450°C, 500°C, 550°C, and 600°C, respectively, finally stabilizing at 5×10^{-6} $\Omega\cdot cm^2$. Both the alloyed and non-alloyed metal contacts showed exceptional capability of stable operation at temperature as high as 600°C in air with low resistivity ~10^{-6} $\Omega\cdot cm^2$, with ρ_c lowering for the non-alloyed contacts with high temperatures.

The p-GaN contacts showed remarkably superior ohmic behavior at elevated temperatures. Both ρ_c and sheet resistance (R_{sh}) of p-GaN decreased by a factor of 10 as

the ambient temperature increased from room temperature to 390°C. The annealed Ni/Au contact showed ρ_c of 2×10^{-3} $\Omega\cdot cm^2$ at room temperature, reduced to 1.6×10^{-4} $\Omega\cdot cm^2$ at 390°C. No degradation was observed after the contacts being subjected to 450°C in air for 48 hours. Indium Tin Oxide (ITO) contacts, which has been widely used as current spreading layer in GaN-base optoelectronic devices, measured an initial ρ_c [the resistivity of the ITO/p-GaN interface, since the metal/ITO ρ_c is negligible] of 1×10^{-2} $\Omega\cdot cm^2$ at room temperature. No degradation was observed after the contact being subjected to 450°C in air for 8 hours.

Accelerated life testing (ALT) was performed to further evaluate the contacts stability at high temperatures quantitatively. The ALT results showed that the annealed Ni/Au to p-GaN contacts is more stable in nitrogen ambient, with a lifetime of 2,628 hours at 450°C which is approximately 12 times longer than that at 450°C in air.

ACKNOWLEDGMENTS

First of all, I would like to express my deepest appreciation to my thesis supervisor, Prof. Srabanti Chowdhury, for introducing me to this interesting field and for her advice, inspiration, encouragement, and continuous support throughout my PhD. Her enthusiasm on the research and her mission for providing high-quality work have made a deep impression on me. I have learnt not only the knowledge in research, but also the dedicating spirit for the work. I am really glad to be associated with a person like Prof. Chowdhury in my life.

I would also like to thank my committee members, Prof. Stephen Goodnick, Prof. Yuji Zhao, and Prof. Robert Nemanich, for giving professional guidance, valuable discussion, and careful corrections. This thesis benefits a lot from their support.

Special thanks must go to Prof. Fernando Ponce and his TEM group for providing TEM analysis which is an important part of my thesis. I have learnt a lot from our discussions and I really enjoy collaborating with them.

I am indebted to all the members in Prof. Chowdhury's research group that I have interacted with over the years. I have learned so much both from their work and from our everyday conversations. Their timely help and friendship shall always be remembered.

I am grateful to the support from the Center for Solid State Electronics Research at ASU, where most experiments were carried out, and the LeRoy Eyring Center for Solid State Science at ASU for providing the characterization service.

I gratefully acknowledge the funding support from the Advanced Research Projects Agency-Energy (ARPA-E).

TABLE OF CONTENTS

Page

LIST OF TABLES vi

LIST OF FIGURES vii

LIST OF SYMBOLS xiii

CHAPTER

1 INTRODUCTION OF GAN HIGH TEMPERATURE ELECTRONICS 1

1.1 Demands for High Temperature (HT) Electronics 1

1.2 Advantages of GaN for HT Electronics 3

1.3 High Temperature InGaN Topping Cells for Hybrid Solar Converters .. 5

1.4 High Temperature Contacts to GaN 7

2 THEORY AND BACKGROUND OF OHMIC CONTACTS TO GAN 9

2.1 A Primer for Semiconductor-Metal Contacts 9

2.2 Schottky Barriers Heights of Metal Contacts to GaN 11

2.3 Summary of Ohmic Contacts to GaN at Room Temperature 12

2.3.1 Ohmic Contacts to n-GaN 12

2.3.2 Ohmic Contacts to p-GaN 14

2.4 Challenge for High Temperature Stable Ohmic Contacts 18

3 EXPERIMENTAL STUDY AND METHODOLOGY TO DEVELOP STABLE HT CONTACTS TO GAN 20

3.1 Transmission Line Method for Characterizing Contact Resistivity 20

3.2 Fabrication of Contacts to GaN 23

3.3 Contacts Characterization 25

CHAPTER Page

3.4 Summary ... 27

4 DEVELOPING OHMIC CONTACTS TO N-GAN FOR HT APPLICATIONS ... 29

4.1 Alloyed Ti/Al/Ni/Au Contacts ... 29

4.2 Non-Alloyed Al/Au Contacts ... 38

4.3 Summary ... 43

5 DEVELOPING OHMIC CONTACTS TO P-GAN FOR HT APPLICATIONS ... 45

5.1 Annealed Ni/Au Contacts to p-GaN ... 45

5.1.1 Electrical Characterization ... 45

5.1.2 Microstructure Characterization ... 57

5.2 Indium Tin Oxide Contacts to p-GaN ... 62

5.3 Summary ... 70

6 LONG TERM RELIABILITY AT HIGH TEMPERATURE ... 71

6.1 Arrhenius Model for Accelerated Life Testing ... 71

6.2 Accelerated Life Testing of the Annealed Ni/Au to p-GaN Contact ... 73

6.3 Summary ... 78

7 CONCLUSION AND FUTURE WORK ... 79

7.1 Conclusion ... 79

7.2 Future Work ... 80

REFERENCES ... 83

LIST OF TABLES

Table Page

1. Values of ρ_c for Contact Sample A, B, and C as a Function of Time under Thermal Stress at 475 °C, 500 °C, and 525 °C, respectively, in Air...................74

2. Comparison of Contact Lifetime (Hours) in Air and in N_2 at Temperatures from 300 °C to 500 °C 78

LIST OF FIGURES

Figure Page

1. High-Temperature Applications with Ambient Temperature Range from 300 °C to 600 °C. 2

2. Semiconductor Intrinsic Carrier Concentration as a Function of Temperature. 4

3. Estimated Practical Electrical Efficiency Limit of a PV Topping Hybrid Solar Converter at 100X Concentration, versus PV Temperature. Dashed Curves Compare the Dispatchable Electricity from Heat without PV and in the Hybrid System. Inset Schematic Shows the Hybrid Converter Configuration 6

4. Metal and n-type Semiconductor Pair before Contact (a) and after Contact (b). The Metal Work Function ϕ_m is Greater than That for the Semiconductor, ϕ_s. 10

5. Metal and p-type Semiconductor Pair before Contact (a) and after Contact (b). The Metal Work Function ϕ_m is Smaller than That for the Semiconductor, ϕ_s. ... 11

6. High-Resolution Transmission Electron Microscopy Image of the Interfacial Area of the Ti/Al/Ni/Au Contacts to n-GaN after Annealing. 13

7. High-Resolution TEM Image of Ni/Au Contact after Annealing in Air Ambient for 20 min at Temperature of 500°C. 17

8. Schematic Drawings of Microstructure at p-GaN/Metal Interface of Ni/Au Contacts, As-Deposited, Annealed in N_2 and Annealed in Air at Temperature of 500~600 °C. 18

9. Schematic Diagrams of Metal Contacts Patterned with TLM Structure on GaN Surface and Measurement of I-V Curves with Four-Point Probes. 21

10. Plot of Total Resistance as a Function of TLM Pad Spacing. 21

Figure Page

11. The Current Flow through the Contacts and the Semiconductor.......................... 23

12. The Layer Structure and Doping Profile of the n-GaN and p-GaN Samples Used for HT Contact Studies. 24

13. Process Flow of the Contact Patterned with TLM Structures.............................. 25

14. Four-Probe I-V Characterization System with a Thermal Chuck Which Can Heat the Sample up to 400 °C during the Measurement in Air.................................... 26

15. A Mini-Brute Furnace for HT Stress with N_2 and Air Flow................................ 27

16. Electrical Characteristics of the Alloyed Ti/Al/Ni/Au Contacts to n-GaN Measured at Room Temperature in Air, (a) I-V Curves Measured between Adjacent TLM Pads with Spacing Increasing from 3um to 30um, and (b) Plot of Measured Resistance versus TLM Contact Spacing.. 29

17. Temperature Dependent *I-V* Characteristics of the Alloyed Ti/Al/Ni/Au Contacts, Taken Between Two Adjacent Pads with Gap Spacing 10um. 31

18. Contact Resistivity and Sheet Resistance of the Alloyed Ti/Al/Ni/Au to n-GaN Contacts as a Function of Measurement Temperature... 31

19. Contact Resistivity and Sheet Resistance of the Ti/Al/Ni/Au to n-GaN Contacts as a Function of Time under 400 °C. 32

20. Microscopy Images of the Alloyed Ti/Al/Ni/Au Contacts Surface, Pre (a) and Post (b) the 450 °C Bake, respectively. Plots of Measured Resistance versus TLM Contact Pads Spacing, Pre (c) and Post (d) the 450 °C Bake, respectively.......... 34

Figure Page

21. The Change of Contact Resistivity and Sheet Resistance of the Alloyed Ti/Al/Ni/Au Contacts after Thermal Stress at 400 °C, 500 °C, 550 °C, and 600 °C for 4 Hours Each with Ambient Air. 35

22. The Change of Contact Resistivity and Sheet Resistance of the Alloyed Ti/Al/Mo/Au Contacts after Thermal Stress at 400 °C, 500 °C, 550 °C, and 600 °C for 4 Hours Each with Ambient Air. 36

23. Cross-Section TEM Images of the Alloyed Ti/Al/Ni/Au Contacts to n-GaN. (a) Low Magnification Image of the Interface and (b) High Resolution Image of the Interfacial TiN Layer. 37

24. Electrical Characteristics of the As-Deposited Al/Au Contacts to n-GaN Measured at Room Temperature in Air, (a) I-V Curves Measured between Adjacent TLM Pads with Spacing Increasing from 3um to 30um, and (b) Plot of Measured Resistance versus TLM Contact Spacing. 39

25. The Change of Contact Resistivity and Sheet Resistance of the Al/Au Contacts after Thermal Stress at 400 °C, 500 °C, 550 °C, and 600 °C for 4 Hours Each with Ambient Air. 40

26. Cross-Section TEM Image of the Al/Au Contacts to n-GaN after Thermal Stress at 600 °C in Air for 4 Hours. 41

27. STEM Image of the Interfacial Area on the Al/Au to n-GaN Contacts after Thermal Stress at 600 °C in Air for 4 Hours. 42

Figure Page

28. (a) EELS Scan Trace, across the 66 nm Interfacial Layer and (b) EELS Spectrum of N, O, Ga, Al, and Au on the Al/Au to n-GaN Sample after Thermal Stress at 600 °C in Air for 4 Hours. 42

29. Extracted Contact Resistivity as a Function of Rapid Thermal Annealing Time at 500 °C, 550 °C, and 600 °C, respectively. 46

30. Measured Resistance versus TLM Pad Spacing after the Ni/Au to p-GaN Contacts were Annealed at 600 °C in N_2 for 3 min. The Inset Picture Shows the I-V Curves Measured between Adjacent Contact Pads with Various Spacing. 46

31. Temperature Dependent I-V Characteristics of the Annealed Ni/Au to p-GaN Contacts, Taken between Two Adjacent Pads with Gap Spacing 5um. 48

32. Temperature Dependent Specific Contact Resistivity ρ_c, (a), and Sheet Resistance R_{sh}, (b), of the Annealed Ni/Au to p-GaN Contacts. 49

33. Measured Resistance versus TLM Pad Spacing after the Annealed Ni/Au Contacts Samples were Subjected to 450 °C in Air for 48 h. The Inset Picture Shows the I-V Curves Measured between Contact Pads with Various Spacing from 3um to 30um. 51

34. Time Evolution of the Specific Contact Resistivity ρ_c, (a), and Sheet Resistance R_{sh}, (b), of the Annealed Ni/Au Contacts over the 48-hour Thermal Stability Test at 450 °C in Air. 53

Figure Page

35. (a) I-V Characteristics Measured at Room Temperature and Taken between Two Adjacent TLM Pads with Gap Spacing 5 um and (b) the Extracted ρ_c of the Ni/Au Contacts after Being Subjected to Thermal Stress at 500 °C, 550 °C, 600 °C, and 650 °C in Series in Air. 55

36. The Extracted R_{sh} of the Ni/Au Contacts after Being Subjected to Thermal Stress at 500 °C, 550 °C, 600 °C, and 650 °C in Series in Air. 56

37. I-V Characteristics of the Ni/Au Contacts Measured at Room Temperature after Being Subjected to 700 °C for 4 hours in Air. 56

38. Cross-Section TEM Image of the Ni/Au Contacts after Post-Deposition Annealing, Showing Three Layers with Two Interfaces. 58

39. High-Resolution TEM Image of the Top Interface, Marked as Interface 1, of the Annealed Ni/Au Contacts. 59

40. High-Resolution TEM Image of the Metal-GaN Interface, Marked as interface 2, of the Annealed Ni/Au Contacts. 59

41. Cross-Section TEM Image of the Ni/Au Contacts after Thermal Stress at 700 °C for 4 hours in Air 61

42. High-Resolution TEM Image of the Interfacial Area on the Ni/Au Contacts after Thermal Stress at 700 °C for 4 hours in Air. 61

43. Two TLM Structures to Test the Contact Resistivity of ITO to p-GaN, (a), and the Sheet Resistance of ITO Film, (b), Respectively. 63

Figure Page

44. (a) I-V Characteristics of the ITO to p-GaN Contact after Post-Deposition Annealing at 500 °C in Air for 1h, Measured on TLM A, and (b) Plot of Measured Resistance versus TLM Contact Spacing. 64

45. (a) I-V Characteristics of the ITO to p-GaN Contact after Thermal Stress at 450 °C in N_2 for 8h, Measured on TLM A, and (b) Plot of Measured Resistance versus TLM Contact Spacing 66

46. (a) I-V Characteristics of the ITO to p-GaN Contact after Thermal Stress at 450 °C in Air for 8h, Measured on TLM A, and (b) Plot of Measured Resistance versus TLM Contact Spacing 68

47. (a) I-V Characteristics of the ITO to p-GaN Contact after Thermal Stress at 500 °C in Air for 8h, Measured on TLM A, and (b) Plot of Measured Resistance versus TLM Contact Spacing 69

48. Increase of ρ_c as a Function of Time under Thermal Stress at 475 °C, 500 °C, and 525 °C, Respectively, in Air. 74

49. Arrhenius Plot of ln (t_f) vs 1/kT in Air. 75

50. Estimated Lifetime in Air versus Temperature according to Arrhenius Model. .. 76

51. Arrhenius Plot of ln (t_f) vs 1/kT in N_2. 77

52. Estimated Lifetime in N_2 versus Temperature according to Arrhenius Model. ... 77

LIST OF SYMBOLS

Symbol Page

1. ρ_c, Specific Contact Resistivity ……………….……………………………………13

2. R_{sh}, Sheet Resistance ……………………….………………………………...22

3. E_a, Activation Energy ……………………………………………………….71

4. t_f, Lifetime ……………………………….....……………………………..72

Chapter 1

INTRODUCTION OF GAN HIGH TEMPERATURE ELECTRONICS

1.1 Demands for High Temperature (HT) Electronics

It is increasingly recognized that semiconductor based electronics that can function at ambient temperatures higher than 150 °C without external cooling could greatly benefit many important applications, especially in the automobiles, aircrafts, gas turbines, oil exploration, and space exploration industries[1]–[5]. More than 40,000 oil and gas wells are being logged every year by the oil industry where electronic and electrical parts range from cabling, connectors, and passive devices to A/D converters, operational amplifiers, motors and solenoids are needed. The temperature in the oil and gas wells can range up to 300 °C for long periods of time during logging. Operational temperatures for the geothermal wells are generally higher than those for oil well and can range up to 400 °C for wells being drilled to depths greater than 11 km. The temperature needs of the automotive industry can range from 150 °C to 800 °C. The lower temperature range, 150 °C to 300 °C, for electronics would include engine block embedded sensors to monitor cylinder pressure and temperature, sensors in brake pads, transmissions, and in chemical fluid reservoirs, while the exhaust gas sensor represents an extreme temperature requirement, 800 °C. The aircraft industry has recognized since the mid-1960s, that placing monitor and control electronics directly on the jet engines could provide many benefits. Electronics capable of operating at 300 °C would satisfy most engine monitoring and control needs, while the engine temperature of high performance aircraft, e.g. supersonic flight at Mach 5, could range from 550 °C to 650 °C. Scientific space missions to other planets and deep space also need high temperature (HT)

electronics. The 465 °C electronic devices are needed for instrumenting Venus surface probe mission, where the maximum surface temperature can reach 465 °C. Fig. 1 shows the major high-temperature applications with ambient temperature range from 300 °C to 600 °C.

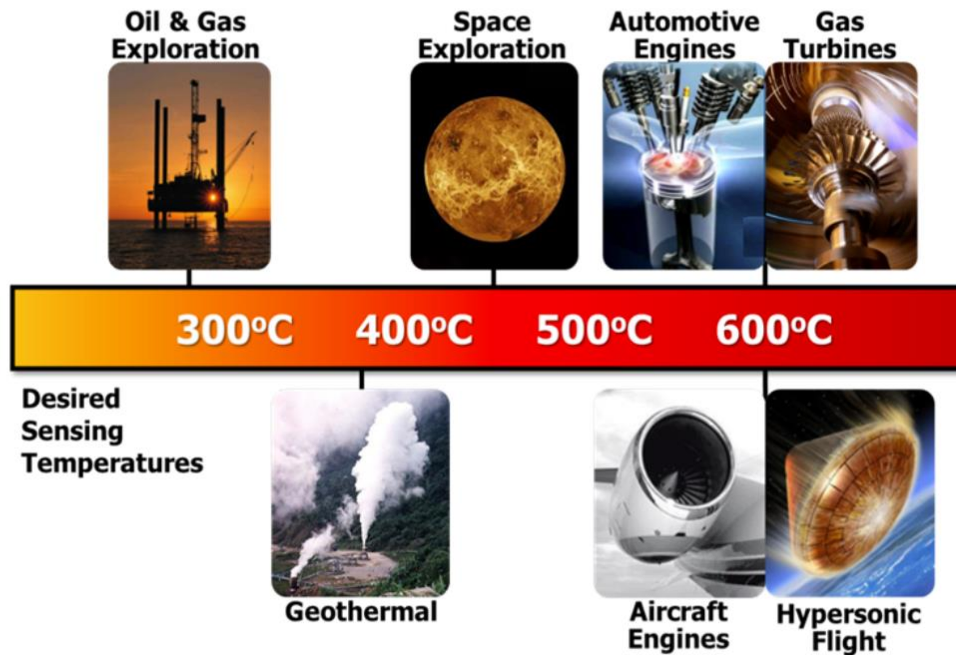

Fig. 1 High-temperature applications with ambient temperature range from 300 °C to 600 °C.

High temperature harsh environments are extremely difficult for electronics to function properly in-situ. Traditionally, engineers rely on active or passive cooling when designing electronics that must function above typical high (150 °C) temperature ranges, or remotely locating the electronics from the high-temperature region. However, active cooling is not always a desired option in many applications or the cost can be very high. The ability to operate electronic systems at high temperatures will not only make new products possible but it will also decrease the cost and increase the reliability of current

products by removing the need for large, massive, complex cooling systems and the cabling and interconnections required for remote placement of the electronics.

1.2 Advantages of GaN for HT Electronics

The temperature limit of semiconductor materials depends highly on their bandgaps. The conventional narrow bandgap silicon devices cannot be operated reliably above 150 °C due to the generation of thermal carriers which can cause leakage, thermal runaway and latch-up at reverse bias[1]. The control of the carrier concentration is crucial for the performance of semiconductor devices. The intrinsic carrier concentration for several semiconductors as a function of temperature is shown in Fig. 2[6], [7]. At temperatures above 300 °C, wide bandgap semiconductor (SiC, GaN, diamond, and AlN) with E_g over 3 eV have much lower intrinsic carrier concentrations compared to Si and GaAs and, thus, do not run into intrinsic carrier conductivity related issues until much higher temperatures. This implies that devices designed for operating above 300 °C should be fabricated from wide-bandgap semiconductors to avoid the deterioration effects of thermally generated carriers.

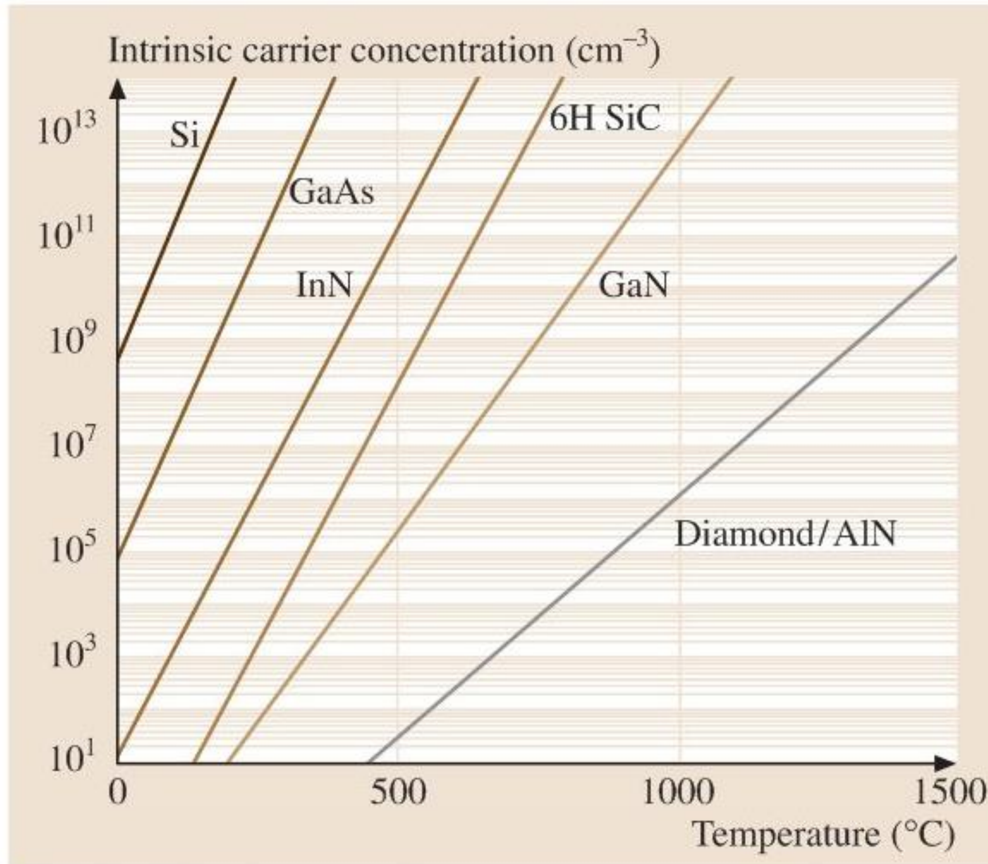

Fig. 2 Semiconductor intrinsic carrier concentration as a function of temperature[6].

SiC-based and GaN based devices are currently the most matured wide-bandgap semiconductors. SiC and GaN technologies are attractive for harsh environment operation because of their high chemical and physical stability; higher atomic displacement energy than many other semiconductor materials. It was reported that the practical temperature limit of GaN and SiC are 600 °C[2], sufficient to support long-term device operation at high temperature. Mass-produced single-crystal SiC wafers have been commercially available while GaN crystals have mostly been grown heteroepitaxially on foreign substrates like sapphire and SiC. SiC crystals have much fewer defects than GaN. Thus, it is not surprising that more research aimed at HT devices has been carried on SiC than GaN. However, GaN also has some important advantages over SiC, i.e.

heterojunction device design capability and a direct energy band gap. The AlGaN/GaN interface forms easily a high-electron mobility two-dimensional electron gas (2DEG) and offers very low channel resistance while SiC devices show rather high channel resistance. GaN-base LED has much higher emission efficiency than SiC because GaN has a direct bandgap whereas SiC has an indirect bandgap which is unfavorable for light emission. In addition, GaN (E_g=3.4 eV) and its alloy with InN (E_g=0.7 eV) has a band gap that is continuously tunable from 0.7 to 3.4 eV[8], which covers a broad solar spectrum from near-infrared to near-ultraviolet wavelength region, offering a great advantage in design and fabrication of high efficiency devices for photovoltaic applications[9], [10]. It is well known that GaN is dominating the lighting and RF industries and entering the power electronics market. Therefore, HT GaN electronics will bring unprecedented advantages in all these applications.

1.3 High Temperature InGaN Topping Cells for Hybrid Solar Converters

Photovoltaic (PV) and concentrating solar power (CSP) are the two main ways of harvest solar energy. However, PV is unlikely to economically supply much more than 10% of the world's electricity due to the high cost of electricity storage[11]. In contrast, CSP collects heat, store heat, and dispatch electricity day and night, but it requires very large and expensive power plants. The hybrid solar converters which combines PV and CSP can address the issue of solar energy storage, and also optimally exploit the solar spectrum to realize higher conversion efficiencies and low electricity costs, while ensuring the availability of inexpensive dispatchable solar power[11]–[13]. The estimated practical electrical efficiency limit of a PV topping hybrid solar converter at 100X concentration, versus PV temperature is shown in Fig. 3[11]. The total efficiency of the

hybrid solar converter is higher than both PV and CSP alone. Despite the drop of PV efficiency at high temperature, the efficiency of CSP increases faster with temperature, thus the total efficiency increases with temperature. Also, the dispatchable fraction of electricity is above 50% when the hybrid solar converter is operating above 400 °C.

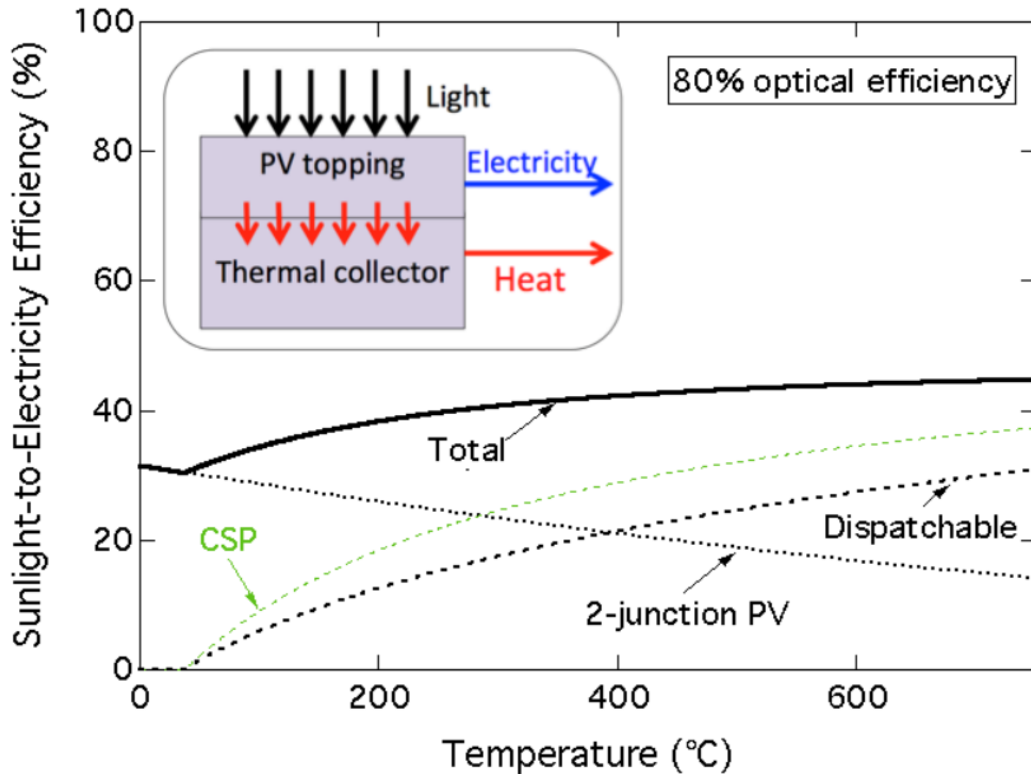

Fig. 3 Estimated practical electrical efficiency limit (black, solid) of a PV topping hybrid solar converter at 100X concentration, versus PV temperature. Dashed curves compare the dispatchable electricity from heat without PV (green) and in the hybrid system (black). Inset schematic shows the hybrid converter configuration[11].

One challenge of the hybrid solar converter is that PV cells, based on wide-bandgap materials, need to be durable for long term operation at high temperatures. GaN and its ternary nitride alloy $In_xGa_{1-x}N$ has the potential application for the HT PV cells due to the wide-bandgap and tunable bandgaps in the range of 0.7 eV and 3.4 eV, covering most of the range of solar spectrum. While GaN alone can withstand high

temperatures above 600 °C, a major challenge is to develop reliable low resistivity ohmic contacts to the device itself. At temperatures higher than 300 °C, failure of the entire cell can occur due to the diffusion of the contact metals, oxidation and reactions at the metal-semiconductor interface. Therefore, the development of thermally and electrically stable ohmic contacts for HT operation is critical for HT GaN electronics, including the hybrid InGaN solar cells.

1.4 High Temperature Contacts to GaN

By contrast with the Si and GaAs devices, which operating temperature is limited by the electronic properties of the semiconductor material, the maximum operating temperature of GaN devices is limited by stability of the contacts. Some device parameters such as response time, output power and etc. depend strongly on the ohmic contact resistivity and its stability at high operating temperatures. For example, in the InGaN PV devices, contact resistance is part of the series resistance. Increase in the series resistance would reduce the fill factor of the PV cells, and thus reduce the efficiency of the InGaN PV cells[14]. Therefore stable and low resistivity ohmic contact is considered as the critical factor determining GaN-based device performance at high temperature. The thermal properties and long term ageing of the ohmic contacts to SiC have been well investigated[15]–[19], which provides insights into approaches to evaluation high-temperature metal contacts to GaN. An InGaN solar cell operating at temperatures in excess of 300 °C, requires thermally stable contacts to both *n*-type GaN and *p*-type GaN capping layers. The focus of this work was specifically derived from the need for appropriate ohmic contacts to both n-type GaN and p-type GaN at elevated temperatures up to 450 °C, also trying to push the contacts temperature limit to 600 °C. The

temperature-dependent contact resistivity of each contacts, their long term stability under high temperature aging, and possible contact degradation mechanism are discussed. We also introduced a method to evaluate the lifetime of ohmic contacts at elevated temperatures using accelerated life testing.

The success of this work enables the possibility of high temperature operation of InGaN solar cell up to 450 °C and unipolar GaN devices, e.g. AlGaN/GaN HEMTs, up to 600 °C in air ambient, making GaN HT devices good supplements to SiC HT electronics. We will be able to use the dispatchable and economic solar energy with better efficiency-to-cost ratio. The work discussed on contacts will significantly benefit HT power electronics and RF electronics where thermal management and thermal stability are of high importance.

Chapter 2

THEORY AND BACKGROUND OF OHMIC CONTACTS TO GAN

2.1 A Primer for Semiconductor-Metal Contacts

Semiconductor device must be connected through metal contacts to the outside world with no adverse change to its current-voltage characteristics and minimum voltage drop across the contact. This can be accomplished through low-resistance ohmic contacts to the semiconductor. Ohmic contacts in a semiconductor are formed such that the majority carriers can flow into the device from an external source (like a voltage or a current supply) with minimal resistance. Conventionally metals with appropriate work functions are chosen to accomplish no barrier to the majority carrier. However in wideband gap semiconductors such as GaN due to lack of metals with appropriate work function or surface pinning effect of the Fermi level, a Schottky based ohmic contact is often more common, where majority carrier transport occurs through the barrier by tunneling. Such designs involve heavy doping in the semiconductor surface so that the carriers can tunnel through the barrier.

The band alignment effect for n-type semiconductor and p-type semiconductor are illustrated in Fig. 4 and Fig. 5, respectively. For metal contact to the n-type semiconductor, the barrier height ϕ_B (before the image force lowering effect) to electrons traveling from metal to semiconductor is $q(\phi_m- \chi)$ while that to electrons traveling from semiconductor to metal is $q(\phi_m- \phi_s)$, ϕ_m the metal work function, ϕ_s the semiconductor work function, and χ the electron affinity. Similarly, for metal contact to the p-type semiconductor, the barrier height to holes traveling from metal to semiconductor is $E_g+q(\chi-\phi_m)$, while that to holes traveling from semiconductor to metal is $q(\phi_s-\phi_m)$.

Therefore, metal with lower work function is preferred to achieve contact to n-type semiconductor, and metal with higher work function is preferred to achieve contact to p-type semiconductor.

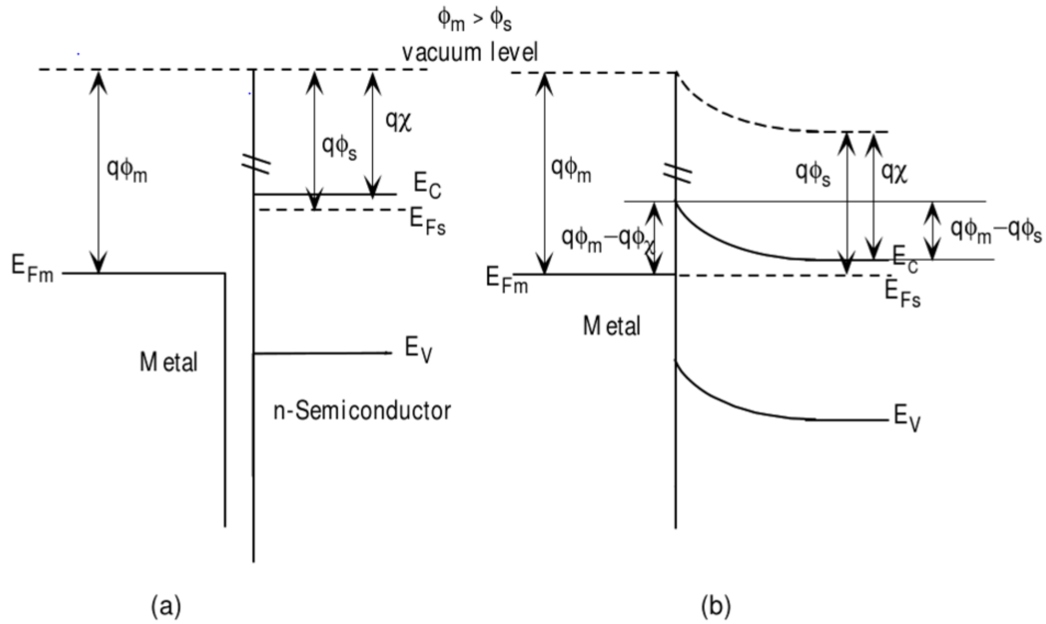

Fig. 4 Metal and n-type semiconductor pair before contact (a) and after contact (b). The metal work function ϕ_m is greater than that for the semiconductor, ϕ_s.

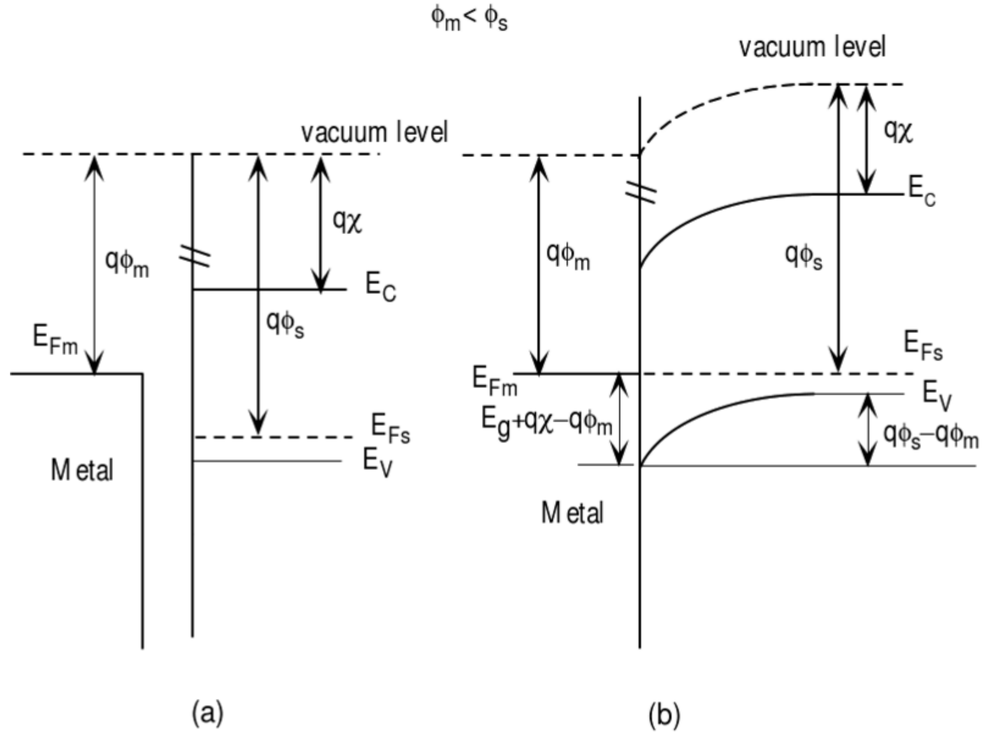

Fig. 5 Metal and p-type semiconductor pair before contact (a) and after contact (b). The metal work function ϕ_m is smaller than that for the semiconductor, ϕ_s.

2.2 Schottky Barrier heights of Metal Contacts to GaN and role of surface states

The above discussion indicates that the Schottky barrier height of metal-semiconductor contact depends highly on the metal work function. However, many researcher have found that the Schottky barriers of metal contacts to GaN depends weakly on the metal work function[20]–[24].

The Schottky barrier heights of Ti, Au, Pd, Ni, Pt, with work functions of 4.3eV, 5.1eV, 5.1eV, 5.15 eV, 5.65 eV, respectively, on n-type GaN are measured to be 0.58eV[22], 0.94eV[24], 0.94eV[24], 0.99eV[23], and 1.04eV[24], respectively. These experimental data illustrates that metal with lower work function has lower Schottky barrier height to n-GaN. However, the difference in the Schottky barrier height among these metals is significantly smaller than the difference in their work functions, implying

that the metal work function is not the only factor affecting the Schottky barriers of metal contacts to n-GaN.

Similarly, the Schottky barrier heights of Ti, Au, Ni, Pt, with work functions of on p-type GaN are measured to be 0.65eV, 0.57eV, 0.5eV, and 0.5eV, respectively[25]. Higher work function metal shows lower Schottky barrier height to p-GaN, but the difference in Schottky barrier heights is small compared to that of metal work function.

The Schottky barrier of metal contacts to GaN is dominated by the fermi level pinning at the surface due to GaN surface states. The minimum barrier height is around 0.5 eV for both n-GaN contact and p-GaN contact. Therefore, selection of appropriate metal alone cannot form low resistivity contact. The presence of high concentration carriers near the metal-GaN interface is essential to form ohmic contact to GaN.

2.3 Summary of Ohmic Contacts to GaN at Room Temperature

2.3.1 Ohmic Contacts to n-GaN

Si has been the preferred n-type dopant for GaN. It acts as a shallow donor with activation energy ~15 meV. Heavy doping can be easily achieved with electron concentration $\sim 10^{20} cm^{-3}$. As a result, ohmic contacts can be formed relatively easily by using metals having a low work function. Ti and Al are commonly used for semiconductor fabrications and they are also popular candidates for ohmic contacts to n-GaN due to their low work functions, 4.33 eV and 4.28 eV, respectively. Ti and Al based metallization schemes, such as Ti-only[26], Al-only[27], Ti/Al bilayer[27], [28], Ti/Al/Ti/Au multilayer[29], and so on, have been used to form ohmic contacts to n type GaN. It was widely believed that a solid phase reaction occurs between Ti and GaN

during the high temperature annealing[29]. Nitrogen out-diffuses from the GaN lattice to form TiN and residual nitrogen vacancies act as donors in GaN. A high-resolution transmission electron microscopy image of the interfacial area of the Ti/Al/Ni/Au contacts to n-GaN after annealing is depicted in Fig. 6, showing the formation of a thin poly-crystalline cubic TiN layer at the metal composite-GaN interface[30]. The interfacial area therefore becomes heavily doped providing the configuration needed for tunneling contacts[29]. Those contacts generally yields specific contact resistivity ρ_c below 1×10^{-5} Ω cm^2.

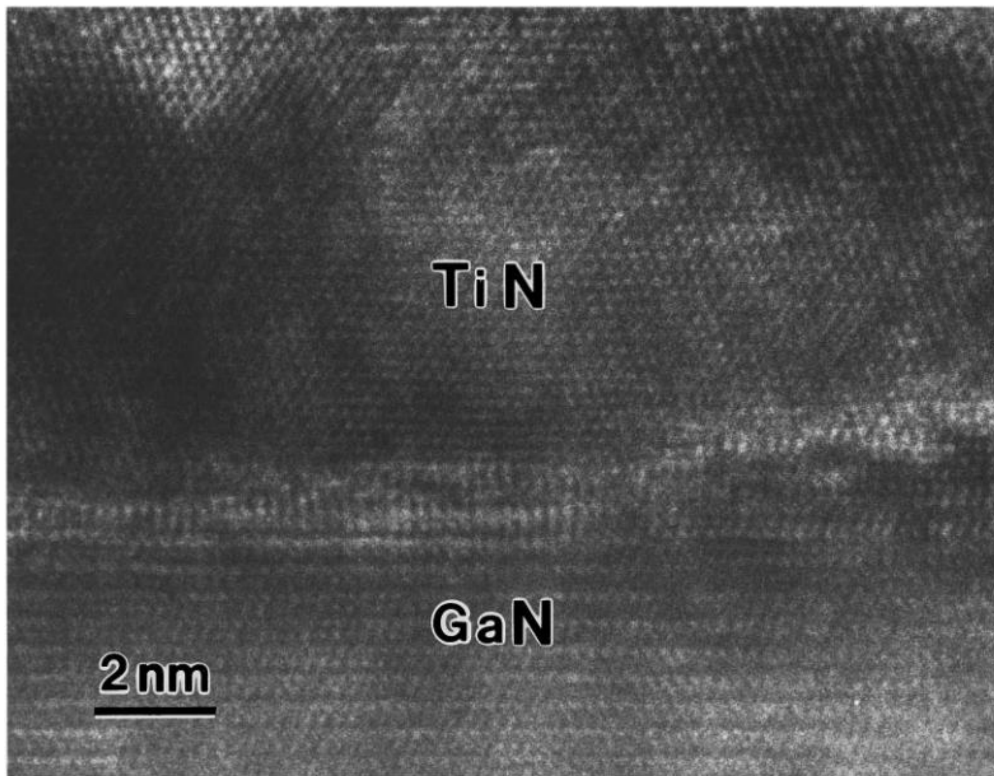

Fig. 6 High-resolution transmission electron microscopy image of the interfacial area of the Ti/Al/Ni/Au contacts to n-GaN after annealing[30].

However, the Ti-only, Al-only, and the Ti/Al bilayer contacts to n-GaN are not reliable for high-power and high-temperature device applications. Both Ti and Al tends to be oxidized, which is unavoidable for HT electronics, especially for Ti. Besides, Al tends

to react with GaN and form wide-band-gap AlN at the interface after annealed at 600 °C[31]. Low melting points of Al (600 °C) presents another problem for thermal stability of the Al-only and Ti/Al contacts. Therefore, those contacts will degrade after high temperature annealing or operation, and thus can't be used for HT electronics.

More complex metallization schemes, such as Ti/Al/Ni/Au multilayer[32]–[34], Ti/Al/Pt/Au[35], [36], Ti/Al/Pd/Au[37], and Ti/Al/Mo/Au[38], are widely studied and tested at high temperature for forming ohmic contacts to n-GaN and AlGaN/GaN HEMTs. In these contact schemes, the low-resistivity Au coating metal is employed to improve the resistance to oxidation of the Ti/Al layer during high temperature annealing. On the other hand, the barrier metal (Ni, Pt, Pd, Mo) between Au and the Ti/Al layer is introduced to prevent the inter-diffusion of Ti, Al, and Au[35], [39], and therefore improve the thermal stability of the contact[40]. Hou *et al*. reported that alloyed Ti/Al/Pt/Au to *n*-type GaN contacts was very stable at 600 °C over 10 hours in an air ambient [41]. The temperature dependence of the specific contact resistivity, between 25 °C and 175 °C in Ti/Al/Ni/Au ohmic contacts to *n*-GaN has been reported[42]. The specific contact resistance ρ_c decreases with increasing measuring temperatures which is explained as the current transport in the contacts occurs by a thermionic field emission mechanism.

2.3.2 Ohmic Contacts to p-GaN

In contrast to n-GaN, stable ohmic contacts with low resistivity to p-GaN are much more difficult to achieve due to lack of suitable work function in metals, surface states in GaN and deep acceptor [Mg] energy level. The strategy to make ohmic contacts to p-type GaN is, in principle, to use metals having a large enough work function to facilitate tunneling transport. However, p-type GaN has fundamental problems, which

make it difficult to form device-quality ohmic contacts with a specific contact resistance that is lower than 1×10^{-4} Ω cm^2. The first problem is the absence of appropriate metals which have a work function that is large than that of the p-type GaN, with bandgap 3.4 eV and electron affinity 4.1 eV. Ni, Au, Pd, and Pt are widely used for p-GaN contacts, and there work function are 5.15 eV, 5.1 eV, 5.12 eV and 5.65 eV, respectively. Thus, a high Schottky-barrier is unavoidable on the metal-semiconductor interface. The second problem arises from the difficulty in growing highly doped p-GaN, with hole concentration above 1×10^{18} cm^{-3}, due to the high activation energy, ~170 meV, of Mg. In growth techniques such as MOCVD reactor where Hydrogen is present during growth, formation of Mg-H complexes causes passivation of Mg[43]. However the passivation of Mg can be recovered by annealing out the H from the crystal at 700 °C and therefore is not a primary issue for high contact resistivity.

Metal schemes with large work function and also easy to use in device processing, such as Ni, Au, Pd, and Pt, have been investigated in order to form low resistance ohmic contacts to p-GaN. Ni/Au double layer contact technology to form ohmic contacts to *p*-type GaN at room temperature has been widely reported, with a standard ρ_c ~1×10^{-3} Ω cm^2 after rapid thermal annealing (RTA) [44]–[56]. However, the mechanism of forming ohmic contact after RTA is still not clear. Ho et al. reported that the decrease of the contact resistivity was due to the formation of NiO during the annealing process in air[45], and the NiO was found to be p-type conducting with hole concentration of 2×10^{17} Ω cm^2[47]. Koide et al. proposed that the ohmic contact was achieved due to the increase of the hole concentration in GaN surface layer caused by removal of hydrogen atoms bonded with Mg acceptors during annealing[57], [58]. Fig. 7 shows a high resolution

image of the Ni/Au contact annealed in the air ambient at 500°C for 20 min. The Au layer is directly in contact with the GaN surface with sharp interface. There is no NiO or other intermixed layer formed at the interface. Ni diffuses away from the metal-GaN interface and reacts with oxygen, forming a NiO compound on top of the Au layer. The Ni and Au layer sequence is inverted after annealing and no reaction between the metals and the GaN is observed at the interface.

Fig. 8 shows the schematic illustrations of the microstructural change of the Ni/Au contacts after annealing in the N_2 or air ambient. Before the metal deposition, there is a thin contaminated layer with a thickness of around 2 nm, which is unavoidable as the GaN epi-layer is exposed to air[59]. Therefore, the as-deposited metal is sitting on top of the contaminated layer, likely Ga_2O_3 (n-type to semi-insulating in nature) offers a higher contact resistivity. After annealing in the N_2 ambient, Ni reacted with the contaminated (oxide) layer and Au, removing the thin contaminated interfacial layer and forming an Au–Ni solid solution which intimately contacted the p-GaN surface. Therefore, reduction of the ρ_c value after annealing in the N_2 ambient was believed to be due to the intimate contact of the metal to the p-GaN surface. Annealing in the air ambient facilitated out-diffusion of Ni to the Au surface, and Ni was then oxidized, forming the NiO on top of the Au layer. Since the Au was not oxidized, the intimate contact of Au to p-GaN occurred as a result of the out-diffusion of Ni to the surface.

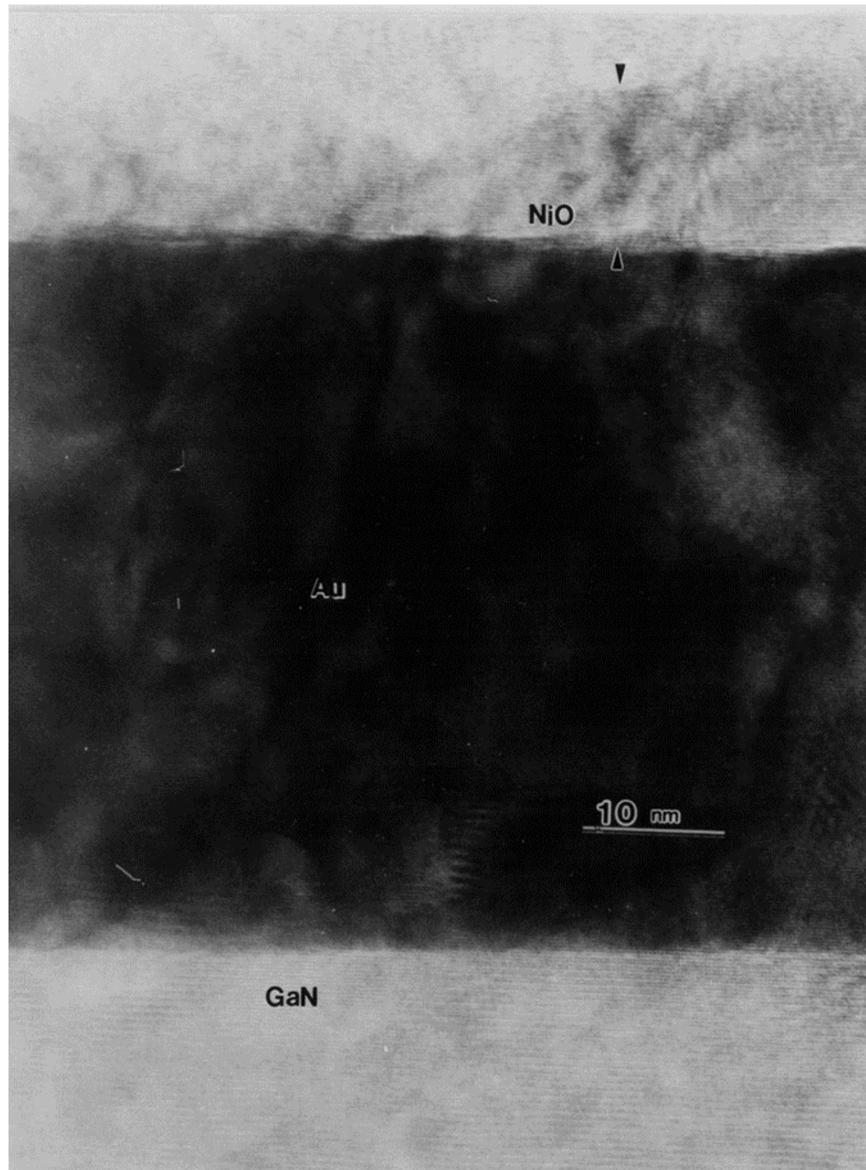

Fig. 7 High-resolution TEM image of Ni/Au contact after annealing in air ambient for 20 min at temperature of 500°C[57].

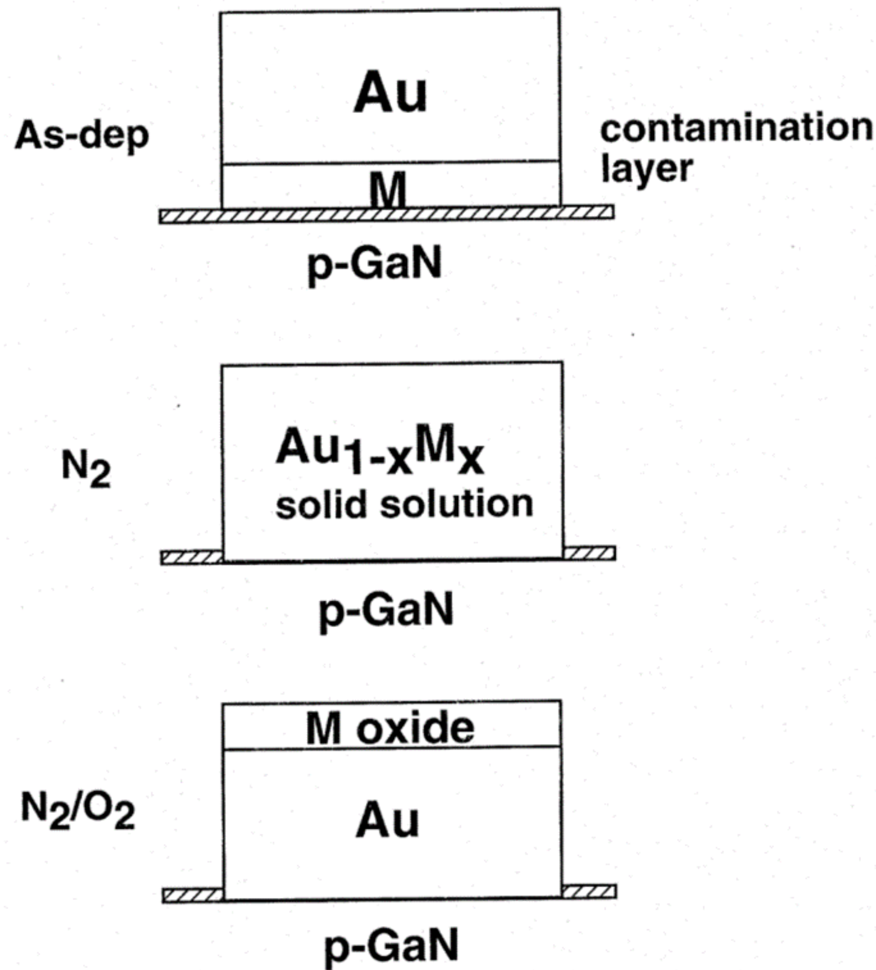

Fig. 8 Schematic drawings of microstructure at p-GaN/metal interface of Ni/Au contacts, as deposited, annealed in N_2 and annealed in air at temperature of 500~600 °C[57].

2.4 Challenges in HT Stable Ohmic Contacts

The ohmic contacts are a critical factor that could restrict the HT device application. The high operating temperatures may cause diffusion processes in the contact layer and reactions between the contact components, which could lead to changes of the contact properties during operation at high temperatures, and deterioration of the devices. Also, possible reaction and diffusion between the metal and GaN occur at high temperature which may result in reduction of carrier concentration on the surface of GaN and thus degrade the ohmic contact. If the contact resistivity is not sufficiently low

inadmissible high voltage drop could arise due to the high current density in the contact of high power devices. Hence, the following requirements to the ohmic contacts are critical for GaN HT applications.

i) Low contact resistivity – in general, the make of low resistivity ohmic contacts is difficult for wide band-gap semiconductors due to the difficulty in doping and, in the case of p-type materials, due to the wide forbidden band-gap.

ii) High temperature stability – this problem is very important in the wide band-gap semiconductors. In the Si and GaAs devices the maximal working temperature is limited by the material stability, because of that the problem of the contact stability is important but not critical. The great potential of III-V nitrides to work at temperatures up to 600 °C and higher, set strong requirements for the thermal stability and reliability of the contacts.

iii) Reproducibility – this requirement is important in the case of the device production. Therefore the contact technology should allow the achievement not only good performance, but good reproducibility.

The listed requirements point that the operation of high temperature and high power GaN-based devices under severe conditions demands development of electrically, thermally and chemically stable metal contacts.

Chapter 3

EXPERIMENTAL STUDY AND METHODOLOGY TO DEVELOP STABLE HT CONATCTS TO GAN

3.1 Transmission Line Method for Characterizing Contact Resistivity

Transmission Line Method (TLM) was used for evaluating the ohmic contacts to n and p type GaN throughout in this study. This technique was proposed by Reeves and Harrison. Details about this method are available in their published work[60].

A schematic diagram of a semiconductor material with ohmic contact pads prepared for TLM tests is shown in Fig. 9. The sample is at first mesa-etched usually to a depth where there is a natural depletion or insulating layer. This is done in order to isolate columns of the conductive epitaxial layer there by restricting current flow within the column or the active device (in this case TLM) area. Metal contact pads, of finite width, *W*, are then deposited on the mesa at a linearly increasing pad spacing, *d*, such that $d_1 < d_2 < d_3$. A constant current is passed between two adjacent pads through two probes; a second set of probes are then used to measure the voltage drop enabling the total resistance between the pads to be obtained. Separate current source and voltage senses are preferred to cancel the resistance of the probes, which otherwise will compromise the accuracy of the method especially when the measured total resistance is relatively low. The process is repeated and the total resistance is plotted on a linear graph as a function of pad spacing, *d*. An example is shown in Fig. 10.

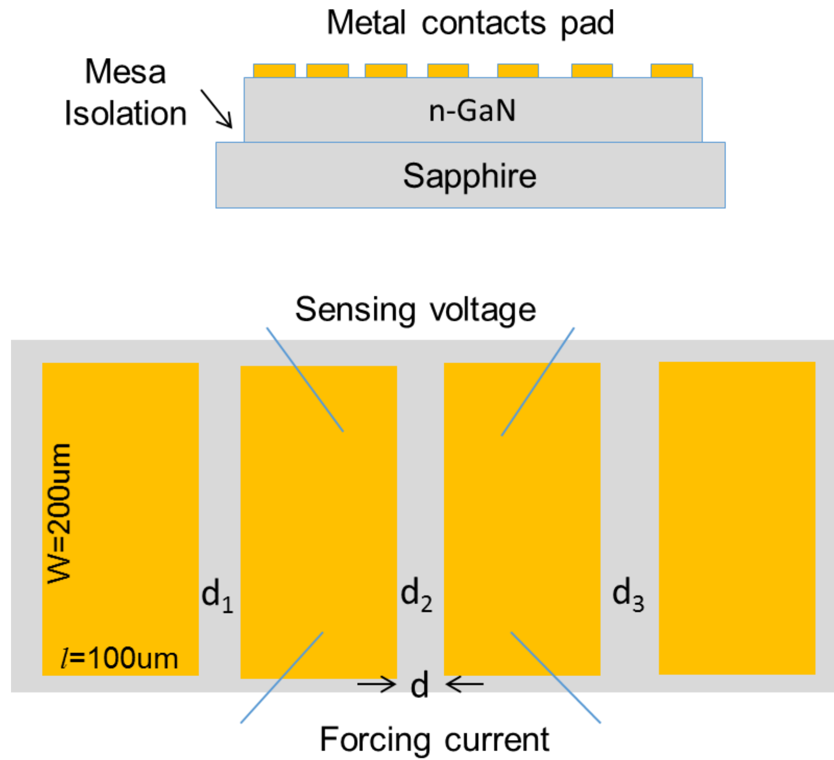

Fig. 9 Schematic diagrams of metal contacts patterned with TLM structure on GaN surface and measurement of I-V curves with four-point probes.

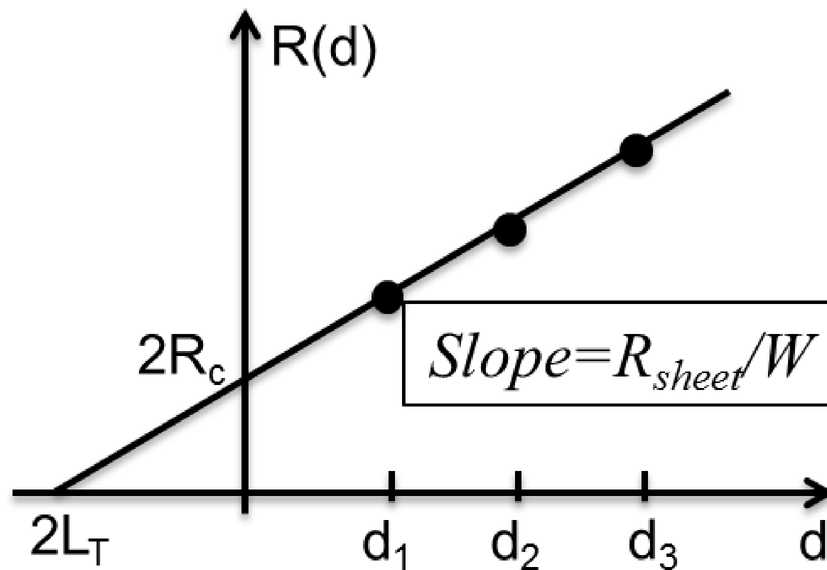

Fig. 10 Plot of total resistance as a function of TLM pad spacing.

The measured total resistance $R(d)$, between two adjacent pads with spacing d, is given by:

$$R(d) = 2R_c+R_{semi}, \tag{1}$$

where, R_c is the resistance due to the contact between metal and semiconductor, and R_{semi} is the resistance due to the semiconductor material.

$$R_{semi} =R_{sh}*d/W, \tag{2}$$

where R_{sh} is the sheet resistance of the semiconductor. Therefore,

$$R(d) = 2R_c + R_{sh}*d/W, \tag{3}$$

Thus the contact resistance and the sheet resistance can be derived by plotting $R(d)$ vs d. The intercept of the $R(d)$ vs d plot gives the contact resistance while the slope gives the sheet resistance.

$$R_c = \text{Intercept}/2, \tag{4}$$

$$R_{sh} = \text{slope}*W, \tag{5}$$

The contact resistance depends on the size of the contact, therefore not a normalized parameter to compare different samples. Therefore, specific contact resistivity, ρ_c

$$\rho_c = R_c*A_c, \tag{6}$$

where, A_c is the effective area of the contact, is chosen as the normalized parameter to quantitatively evaluate and compare the quality of contacts. However, it is not the same as the physical area of the contact metal, since the current does not flow uniformly in the contact, as shown in Fig. 11. At the edge of the contact, the current flowing in (or out) is significant. Moving away from that edge, the current drops off until, at the far edge, there is no current[61]. This is known as "current crowding". The transfer length, L_T, is

introduced, which describes the average distance that an electron (or hole) travels in the semiconductor beneath the contact before it flows up into or out of the contact. $L_T = \frac{R_c}{Slope}$, is extracted from the standard plot shown in Fig. 10.

Therefore, the effective area of the contact can be treated as $L_T * W$. Thus,

$$\rho_c = R_c * L_T * W = \frac{R_c^2 W}{Slope}, \quad (7)$$

Therefore, both R_{sh} and ρ_c can be extracted from the linear plot of $R(d)$ vs d.

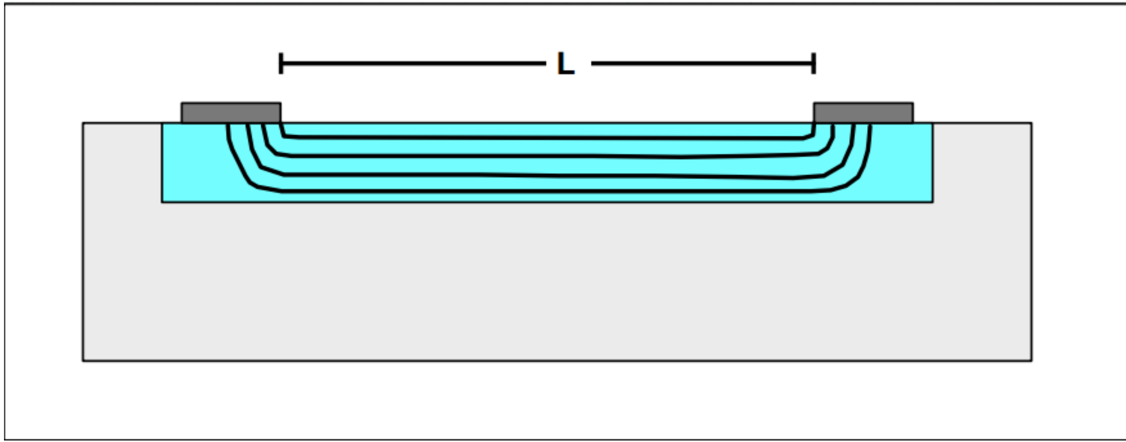

Fig. 11 The current flow through the contacts and the semiconductor[61].

3.2 Fabrication of Contacts to GaN

The epitaxial layers of n-GaN and p-GaN were grown by Metal Organic Chemical Vapor Deposition (MOCVD). The layer structure and doping profile is shown in Fig. 12. For the n-GaN samples, an unintentionally doped *c*-plane GaN buffer layer (3.1 um) was first grown on sapphire substrate, followed by 300 nm thick *n*-type GaN with a Si doping concentration of 1×10^{17} cm^{-3}. Then, the n-GaN structure was capped with 100 nm thick heavily doped *n*-type GaN with a Si doping concentration of 1.7×10^{19} cm^{-3}. For the *p*-type contact studies,, an unintentionally doped *c*-plane GaN buffer layer (3.1 um) was first grown on sapphire substrate, followed by 300 nm thick *n*-type GaN with a Si doping

concentration of 1×10^{17} cm^{-3} and 100 nm thick *p*-type GaN with a Mg doping concentration of 3×10^{19} cm^{-3}. The p-GaN structure was capped with 10 nm of p^+GaN with a Mg doping concentration of 1×10^{20} cm^{-3}. The p-GaN samples were activated by annealing at 700 °C in N_2 ambient for 30 min.

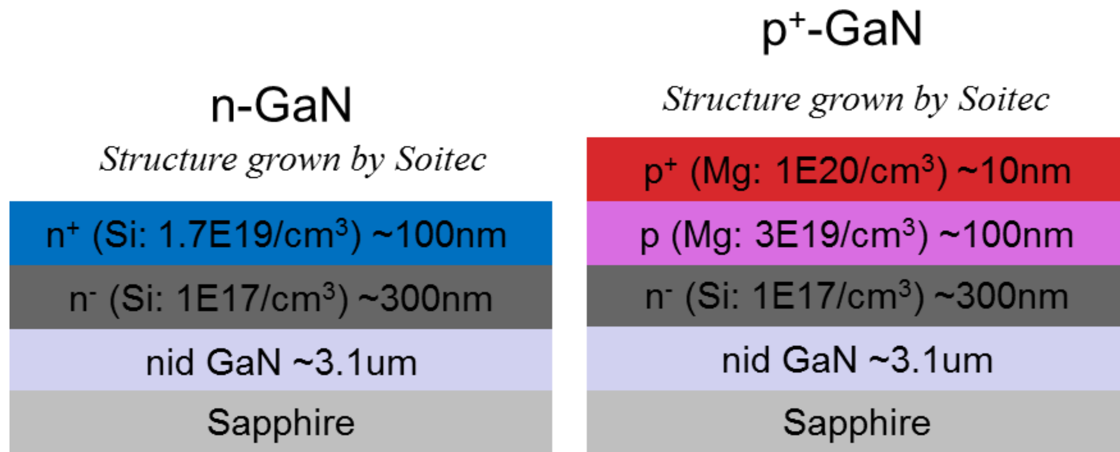

Fig. 12 The layer structure and doping profile of the n-GaN and p-GaN samples used for HT contact studies.

The determination of the specific contact resistivity (ρ_c) and sheet resistance (R_{sh}) were carried out by the TLM measurement. TLM test structures were fabricated on both n-GaN and p-GaN samples with layer structures as shown in Fig.12. Fig. 13 shows the process flow of the contacts patterned with TLM structures. First, mesa regions for TLM measurements were defined using inductively coupled plasma (ICP) etching to etch down to the lightly doped *n*-type GaN. Next, TLM contact pads, with an area of 100×200 μm^2, were deposited by e-beam evaporation. A 1-min dip in HCl: DI water (1:3) mixture was conducted to remove the native oxide layers prior to e-beam evaporation of the contact pads. After deposition and lift-off of the metal contacts, we subjected the samples to a rapid thermal annealing (RTA). The RTA conditions are different for each contact.

Further details about the RTA conditions have been discussed in the following two chapters.

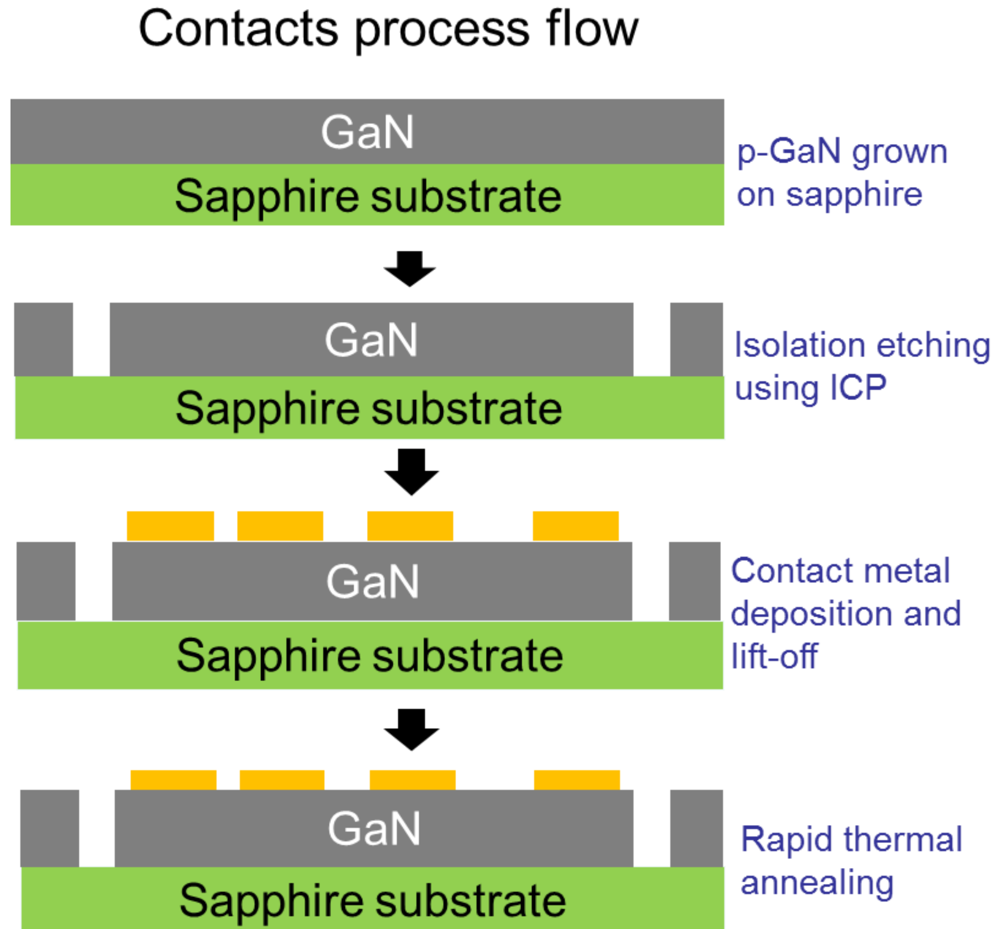

Fig. 13 Process flow of the contact patterned with TLM structures.

3.3 Contacts Characterization

The current-voltage (*I*-*V*) characteristics of the annealed contacts were measured using a four-point probe station equipped with a Keithley 4200-SCS parameter analyzer. The temperature dependence of ρ_c and R_{sh} were studied in the range from 25 °C to 400 °C, varying the chuck temperature by using an Instec mK2000 temperature controller, as shown in Fig. 14. To evaluate the stability of the contacts above 400 °C, a Minibrute

furnace, shown in Fig. 15, with N_2 or air ambient was used for HT stress test. The contact samples were measured before and after the HT stress to see if there is any degradation.

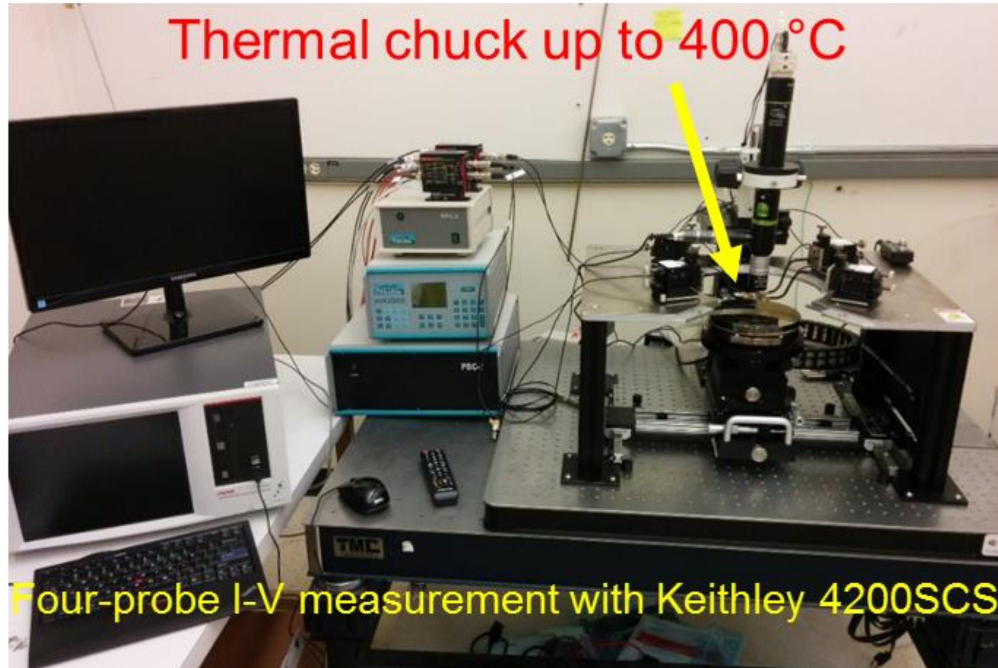

Fig. 14 Four-probe I-V characterization system with a thermal chuck which can heat the sample up to 400 °C during the measurement in air.

Fig. 15 A Mini-brute furnace for HT stress with N_2 and air flow.

To understand the mechanism that whether the ohmic contact is stable at high temperature or it degrades due to the high temperature, high-resolution transmission electron microscope (HR-TEM) was used to study the interface between metal and GaN. The contacts samples were prepared by either focused ion beam (FIB) or wedge polishing technique. Scanning transmission electron microscope (STEM) and *in situ* electron energy loss spectroscopy (EELS) were employed to analyze the interfacial layer or phase created by HT thermal stress. The electron microscopy provided strong explanation to support the electrical characterization.

3.4 Summary

TLM structures were prepared to evaluate various contact metallurgy schemes. Besides the electrical characterization done using TLM, the microscopic study of the contacts was done with TEM, STEM and EELS. Electrical behavior along with the

microstructure images revealed all the information about the contacts and their degradation mechanism. Chapters 4 and 5 describe the details of our study. Chapter 6 shows the application of the TLM results to derive the lifetime of the contacts.

Chapter 4

DEVELOPING OHMIC CONTACTS TO N-GAN FOR HT APPLICATIONS

4.1 Alloyed Ti/Al/Ni/Au Contacts

The Ti/Al/Ni/Au multilayer (of thicknesses - 20nm, 120nm, 30nm, and 50nm, respectively) metal contacts to n-GaN show excellent ohmic behavior after RTA at 800 °C in N_2 for 30s, as was discussed in Chapter 2. We first measured the TLM structures at room temperature in air. The I-V curves, shown in Fig. 16 (a), are quite linear, resulting in the plot of measured resistance versus TLM contact spacing, as shown in Fig. 16 (b). A sheet resistance, R_{sh}, of 288 Ω/□ and the specific contact resistivity, ρ_c, of 6.8×10^{-6} Ω cm^2 was derived from the TLM data calculated using the method introduced in Chapter 3.

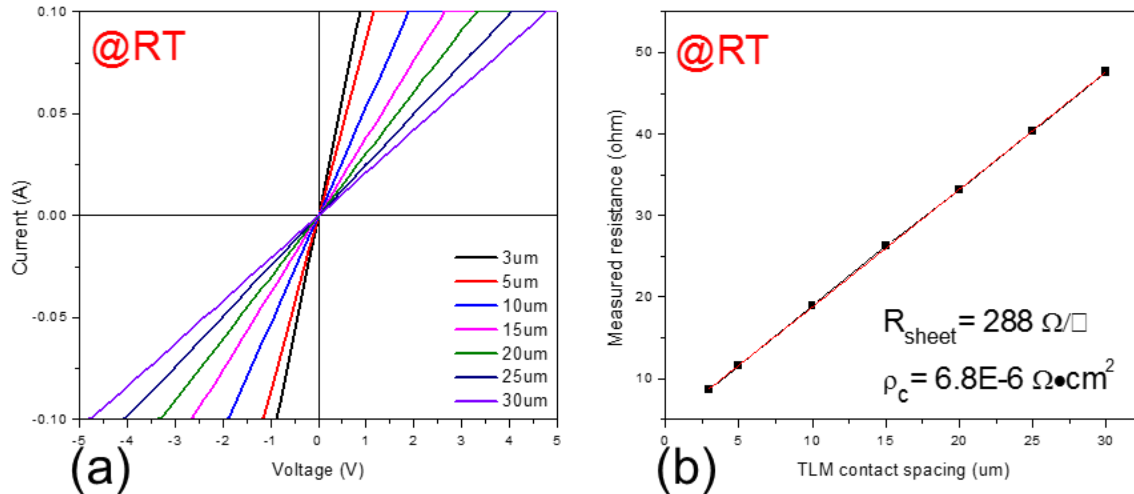

Fig. 16 Electrical characteristics of the alloyed Ti/Al/Ni/Au contacts to n-GaN measured at room temperature in air, (a) I-V curves measured between adjacent TLM pads with spacing increasing from 3um to 30um, and (b) plot of measured resistance versus TLM contact spacing.

To understand the HT behavior, the sample was heated up to 400 °C in air and the TLM measurements were taken at 300 °C and 400 °C, respectively. The temperature dependent I-V characteristics of the alloyed Ti/Al/Ni/Au contacts, measured between two adjacent pads with a spacing of 10um, is shown in Fig. 17. As the measurement temperature increased, the I-V curves remained linear, but the current reduced slightly, indicating an increase of the measured resistance. Fig. 18 shows the temperature dependent contact resistivity and sheet resistance of the alloyed Ti/Al/Ni/Au to n-GaN contacts. ρ_c, ~6×10^{-6} Ω cm^2, is indeed independent of the measurement temperature, while R_{sh} increases significantly as the measurement temperature increases, from 288 Ω/□ at room temperature to 370 Ω/□ at 400 °C. The increase of n-GaN sheet resistance is most likely due to the decrease of electron mobility at high temperature. Therefore, although the contacts resistivity of the alloyed Ti/Al/Ni/Au to n-GaN contacts did not change with the ambient temperature, the n-GaN layers became more resistive as the temperature increased.

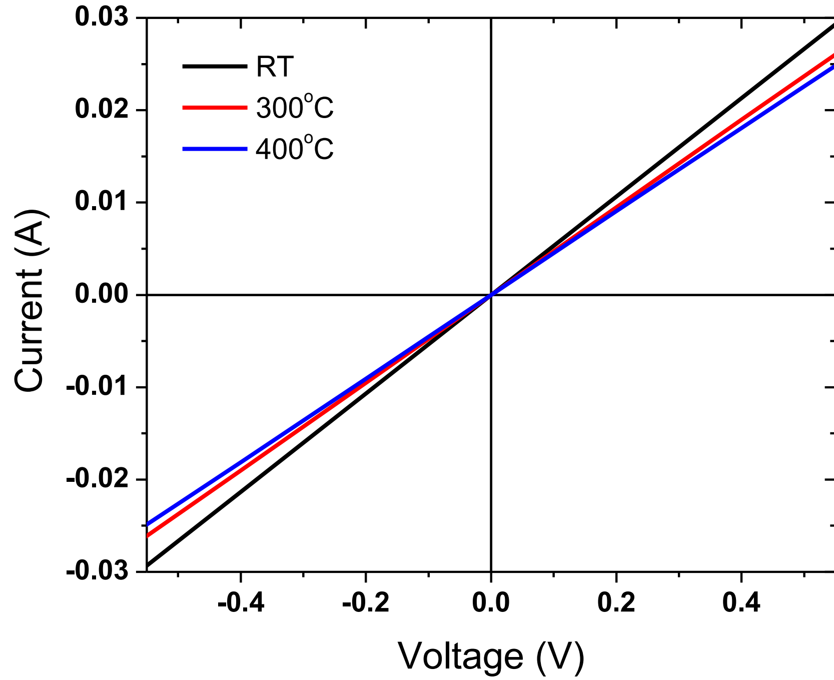

Fig. 17 Temperature dependent *I-V* characteristics of the alloyed Ti/Al/Ni/Au contacts, measured between two adjacent pads with gap spacing 10um.

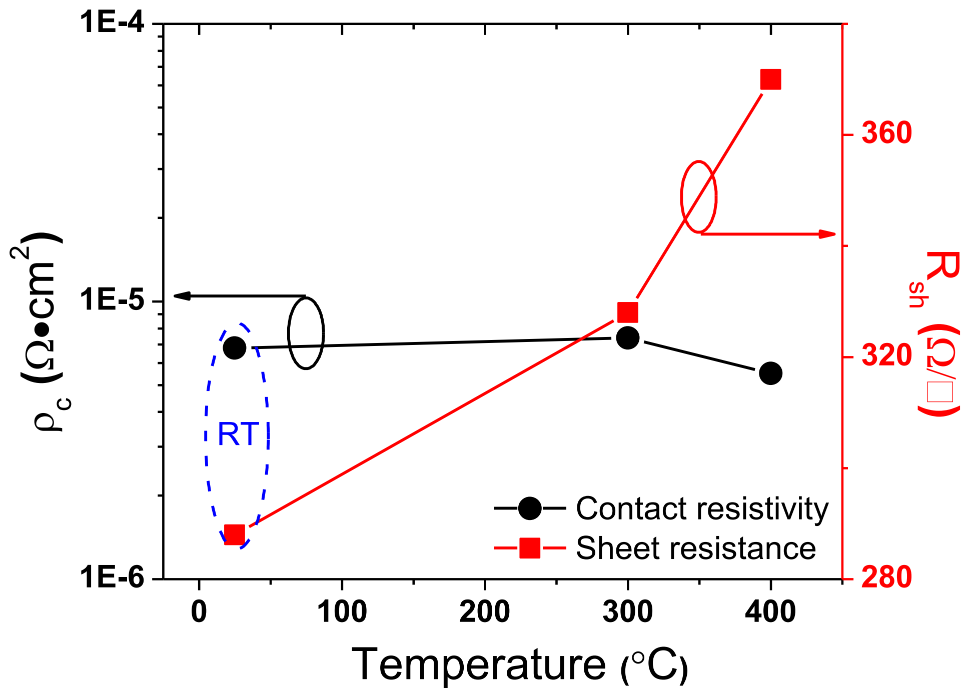

Fig. 18 Contact resistivity and sheet resistance of the alloyed Ti/Al/Ni/Au to n-GaN contacts as a function of measurement temperature.

To further investigate the thermal stability of the alloyed Ti/Al/Ni/Au to n-GaN contacts at 400 °C in air, the samples were held at 400 °C for 3h, during which the TLM structures were measured multiple times. Fig. 19 shows the time evolution of contact resistivity and sheet resistance as the samples were held at 400 °C for 3 h. Both ρ_c and R_{sh} were very consistent at 400 °C and no degradation could be observed during the 3h high temperature testing. When the sample was cooled down to room temperature, both ρ_c and R_{sh} returned to their initial values measured prior to the high temperature testing. Based on the above analysis, the sheet resistance of n-GaN is a function of measurement temperature, but it is independent of the time subjected at those high temperatures. The change in sheet resistance was reversible when the sample was cooled down to room temperature. The contact resistivity is independent of the measurement temperature and it was very steady at 400 °C with ambient air.

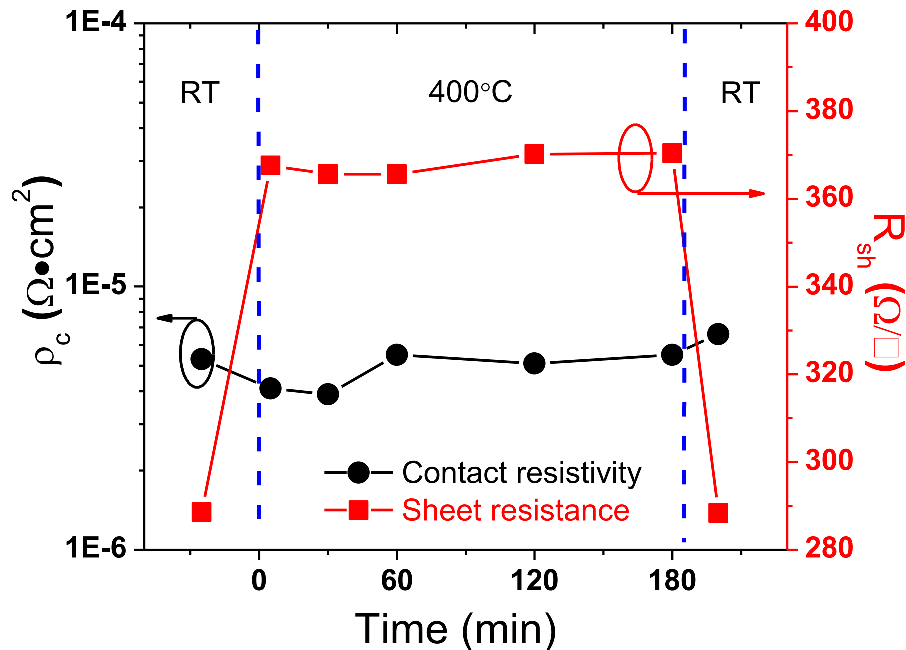

Fig. 19 Contact resistivity and sheet resistance of the Ti/Al/Ni/Au to n-GaN contacts as a function of time under 400 °C.

To test the stability of the alloyed Ti/Al/Ni/Au to n-GaN contacts at 450 °C in air, the sample was subjected to a Minibrute furnace and baked at 450 °C for 8 hours. Fig. 20 (a) and (b) shows the comparison of contacts surface before and after the 8-hour bake at 450 °C in air, respectively. No visible difference was observed. Also, there was negligible change in contact resistivity and sheet resistance that were extracted from the plots of measured resistance versus TLM contact pads spacing, pre-bake (c) and post-bake (d).

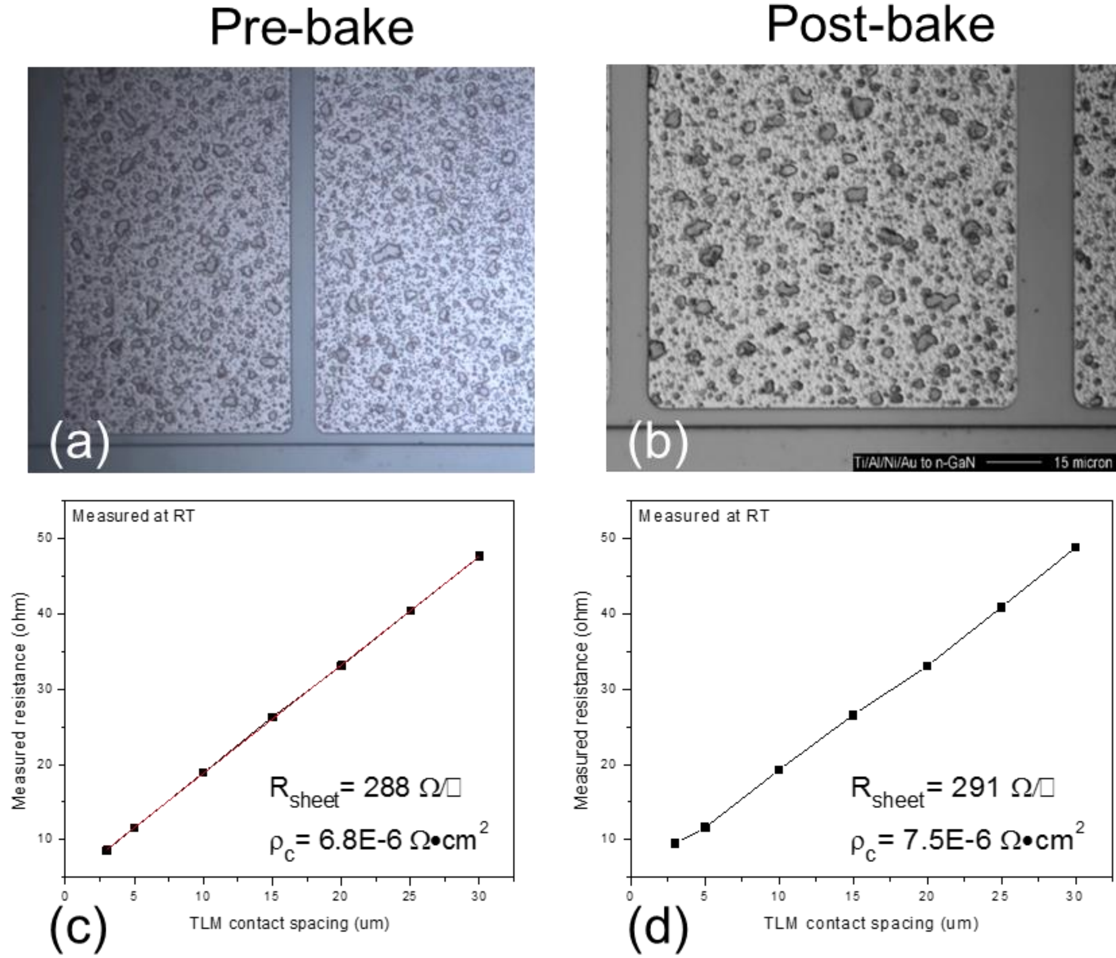

Fig. 20 Microscopy images of the alloyed Ti/Al/Ni/Au contacts surface, pre (a) and post (b) the 450 °C bake, respectively. Plots of measured resistance versus TLM contact pads spacing, pre (c) and post (d) the 450 °C bake, respectively.

To find out the temperature limit of the contact in air ambient, a new sample was prepared. The sample with the alloyed contacts after post-deposition RTA offered a ρ_c of 5.9×10^{-6} Ω cm^2 with a R_{sh} of 441 Ω/□. Then the sample was sequentially subjected to 400 °C, 500 °C, 550 °C, and 600 °C in the Minibrute furnace with air ambient for 4 hours at each temperature. The sample was taken out and cooled down to RT for the TLM measurement after the thermal stress at each temperature. The change of ρ_c and R_{sh} are shown in Fig. 21. The sheet resistance was very consistent after each thermal stress,

showing values around 445 Ω/□, indicating thermal stress up to 600 °C did not cause significant change in the conduction layer of n-GaN. The contact resistivity increased after thermal stress at 500 °C for 4 hours, but it then decreased after thermal stress at 550 °C for 4 hours. Finally, ρ_c showed a tendency to stabilized around 1×10^{-6} Ω cm^2 after thermal stress at 600 °C for 4 hours.

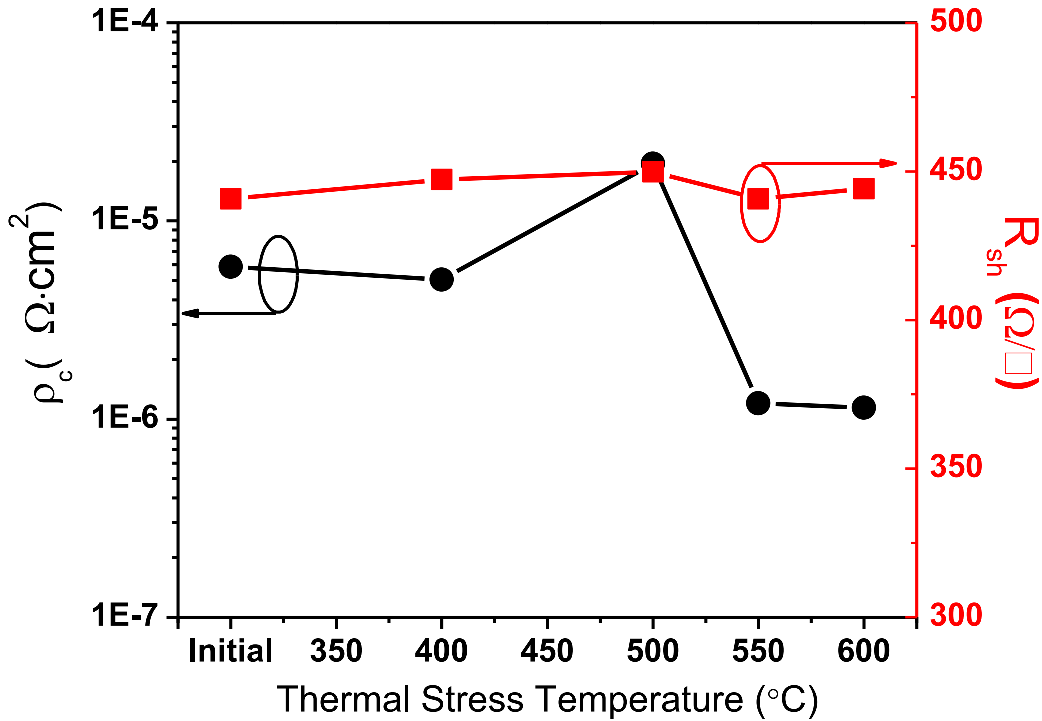

Fig. 21 The change of contact resistivity and sheet resistance of the alloyed Ti/Al/Ni/Au contacts after thermal stress at 400 °C, 500 °C, 550 °C, and 600 °C for 4 hours each with ambient air.

Similar study was done on the Ti/Al/Mo/Au contacts, which uses a layer of Mo instead of Ni for the diffusion barrier. The Ti/Al/Mo/Au contacts, with thicknesses of 20nm, 120nm, 30nm, and 50nm, respectively, were also subject to RTA at 800 °C in N_2 for 30s. The TLM test structures showed good ohmic behavior with ρ_c of 3.7×10^{-5} Ω cm^2 and R_{sh} of 314 Ω/□. Fig. 22 shows the change of ρ_c and R_{sh} of the alloyed Ti/Al/Mo/Au contacts after thermal stress at 400 °C, 500 °C, 550 °C, and 600 °C for 4 hours each with

ambient air. Similar to those with the alloyed Ti/Al/Ni/Au contacts, sheet resistance was not affected by the thermal stress at temperatures up to 600 °C while contact resistivity increased after the 500 °C thermal stress and decreased after the 550 °C thermal stress.

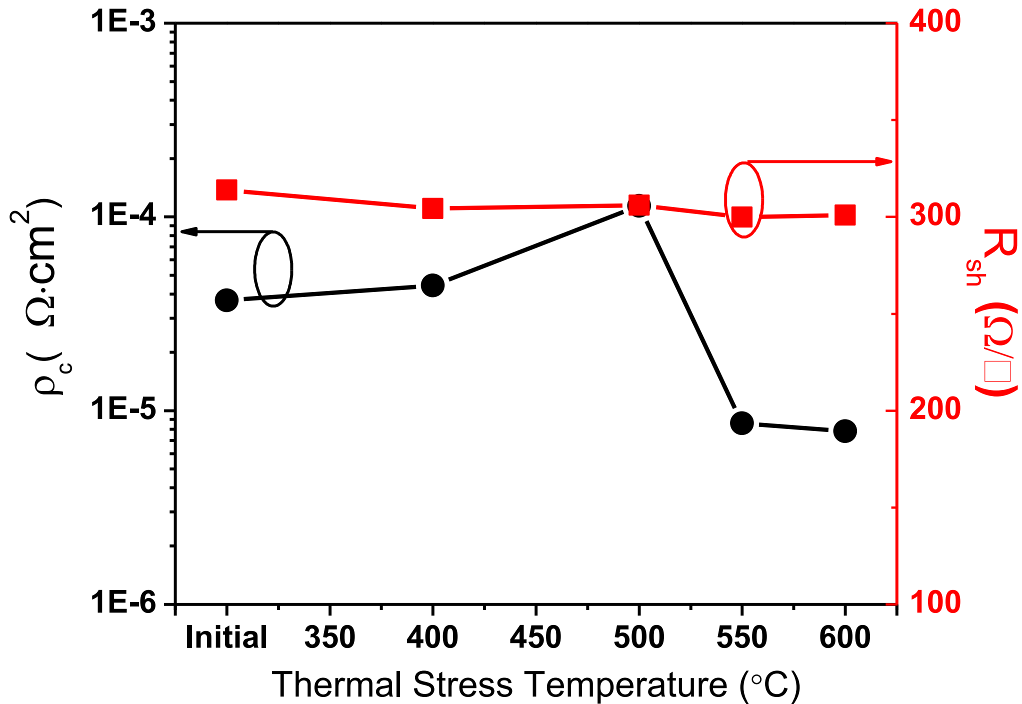

Fig. 22 The change of contact resistivity and sheet resistance of the alloyed Ti/Al/Mo/Au contacts after thermal stress at 400 °C, 500 °C, 550 °C, and 600 °C for 4 hours each with ambient air.

In summary, the Ti/Al/Ni/Au contacts as well as the Ti/Al/Mo/Au contacts showed very low contact resistivity and very good stability after the post-deposition RTA at 800 °C. High temperature stress, up to 600 °C, did not affect the sheet resistance of n-GaN. 500 °C thermal stress would increase the contact resistivity, but higher temperature (> 550 °C) stress tends to improve the contact resistivity.

To understand the underlying reason for the high temperature stability of the alloyed contacts, transmission electron microscope (TEM) was used to study the microstructure of the contacts interface. Fig. 23 shows the TEM images of the alloyed

Ti/Al/Ni/Au contacts to n-GaN. Clearly there is a thin layer between the GaN and the metal alloy, shown in Fig. 23 (a). This layer is identified as TiN because it has a cubic crystal structure and shows a lattice constant of 4.23 Å, shown in Fig. 23 (b), matching that of TiN. The layer of TiN was formed by the reaction between Ti and the N atoms from GaN lattice during the RTA at 800 °C. As mentioned in Chapter 2, the formation of TiN, creating a lot of N vacancies, is responsible for the low contact resistivity of the alloyed contacts. On the other hand, TiN is a hard, dense, refractory material with high electrical conductivity[62], [63]. It has a melting point of 2,930 °C and it won't oxidize until 800 °C[63]. The good corrosion and erosion resistance of TiN, and its relative inertness make it widely used as diffusion barriers in microelectronic devices. Therefore, the layer of TiN is the key for the stability of the alloyed contacts at high temperature, very stable itself and preventing further interfusion and reaction between metal and GaN.

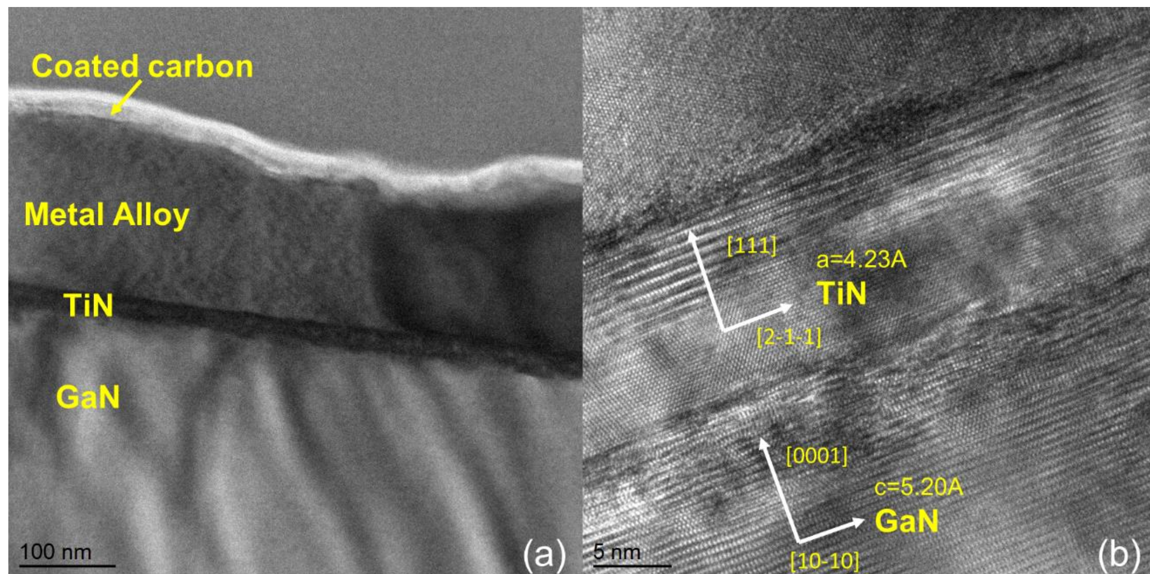

Fig. 23 Cross-section TEM images of the alloyed Ti/Al/Ni/Au contacts to n-GaN. (a) Low magnification image of the interface and (b) high resolution image of the interfacial TiN layer.

4.2 Non-Alloyed Al/Au Contacts

In the previous discussion, the alloyed Ti/Al/Ni/Au contacts showed very low contact resistivity, ρ_c ~6×10^{-6} Ω cm^2, and very good stability up to 600 °C in air. However, the contact surface is very rough, with root-mean-square (rms) roughness of 70 nm, probably due to the low melting point of Al, causing the lateral diffusion of Al and ball up. Also the alloyed contacts have several complex phases, e.g. Al-Au, Al-Ni, Ti-Al and TiN, which could also increase the surface roughness. Besides, the interface of metal and GaN is relatively rough, shown in Fig. 23(a), due to the reaction between metal and GaN during the 800 °C annealing. In addition, Fig. 23 (b) shows that there is a thin layer with thickness of 5nm-10nm "damaged" by the alloying, giving the possibility of metal diffusion or spiking into GaN surface. The diffusion of metal into GaN could kill some GaN devices in which the surface layer is very thin, only a few nanometers. Therefore, the non-alloy ohmic contacts is also necessary for GaN high temperature applications.

As discussed in Chapter 2, Al forms ohmic contact to n-GaN without annealing. Adding a cap layer of Au could help to prevent the oxidation of Al and increase the metal conductivity as well. The Al/Au bilayer contacts with thickness of 30nm and 300nm, respectively, were tested at room temperature. Fig. 24(a) shows the I-V curves measured on the TLM structures and Fig. 24(b) shows the plot of measured resistance versus TLM contact pad spacing. The extracted R_{sh} and ρ_c were 548 $\Omega/\square$ and 3×10^{-4} Ω cm^2, respectively. Although the contact resistivity is much higher than that of the alloyed contacts, it is low enough for the purpose of photovoltaic applications.

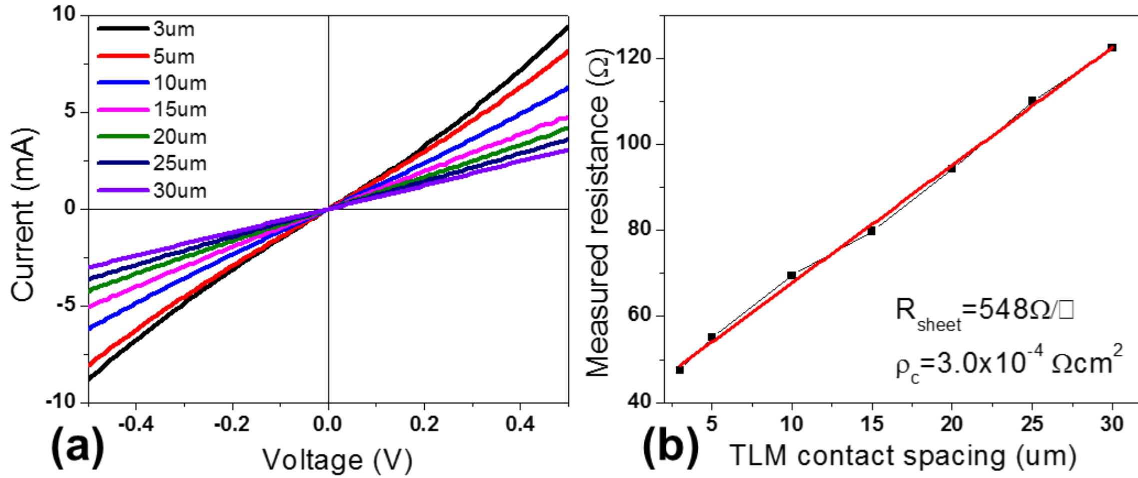

Fig. 24 Electrical characteristics of the as deposited Al/Au contacts to n-GaN measured at room temperature in air, (a) I-V curves measured between adjacent TLM pads with spacing increasing from 3um to 30um, and (b) plot of measured resistance versus TLM contact spacing.

To study the high temperature stability and limit of the Al/Au ohmic contacts, the contact sample was subjected to 400 °C, 500 °C, 550 °C, and 600 °C, sequentially, in the Minibrute furnace with air ambient for 4 hours at each temperature. The change of ρ_c and R_{sh} is shown in Fig. 25. R_{sh} increased from 548 Ω/□ to 600 Ω/□ after thermal stress at 400 °C for 4 hours, indicating possible reaction between the metal and n-GaN surface layer, but it did not increase further after higher temperature stress. ρ_c was reduced significantly by the 400 °C thermal stress, from 3×10^{-4} Ω cm^2 to 1.6×10^{-5} Ω cm^2. Higher temperature stress caused slight reduction in ρ_c. The R_{sh} and ρ_c measured after thermal stress at 600 °C for 4 hours are 601 Ω/□ and 5×10^{-6} Ω cm^2, respectively. Therefore, the non-alloyed Al/Au contacts also show very low contact resistivity and very good stability for 600 °C operation.

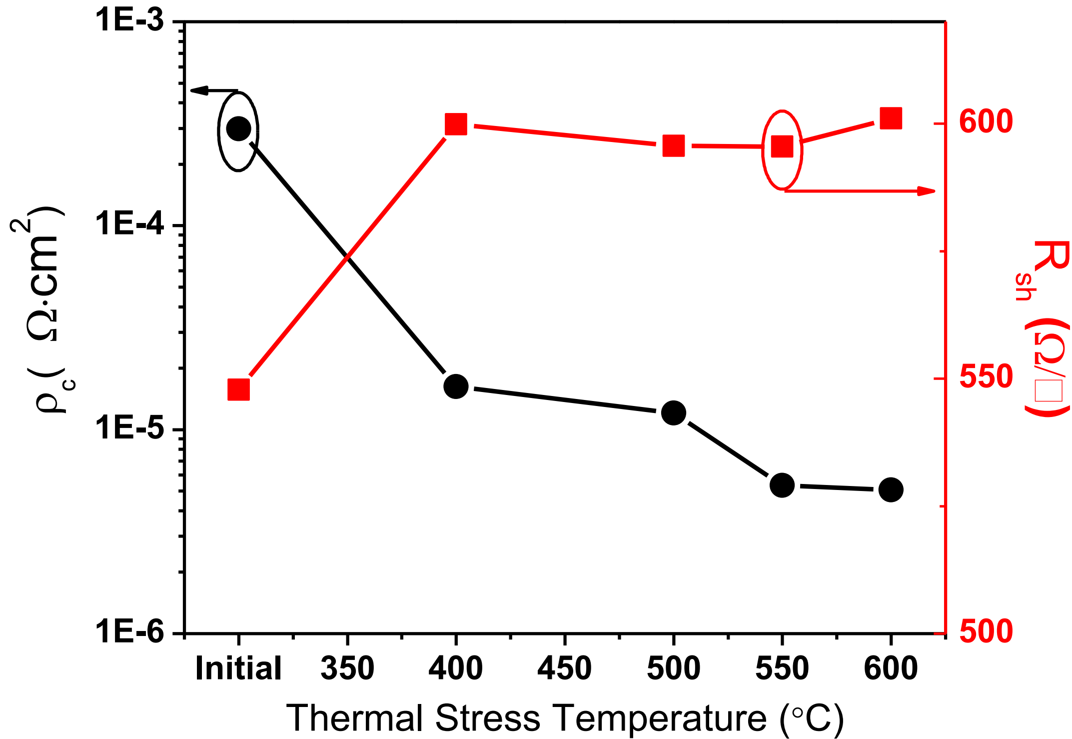

Fig. 25 The change of contact resistivity and sheet resistance of the Al/Au contacts after thermal stress at 400 °C, 500 °C, 550 °C, and 600 °C for 4 hours each with ambient air.

To understand the underlying mechanism of forming such contacts with low resistivity and high temperature stability, TEM study was conducted on the Al/Au sample after the 4 hour thermal stress at 600 °C in air. The cross-section view of metal-GaN interface is shown in Fig. 26. The TEM image indicates that there is a metal layer with thickness around 66nm on the interface and another layer with thickness around 237nm on top of that, while the as deposited thickness of Al and Au are 30nm and 300nm, respectively. Scanning transmission electron microscope (STEM) and *in situ* electron energy loss spectroscopy (EELS) were used to identify these two layers. Fig. 27 shows a high resolution STEM image of the metal-GaN interfacial area. A flat and sharp interface is observed, indicating that the reaction between metal and GaN and the diffusion of

metal into GaN are negligible. EELS scan was conducted across the 66nm interfacial layer, shown in Fig. 28(a). The EELS spectrum of N, O, Ga, Al, and Au are shown in Fig. 28(b), clearly indicating that the 66 nm interfacial metal layer consists of Al, O , and Au, while the top layer consists of only Au. This suggests that there was gold diffusion into the interface and oxygen reaction with aluminum during the thermal stress in air. It is interesting that inspite of the presence of oxygen with Au, which has high work function, the the interfacial layer complex allows the formation of low resistivity contacts to n-GaN. Further study of the Al-O-Au complex in forming ohmic contact is needed. However, it seems that this Al-O-Au complex reaches a saturation state, which is very stable at high temperature.

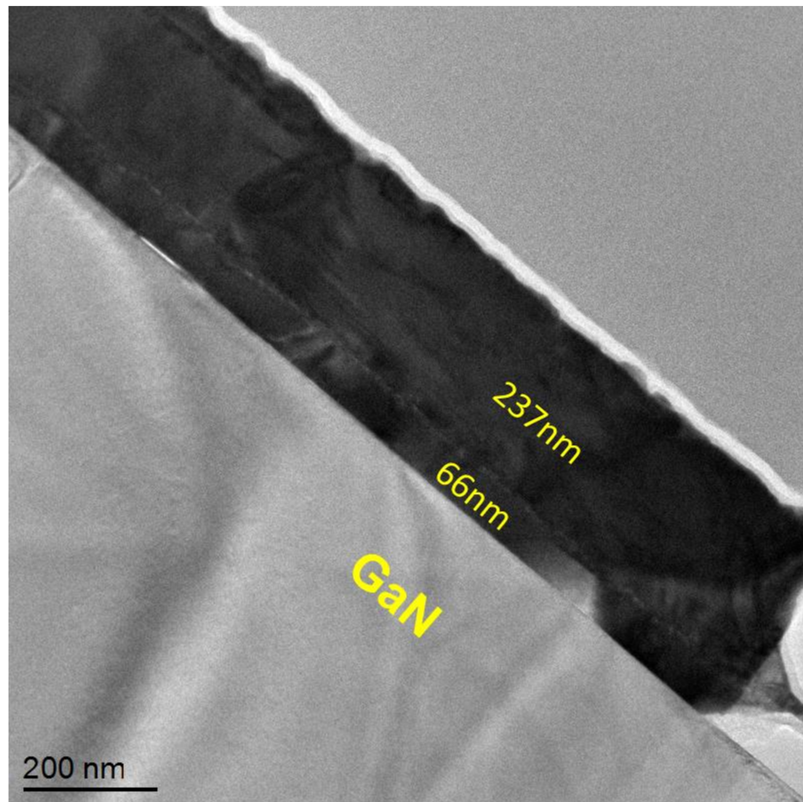

Fig. 26 Cross-section TEM image of the Al/Au contacts to n-GaN after thermal stress at 600 °C in air for 4 hours.

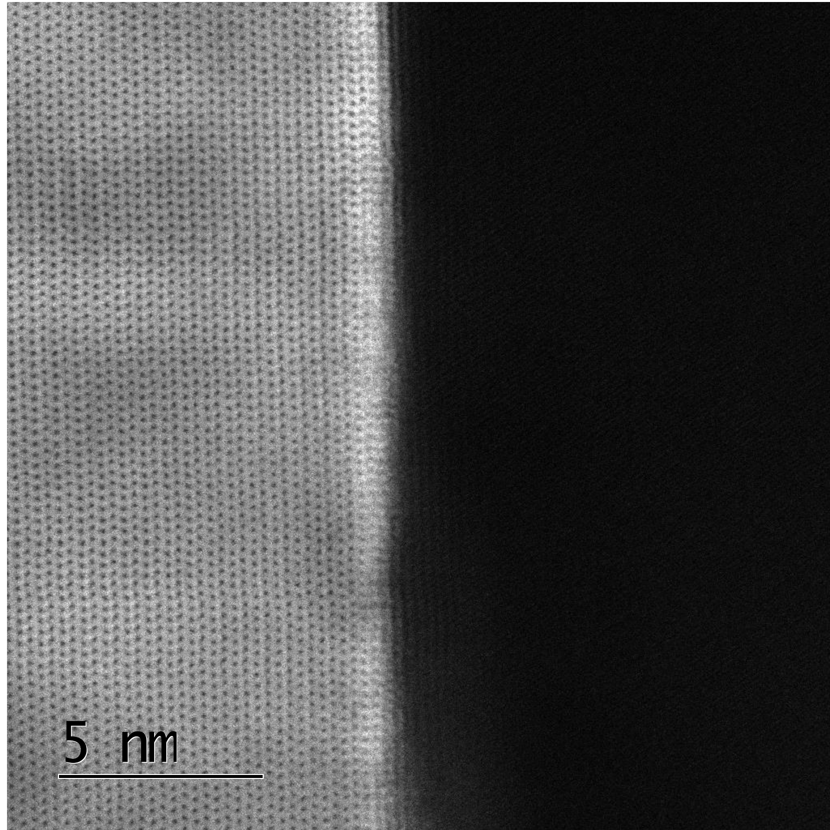

Fig. 27 STEM image of the interfacial area on the Al/Au to n-GaN contacts after thermal stress at 600 °C in air for 4 hours.

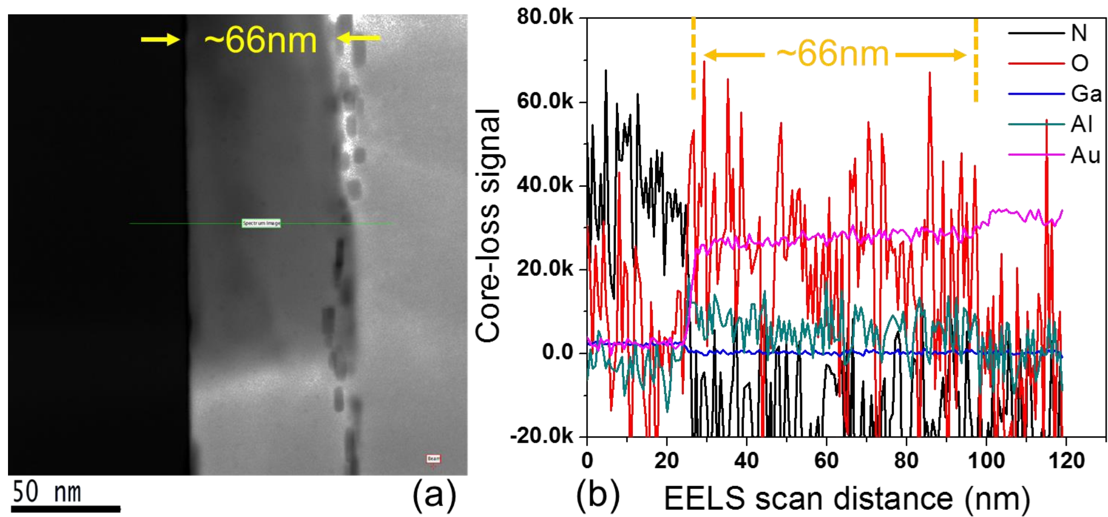

Fig. 28 (a) EELS scan trace, across the 66 nm interfacial layer and (b) EELS spectrum of N, O, Ga, Al, and Au on the Al/Au to n-GaN sample after thermal stress at 600 °C in air for 4 hours.

4.3 Summary

In this chapter, both alloyed and non-alloyed contacts to n-GaN were developed for high temperature applications. Both of them show low resistivity, ~10^{-6} Ω cm^2, and good stability up to 600 °C in air.

The alloyed Ti/Al/Ni/Au contact can be easily achieved, showing ρ_c ~ 6.8×10^{-6} Ω cm^2 at room temperature. Temperature dependent measurements, up to 400 °C, show that the contact resistivity is independent of the measurement temperature while the sheet resistance of n-GaN increased from 288 Ω/□ at room temperature to 370 Ω/□ at 400 °C, due to the decrease of electron mobility at high temperature. It must be mentioned that the change in the sheet resistance of n-GaN was reversible. After the contacts were cooled down to room temperature the contact resistivity restored its initial value. Stability of the contact was first tested by subjecting the sample to 450 °C for 8 hours. No degradation in contact resistivity and sheet resistance was observed after the thermal stress. The contact was tested further at higher temperature up to 600 °C. No change in sheet resistance of n-GaN was observed, and in fact the contact resistivity improved slightly after the contacts were subjected to 600 °C for 4 hours in air. The alloyed Ti/Al/Mo/Au contact showed similar properties to the alloyed Ti/Al/Ni/Au contact, but offered higher contact resistivity. TEM study of the contact microstructure indicates that the formation of TiN on the metal-GaN interface is responsible for the low resistivity and high stability contact.

The non-alloyed Al/Au contact offered a ρ_c ~ 3×10^{-4} Ω cm^2 before any high temperature testing was conducted. The contact resistivity decreased after thermal stress at 400 °C, 500 °C, 550 °C, and finally stabilized to 5×10^{-6} Ω cm^2, same as that of the

alloyed contact, after thermal stress at 600 °C for 4 hours in air. Instead of showing degradation, ρ_c was reduced by two orders of magnitude. TEM, STEM, and EELS studies showed the formation of Al-O-Au complex at the interface, caused by the thermal stress in air. The interfacial Al-O-Au played an important role in reducing the contact resistivity and maintaining good stability at temperatures up to 600 °C in air.

Chapter 5

DEVELOPING OHMIC CONTACTS TO P-GAN FOR HT APPLICATIONS

5.1 Annealed Ni/Au Contacts to p-GaN

5.1.1 Electrical Characterization

The most commonly used metallization structure for p-GaN ohmic contacts has been the Ni/Au stack. In fact, such metallization scheme was used even in the early generations of GaN blue LEDs as early as 1993[64].

After the deposition and lift-off of the Ni/Au layers of thickness 20 nm/200 nm, the samples were subjected to a rapid thermal annealing (RTA) process at 500 °C, 550 °C, and 600 °C in a N_2 ambient for various time intervals. The current-voltage (*I*-*V*) characteristics of the annealed contacts were measured using a four point probe station equipped with a Keithley 4200-SCS parameter analyzer. Fig. 29 shows the extracted contact resistivity as a function of RTA time at 500 °C, 550 °C, and 600 °C, respectively. The contacts formed by RTA at 600 °C for 3 minutes showed the lowest specific contact resistivity ρ_c, 1.6×10^{-3} Ω•cm^2, with a sheet resistance R_{sh} of 1.3×10^5 $\Omega/\square$. ρ_c and R_{sh} were extracted from the linear plot of measured resistance ($R_{measured}$) versus contact pad spacing, shown in Fig. 30, according to the TLM model. The linear *I*-*V* curves of this optimized contacts are shown in the graph inset of Fig. 30, depicting very good ohmic behavior at room temperature (25 °C). This optimized Ni/Au contact were then subjected to the study for high temperature applications.

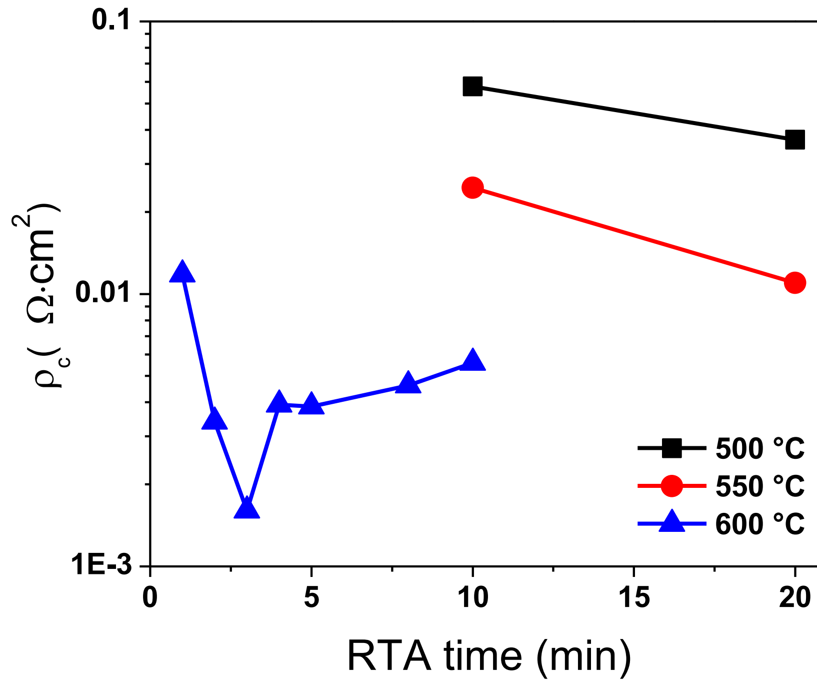

Fig. 29 Extracted contact resistivity as a function of rapid thermal annealing time at 500 °C, 550 °C, and 600 °C, respectively.

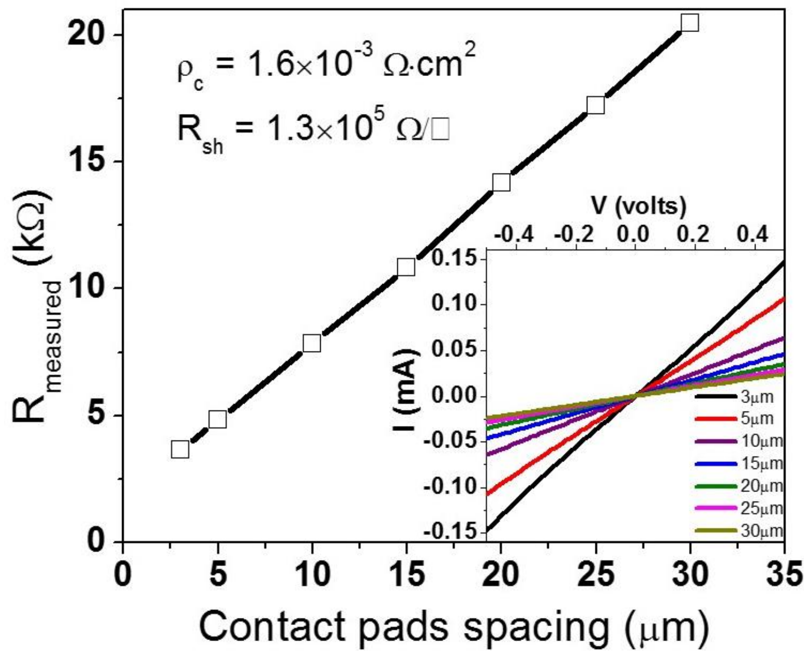

Fig. 30 Measured resistance versus TLM pad spacing after the Ni/Au to p-GaN contacts were annealed at 600 °C in N_2 for 3 min. The inset picture shows the I-V curves measured between adjacent contact pads with various spacing.

A. Dependence of ρ_c and R_{sh} on temperatures up to 390 °C

The temperature dependence of the specific contact resistivity and sheet resistance were studied in the range of 25-390 °C, varying the temperature of the probe station chuck by using an Instec mK2000 temperature controller. Fig. 31 shows the *I-V* characteristics of the contacts, measured at various temperatures between 25 °C and 390 °C, taken between two adjacent TLM pads with gap spacing 5 um. The contacts remain ohmic at all temperatures from 25 °C to 390 °C with the current increasing with the increasing temperature. The current at 390 °C was 10 times higher than that at 25 °C. The ρ_c and R_{sh} values of the contacts, extracted from the TLM measurements, as a function of the measurement temperature are shown in Fig. 32 (a) and (b), respectively. Both specific contact resistivity and sheet resistance decreased with increasing measurement temperature. ρ_c decreased by a factor of 10, i.e., from 1.6×10^{-3} Ω•cm^2 at 25 °C to 1.6×10^{-4} Ω•cm^2 at 390 °C. R_{sh} decreased by a factor of 11, i.e., from 1.3×10^5 Ω/□ at 25 °C to 1.2×10^4 Ω/□ at 390 °C. The reduction in ρ_c and R_{sh} was due to the increased hole concentration at high temperature, as expected [65], leading to 10 times increase in the current. Therefore, although ohmic contacts to p-GaN is difficult to achieve at RT, the Ni/Au to p-GaN contacts shows superior ohmic behavior at elevated temperatures.

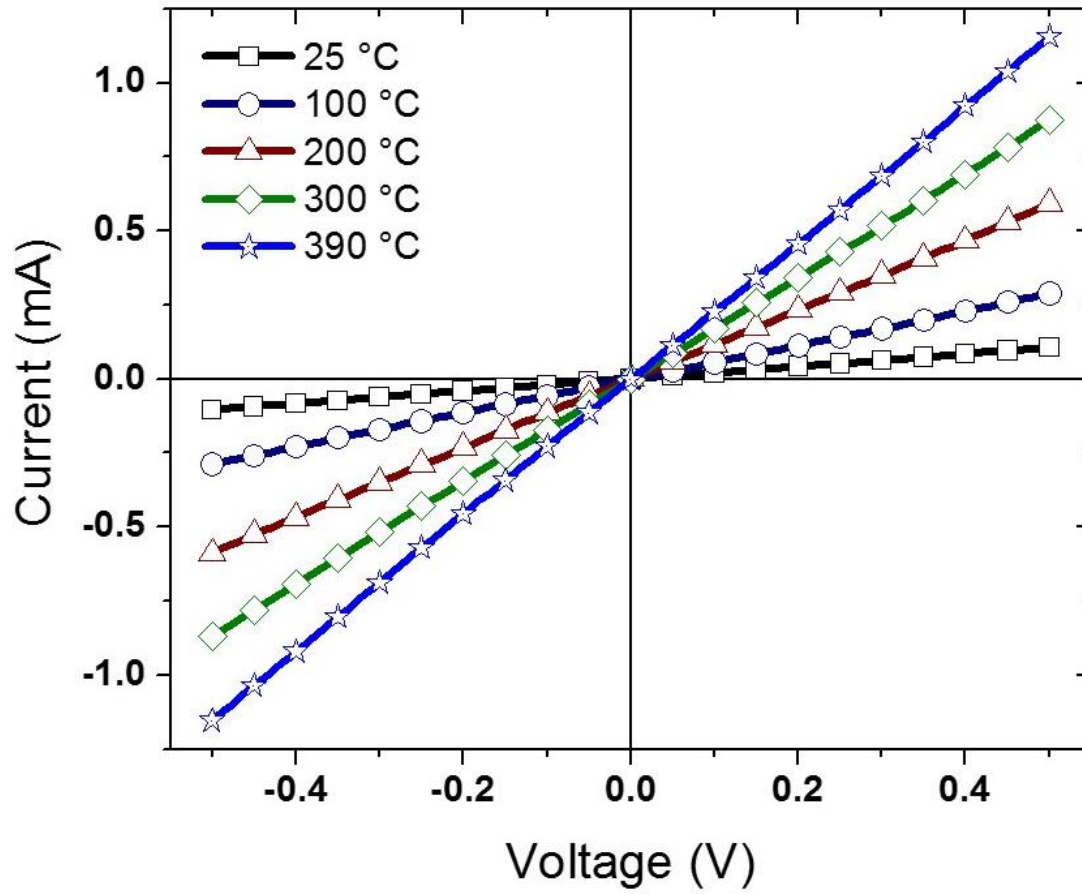

Fig. 31 Temperature dependent I-V characteristics of the annealed Ni/Au to p-GaN contacts, taken between two adjacent pads with gap spacing 5um.

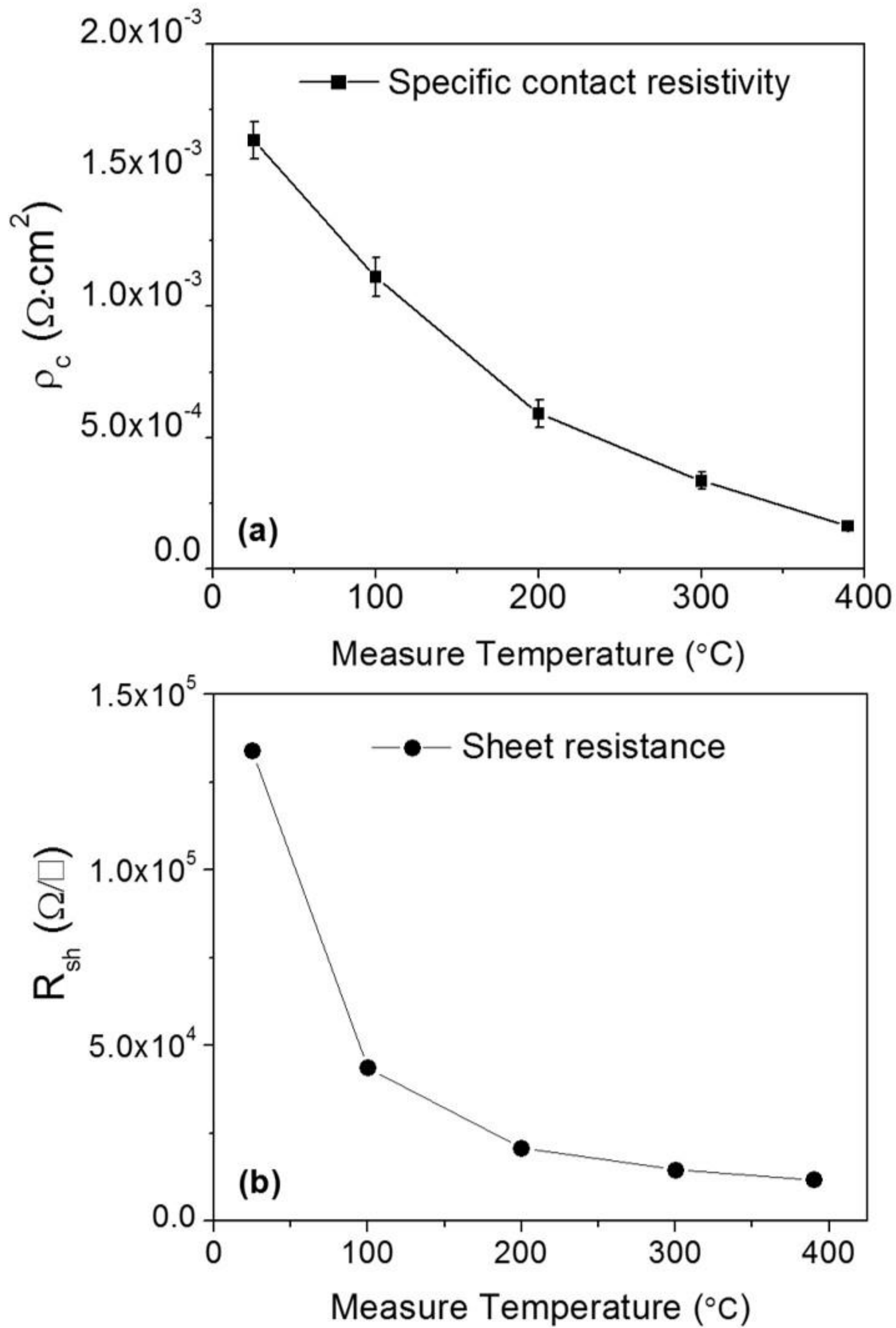

Fig. 32 Temperature dependent specific contact resistivity ρc, (a), and sheet resistance Rsh, (b) of the annealed Ni/Au to p-GaN contacts.

B. Stability of the contacts at 450 °C in air

The thermal stability of the annealed Ni/Au to *p*-GaN contacts was tested on several samples with the optimized annealing condition, showing an average initial ρ_c of 2.2×10^{-3} $\Omega\cdot cm^2$. The samples were placed in a Minibrute furnace at 450 °C with ambient air for a maximum time of 48 hours. During this 48 hours of test the samples were taken out of the furnace and the *I-V* characteristics were measured at room temperature at regular intervals. Fig. 33 shows the plot of measured resistance versus contact pad spacing after the sample was subjected to 450 °C in the ambient of air for 48 hours. The *I-V* curves obtained after 48 hours of high temperature thermal stress, as shown in the inset of Fig. 33, validate that the contacts maintained very good ohmic behavior. The ρ_c and R_{sh} extracted from Fig. 33 are 1.4×10^{-3} $\Omega\cdot cm^2$ and 1.32×10^5 Ω/□, respectively. The reduction in ρ_c and R_{sh}, compared with those before the high temperature stress, are approximately -36% and 6%. While the change of R_{sh} was negligible while the improvement in the ρ_c was possibly a result of further annealing of the contacts, leaving some room for typical errors incurred in the TLM method [66].

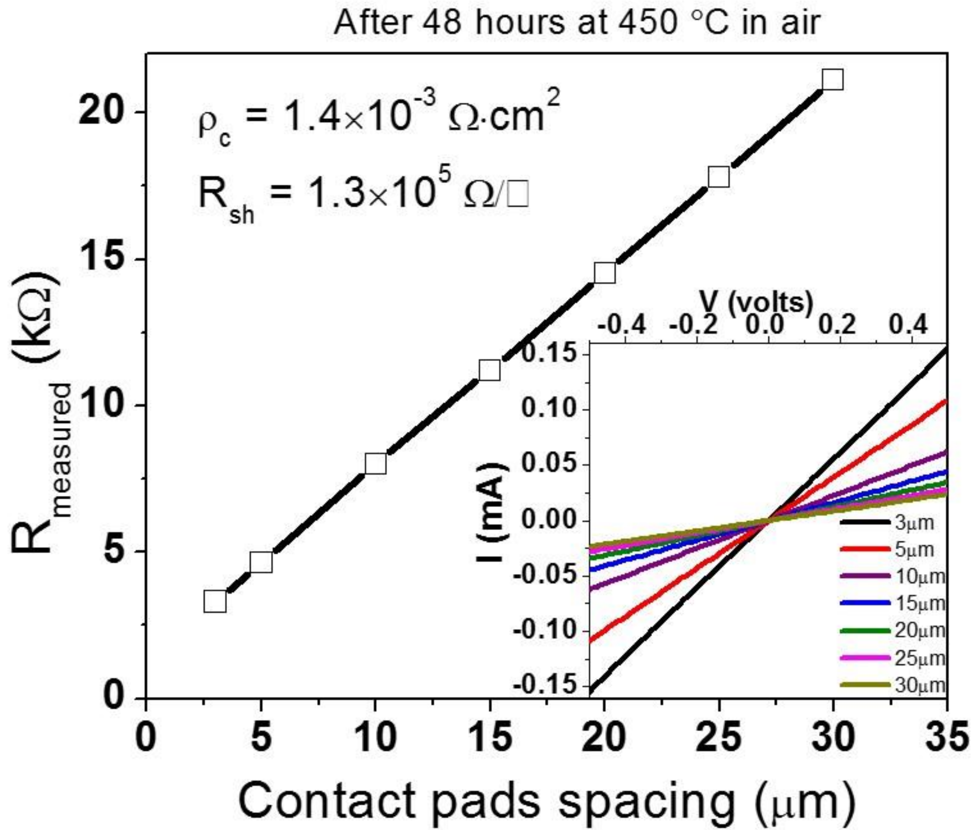

Fig. 33 Measured resistance versus TLM pad spacing after the annealed Ni/Au contacts samples were subjected to 450 °C in air for 48 h. The inset picture shows the I-V curves measured between contact pads with various spacing from 3um to 30 um.

Fig. 34 (a) shows the time evolution of the specific contact resistivity measured and averaged over at least four samples after thermal stress at 450 °C in air for up to 48 hours. A significant increase and then decrease in ρ_c was observed during the initial 10-hour "burn-in" period[41]. After the first 10 hours, the ρ_c decreased slowly and stabilized at ~2×10^{-3} $\Omega\cdot cm^2$. No degradation was observed thereby demonstrating excellent thermal stability of these contacts at 450 °C in air. Fig. 34 (b) shows the time evolution of the sheet resistance during the 48-hour thermal stress at 450 °C in air, obtained from the same TLM readings. The change in R_{sh} is negligible, as expected, because the both

metals, Ni and Au, don’t react with GaN and 450 °C is far below the dissociation temperature limit of GaN[2], [67]. The measurements were repeated for multiple TLM structures across the samples and the results were consistent, showing excellent stability of our contact process.

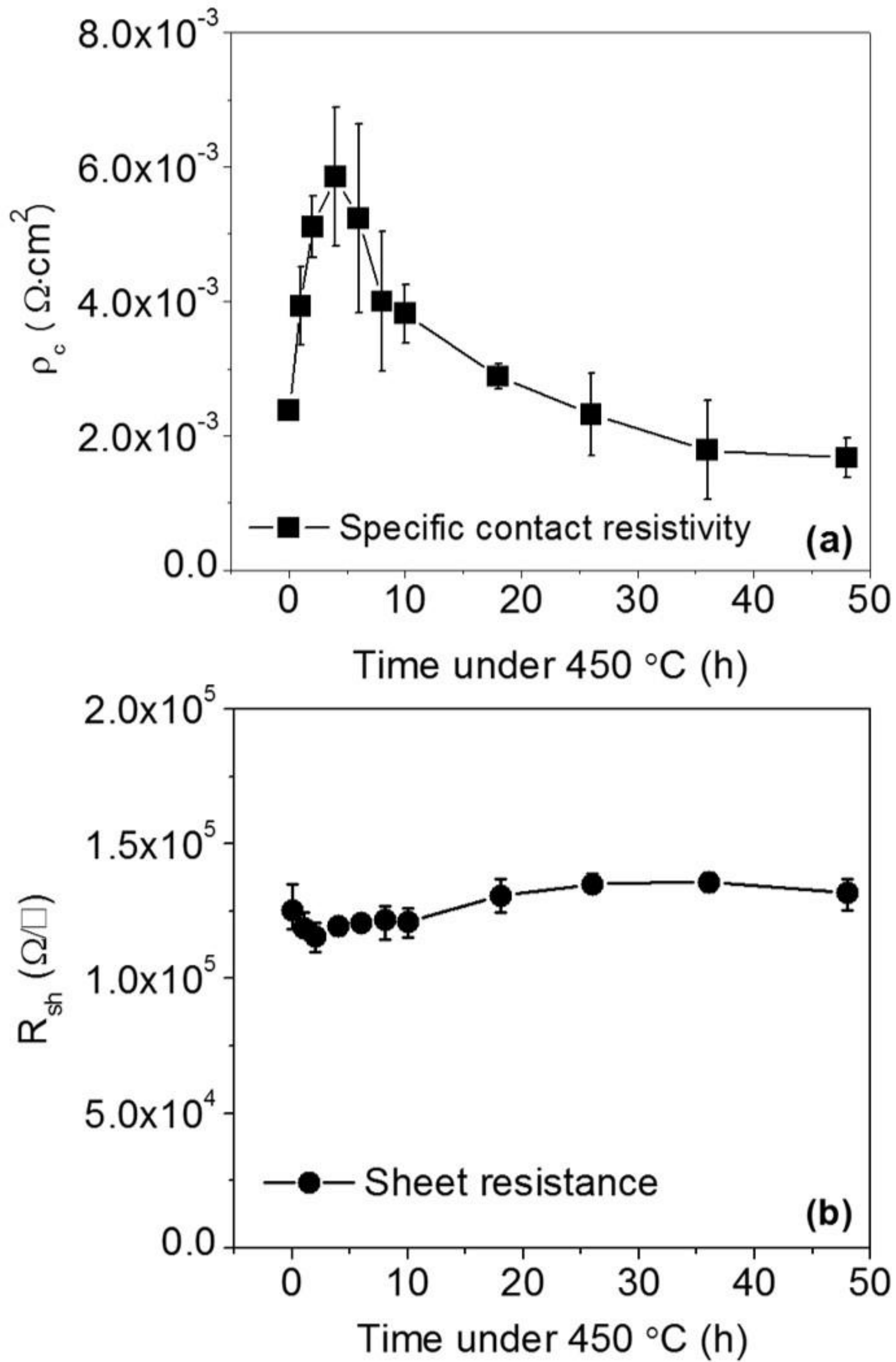

Fig. 34 Time evolution of the specific contact resistivity ρ_c, (a), and sheet resistance R_{sh}, (b), of the annealed Ni/Au contacts over the 48-hour thermal stability test at 450 °C in air.

C. Contacts degradation above 450 °C

To identify the high temperature limit of the contacts, the test sample was sequentially subjected to thermal stress at 500, 550, 600, 650, and 700 °C for 4 hours each in the Minibrute furnace with ambient air. *I-V* characteristics were measured at room temperature after each thermal stress and the specific contact resistivity was extracted. Fig. 35 (a) shows the *I-V* characteristics of the contacts between two adjacent TLM pads with a spacing of 5 μm, at room temperature and then before and after each thermal stress cycle at temperatures up to 650 °C. The *I-V* curves remain linear even after thermal stress at 650 °C for 4 hours, but the current is significantly reduced as the temperature increases to 650 °C. Fig. 35 (b) shows the evolution of the specific contact resistivity caused by the thermal stress at temperatures above 450 °C. ρ_c increases by 69% after 4 hours of thermal stress at 500 °C, further increasing by 400% after 4 hours of thermal stress at 550 °C, by 180% after 4 hours of thermal stress at 600 °C, and by 152% after 4 hours of thermal stress at 650 °C. The sheet resistance of p-GaN also increased significantly especially after thermal stress at 600 °C and 650 °C, shown in Fig. 36, indicating that the hole concentration at the surface was reduced probably caused by high temperature thermal stress. The reduction in the surface hole concentration is responsible for the degradation in contact resistivity. The contacts showed rectifying *I-V* curves after being subjected to 700 °C in air for 4 hours and the current was reduced by three orders of magnitude compared to the initial value, shown in Fig. 37.

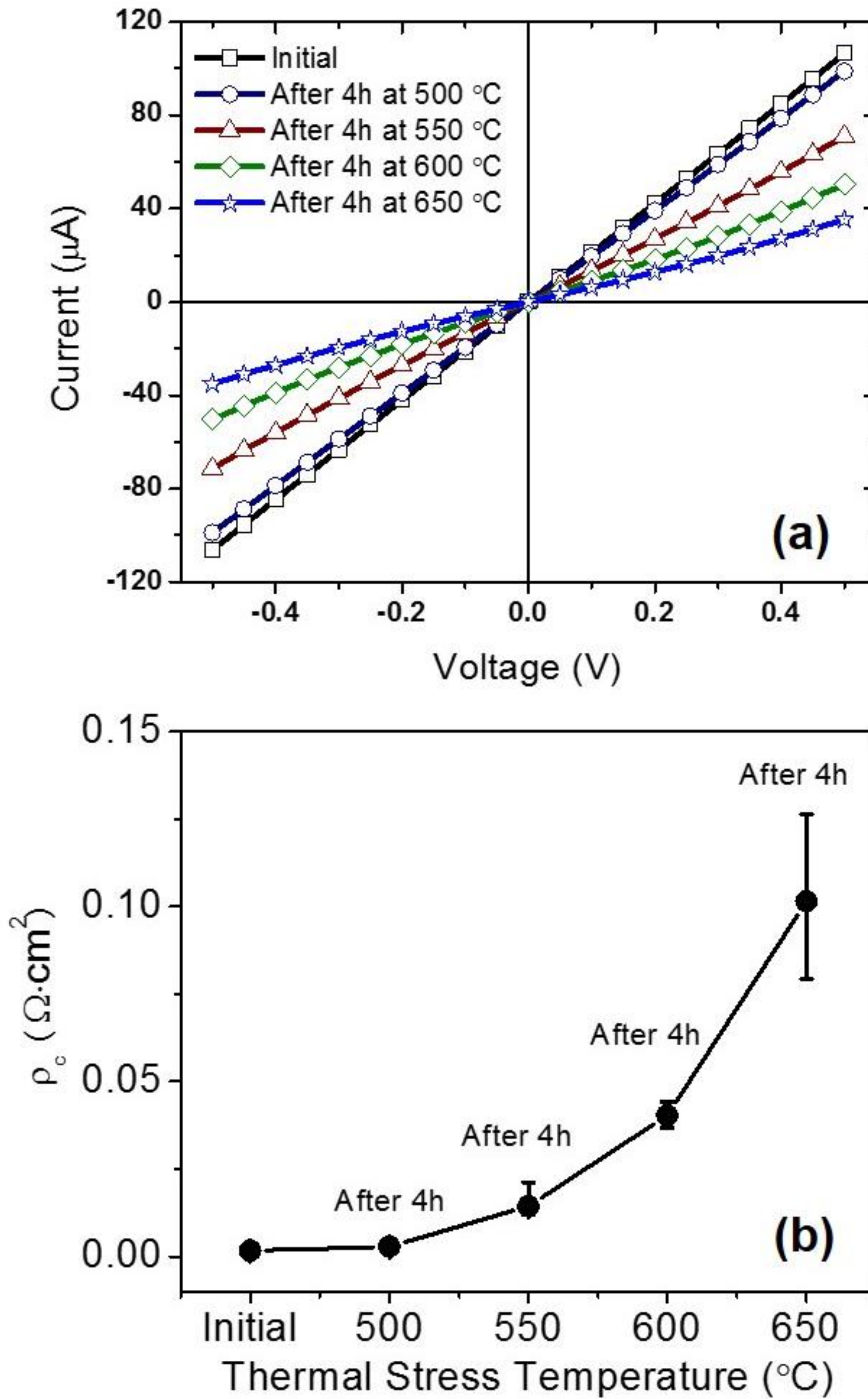

Fig. 35 (a) I-V characteristics measured at room temperature and taken between two adjacent TLM pads with gap spacing 5 um and (b) the extracted ρ_c of the Ni/Au contacts after being subjected to thermal stress at 500 °C, 550 °C, 600 °C, and 650 °C in series in air.

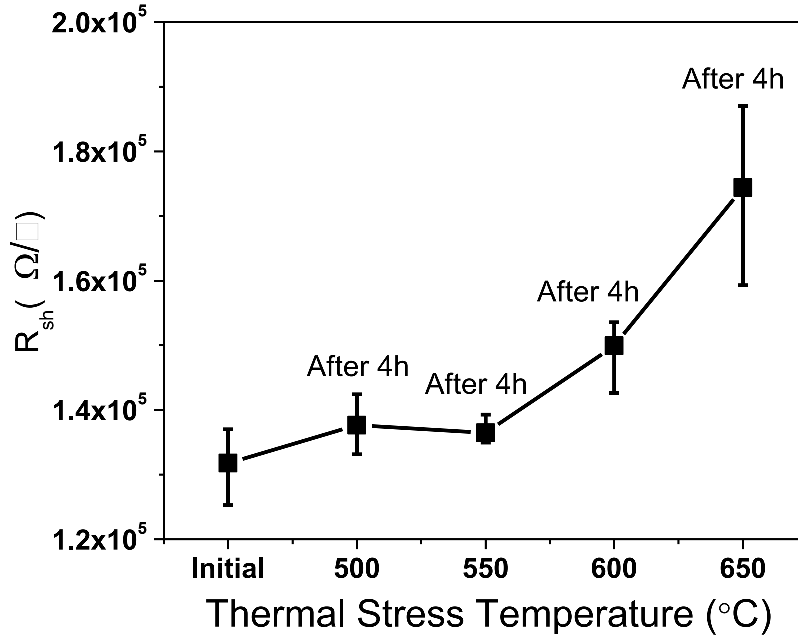

Fig. 36 The extracted R_{sh} of the Ni/Au contacts after being subjected to thermal stress at 500 °C, 550 °C, 600 °C, and 650 °C in series in air.

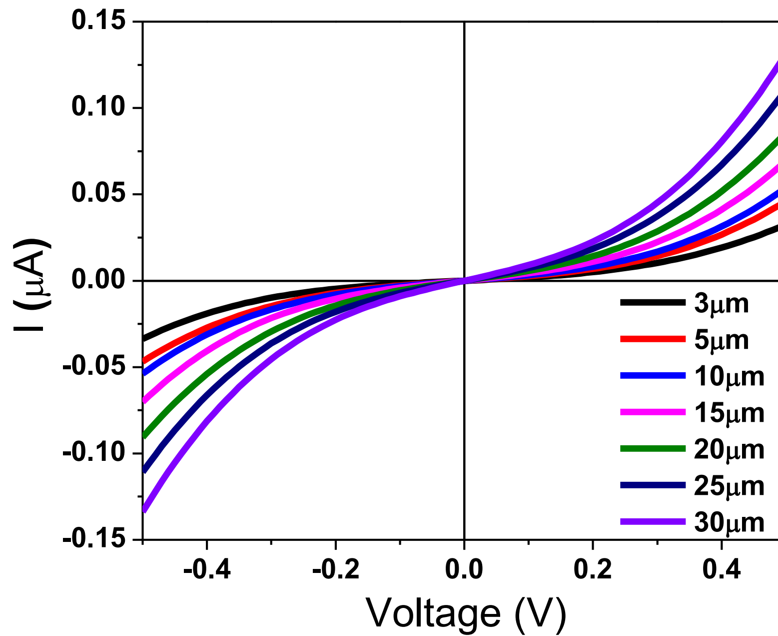

Fig. 37 I-V characteristics of the Ni/Au contacts measured at room temperature after being subjected to 700 °C for 4 hours in air.

5.1.2 Microstructure Characterization

In order to understand the root cause for the good stability of the annealed Ni/Au contacts at high temperatures up to 450 °C in air, we performed transmission electron microscopy (TEM) study on the contact interface. The first set of TEM was conducted after the sample was annealed, but before any further thermal stress.

The cross-section image of the annealed contacts is shown in Fig. 38. Clearly it has three layers and two interfaces, marked as interface 1 and interface 2. The high-resolution TEM images of interface 1 and interface 2 are shown in Fig. 39 and Fig. 40, respectively. The three layers are identified as NiO, Au, and GaN by the lattice parameters measured from the high-resolution TEM images, shown in Fig. 39 and Fig. 40. The TEM study provides direct evidence of the layer reversal between the as deposited Ni and Au. Au diffuses into the metal-GaN interface while Ni diffuses out to the surface of Au and reacts with air to form NiO during the post-deposition annealing. In addition, Fig. 40 shows very flat and sharp interface between Au layer and GaN layer, with Au lattice grown epitaxially on GaN lattice. The epitaxial structure of Au-GaN interface is believed to play an important role in forming good ohmic contacts to p-GaN. Early reports show that direct deposition of Au on p-GaN surface does not result in low-resistance ohmic contacts [68], [25]. It must be mentioned here that the deposition of Au, as a noble metal, will start with nucleation of gold particles, followed by lateral cluster growth, then coarsening, and finally a continuous layer [69]. Therefore, the Au layer would be polycrystalline or non-crystalline, and it won’t form epitaxial structure with GaN. However, in the Ni/Au contacts system, a wetting layer of Ni is used to remove the surface oxide by reacting with O and diffusing out to the surface of Au while Au diffuses

into the metal-GaN interface and form intimate epitaxial structure with GaN lattice. The epitaxial structure of Au on p-GaN is also responsible for the high temperature stability of the contacts because Au doesn't react with GaN and Au doesn't diffuse into GaN unless the temperature is very high.

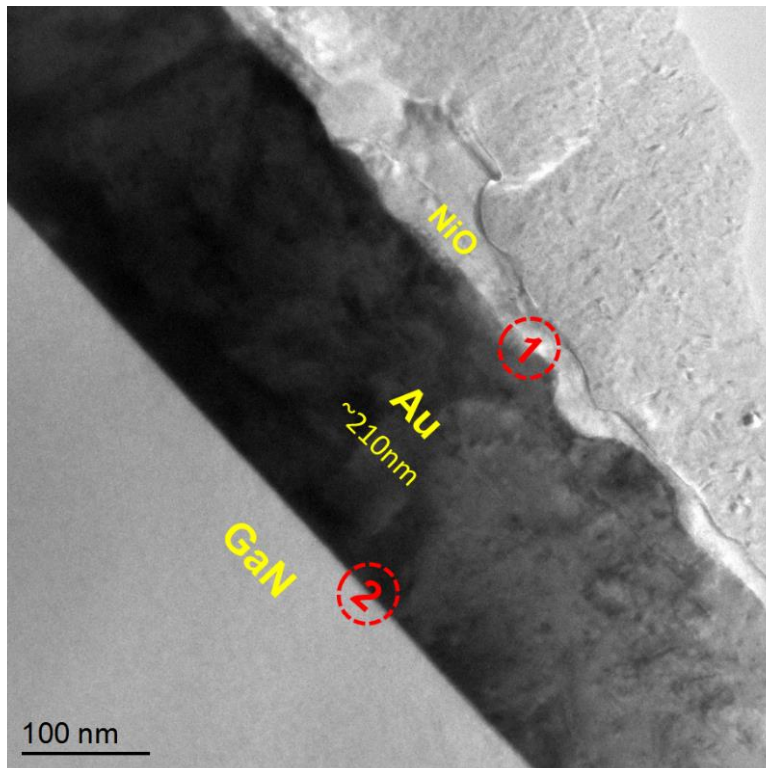

Fig. 38 Cross-section TEM image of the Ni/Au contacts after post-deposition annealing, showing three layers with two interfaces.

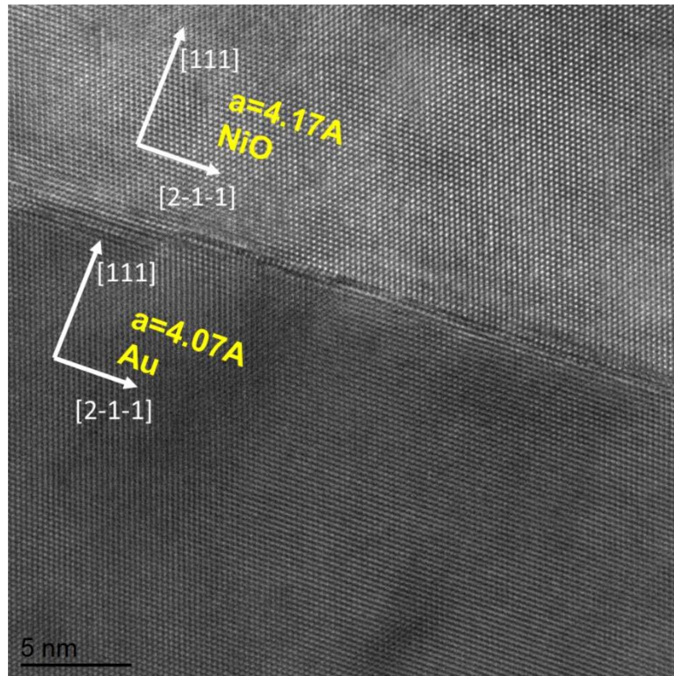

Fig. 39 High-resolution TEM image of the top interface, marked as interface 1, of the annealed Ni/Au contacts.

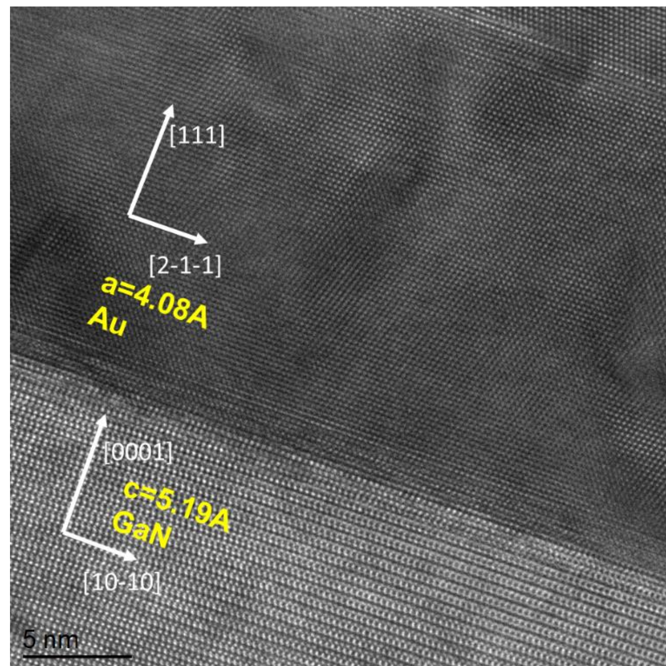

Fig. 40 High-resolution TEM image of the metal-GaN interface, marked as interface 2, of the annealed Ni/Au contacts.

The samples with the TLM test structures were subjected to thermal stress at 700 °C for 4 hours in air, showing rectifying I-V characteristics, was also prepared for TEM analysis to investigate the degradation mechanism.

The cross-section TEM image of the degraded contacts is shown in Fig. 41. Both the metal-GaN interface and GaN surface are very rough with a new layer formed between GaN and metal, indicating strong reaction on the interface during the thermal stress at 700 °C in air. The high resolution TEM image for the interfacial area is shown in Fig. 42. Au and GaN are identified by the lattice parameters and the interfacial layer shows similar lattice parameter to GaN, implying the formation of Gallium oxide. The insulating gallium oxide layer can be produced by thermal oxidation of Gallium-polar GaN at high temperature [70]–[73]. Therefore, the formation of Gallium oxide on the contacts interface is believed to be the root cause for the degradation in contact resistivity.

The study of the degradation mechanism provided us with evidences of oxidation. Extension of the lifetime or increase of the operating temperature limit should be possible by encapsulation of the GaN surface with SiN with appropriate wire bonding techniques, so that there is no path for the oxygen to react with GaN.

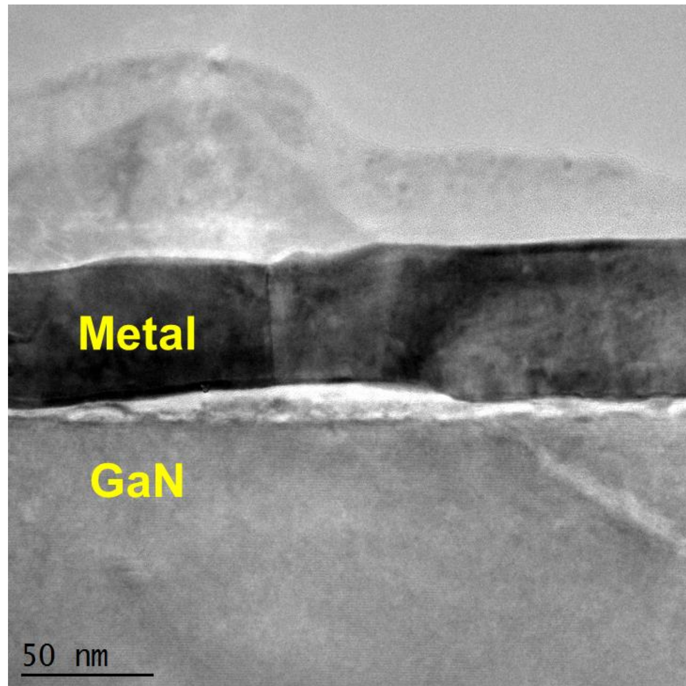

Fig. 41 Cross-section TEM image of the Ni/Au contacts after thermal stress at 700 °C for 4 hours in air.

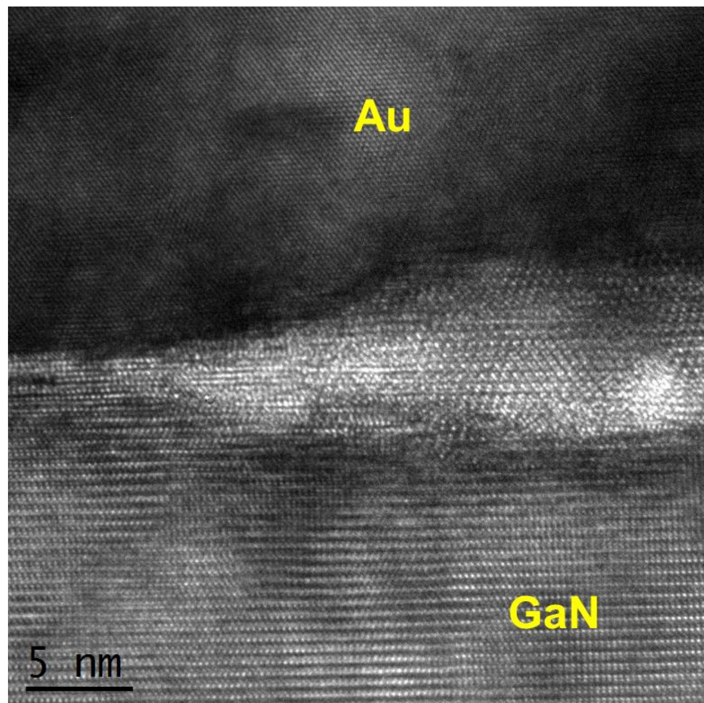

Fig. 42 High-resolution TEM image of the interfacial area on the Ni/Au contacts after thermal stress at 700 °C for 4 hours in air.

5.2 Indium Tin Oxide Contacts to p-GaN

Previous section shows that the annealed Ni/Au to p-GaN contact is very stable at temperatures up to 450 °C in air and the contact resistivity increases only slightly after 4 hours at 500 °C. However, the low transmittance associated with this metal contact, with total thickness of 220 nm, acts as a bottleneck when applied to optoelectronics, e.g. LED and solar cell. Although the transmittance can be increased by using very thin metal layer, it leads to large series resistance effects that in turn cause lower efficiency, increased device temperature, non-uniform light emission, and so on. Transparent and conducting contacts can be used to combat this problem. Indium tin oxide (ITO) has been widely used as the transparent conductive electrodes in organic and inorganic optoelectronic devices because of its high optical transmittance in the visible wavelength and good electrical conductivity [74]–[76]. In commercial GaN-base LEDs and solar cells, ITO is deposited on p-GaN is used as the transparent conductive electrodes to spread the current more uniformly, and many studies on the ITO ohmic contacts to p-GaN have been reported [77]–[80].

In addition to the contact resistivity between ITO and p-GaN, the film resistivity of ITO is another factor affecting the series resistance of InGaN solar cell, because ITO is a semiconductor with typical resistivity two orders of magnitude higher than that of metal, so the film resistivity is not negligible. The conductivity of ITO is attributed to oxygen vacancies in the film, substantial tin donor dopants, and film crystallinity [81]–[83]. Therefore, the resistivity is highly dependent to the growth condition, annealing temperature, and oxygen pressure. In the high temperature solar cell, the resistivity of ITO film could be affected by the operating temperature and ambient.

The ITO contact used for high temperature InGaN solar cell was prepared by the company of Photonitride Devices Inc. The ITO film with thickness of 150 nm was deposited in vacuum by e-beam evaporation using a source composed of 90 wt% In_2O_3 and 10 wt% SnO_2. Since the as-deposited ITO film is not transparent due to oxygen deficiency, annealing at 500 °C in air for 1 hour is needed to turn the opaque film into a transparent film. Two TLM structures, A and B shown in Fig. 43 (a) and (b), respectively, were made to test the contact resistivity and film resistivity. Measurements on TLM A gave the contact resistivity of ITO to p-GaN contact while measurements on TLM B gave the sheet resistance of ITO layer.

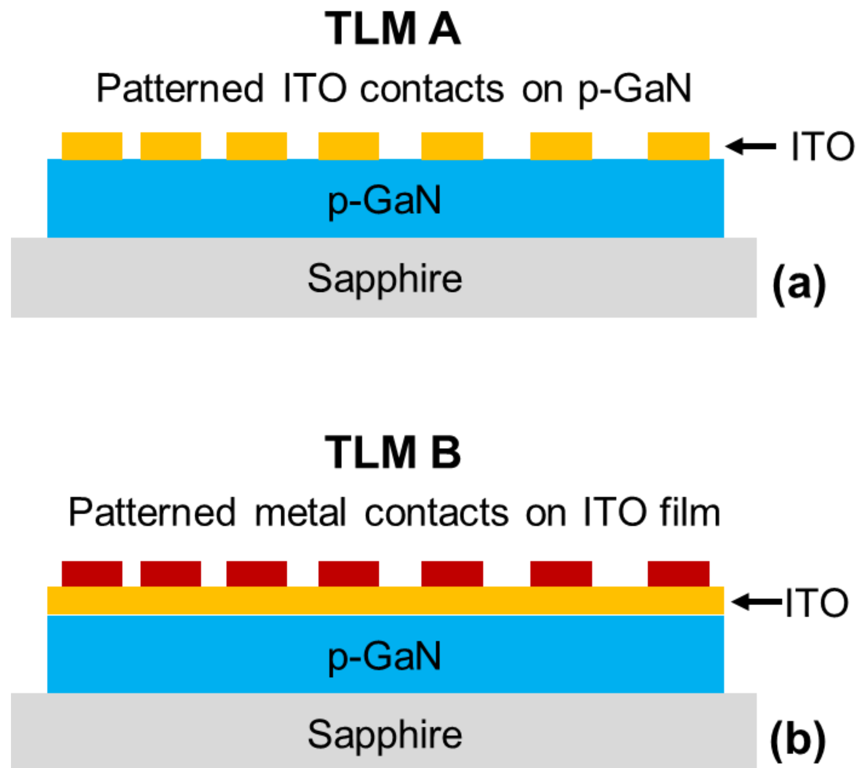

Fig. 43 Two TLM structures to test the contact resistivity of ITO to p-GaN, (a), and the sheet resistance of ITO film, (b), respectively.

Fig. 44 (a) shows the I-V characteristics of the ITO to p-GaN contact after post-deposition annealing at 500 °C in air for 1h, measured on TLM A, depicting good ohmic behavior of the contact. The plot of measured resistances versus TLM contact spacing, shown in Fig. 44 (b), gives ρ_c of 9.4×10^{-3} Ω·cm². The sheet resistance of ITO film, extracted from measurements on TLM B, is 27.8 Ω/☐. The converted resistivity of ITO is 4.2×10^{-4} Ω·cm, showing very good conductivity.

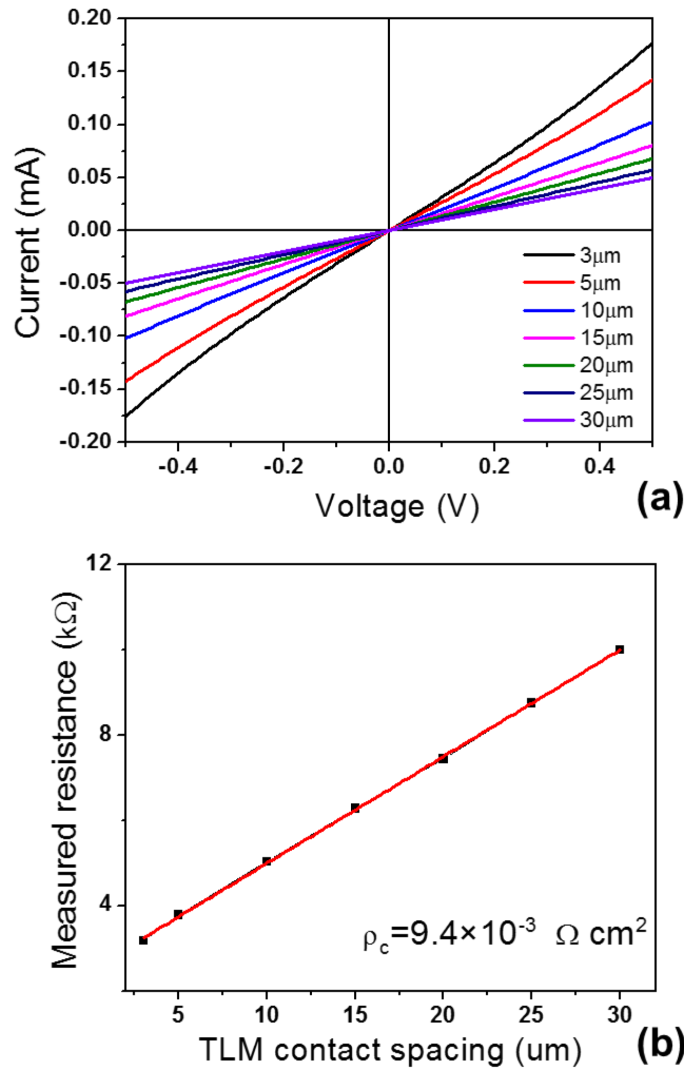

Fig. 44 (a) I-V characteristics of the ITO to p-GaN contact after post-deposition annealing at 500 °C in air for 1h, measured on TLM A, and (b) plot of measured resistance versus TLM contact spacing.

The high temperature stress tests were performed in a N_2 ambient first, because the high temperature solar cell was preferred to operating in a non-oxidizing ambient. The annealed samples were subjected to the Mini-brute furnace at temperatures up to 450 °C with N_2 flow, which was not a pure N2 ambient.

Fig. 45 (a) shows the I-V characteristics measured on TLM A of the ITO to p-GaN contact after thermal stress at 450 °C in N_2 for 8h,. The currents were significantly reduced compared with those before the thermal stress, indicating the degradation of the contacts. The plot of measured resistance versus TLM contact spacing, shown in Fig. 45 (b), gives ρ_c of $2.7\times10^{-2}\ \Omega\cdot cm^2$. The sheet resistance of ITO film, extracted from measurements on TLM B, is 11.5 Ω/□, much lower than that before the thermal stress at 450 °C in N_2. The reduction in the sheet resistance is possibly due to the out-diffusion of oxygen in the ITO film during the thermal stress in N_2 ambient, which would increase the carrier concentration by introducing more oxygen vacancies, and thus the ITO film becomes more conductive. The out-diffusion of oxygen is most likely the cause for the shift of ITO work function. ITO was reported to have work functions between 4.8 and 5 eV, which can be controlled by altering the chemical composition[84]. The work function of ITO decreases as the carrier concentration increases[85], [86]. Out-diffusion of oxygen will reduce the work function of ITO, while absorption of oxygen will increase the work function. The decrease in the work function of ITO, caused by the thermal stress in N_2 ambient, is believed to be responsible for the contact degradation. To take a close look at this phenomenon, thermal stress test at lower temperatures in N_2 were performed. No degradation was observed after a 8h thermal stress at 300 °C in N_2, however, ρ_c increased

by 25% when the thermal stress was conducted at 350 °C in N_2 for 8h. Therefore, the out-diffusion of oxygen happens at temperature around 350 °C in non-oxygen ambient.

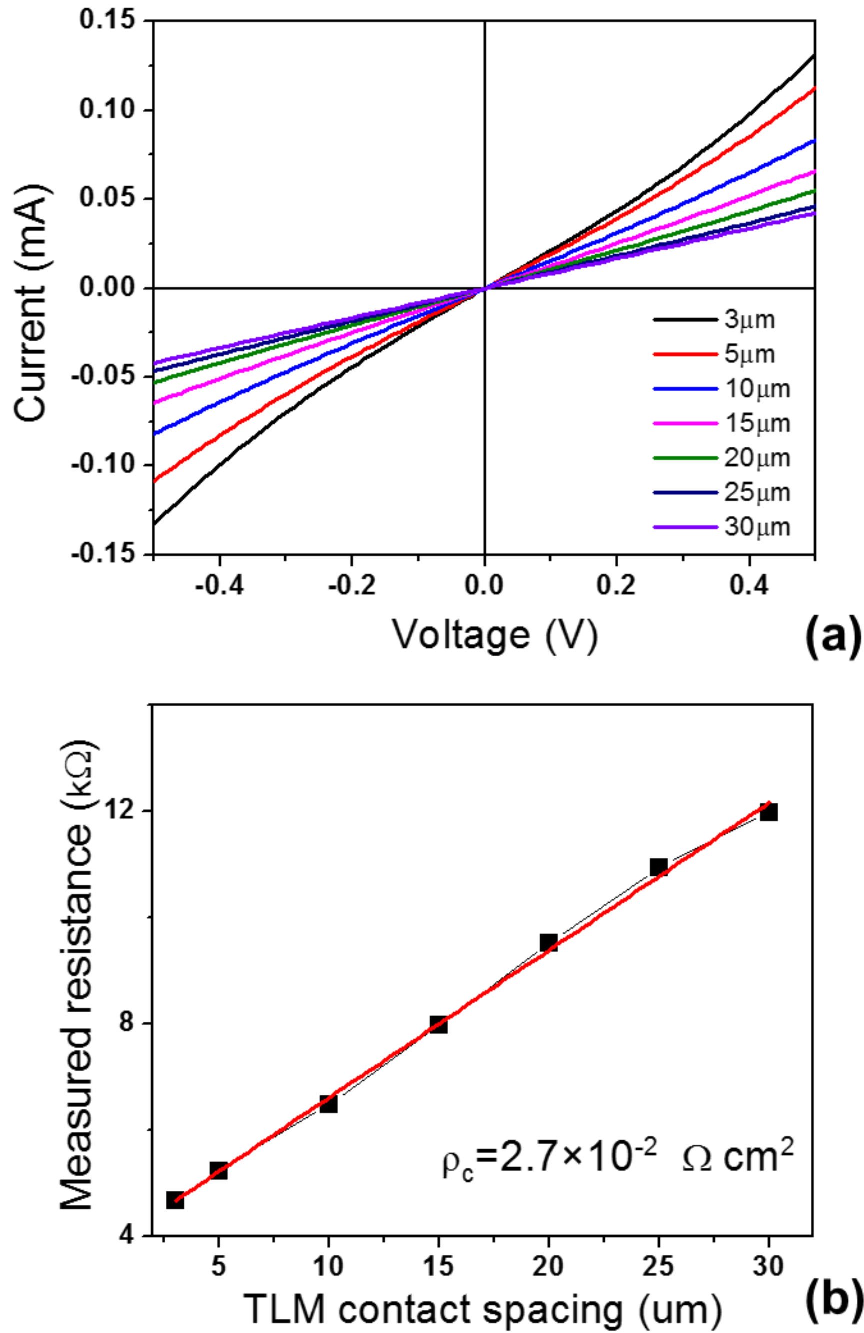

Fig. 45 (a) I-V characteristics of the ITO to p-GaN contact after thermal stress at 450 °C in N_2 for 8h, measured on TLM A, and (b) plot of measured resistance versus TLM contact spacing.

The above discussion indicates that the ITO to p-GaN contact is stable up to 300 °C in N_2 ambient. Higher temperature stress in non-oxygen ambient will cause out-diffusion of oxygen, reducing the work function of ITO which in turn increases the contact barrier. To solve this problem, thermal stress tests were conducted in air as well carrying plentiful oxygen supply. Fig. 46 (a) shows the I-V characteristics of the ITO to p-GaN contact after thermal stress at 450 °C in air for 8h, measured on TLM A are very similar to those before the thermal stress test. The ρ_c extracted from the plot of measured resistance versus TLM contact spacing, shown in Fig. 46 (b), is 9.2×10^{-3} $\Omega\cdot cm^2$. The sheet resistance of ITO film, extracted from measurements on TLM B, is 28.9 Ω/☐. The difference in those values, before and after thermal stress, is negligible, indicating good stability of the ITO contact at temperatures up to 450 °C in air.

The sample was then thermally stressed at 500 °C in air for 8 hours. The currents measured on the TLM A were significantly reduced, shown in Fig. 47 (a). The extracted ρ_c was 3.6×10^{-2} $\Omega\cdot cm^2$, shown in Fig. 47 (b), three times higher than that after the 450 °C thermal stress in air. The sheet resistance of ITO film, extracted from measurements on TLM B, also increased significantly from 28.9 Ω/☐ to 48 Ω/☐. The increase in sheet resistance is probably due to the reduction of oxygen vacancy. Thermal stress at high temperature in air will introduce more oxygen into ITO, so the oxygen deficiency can be recovered. In addition, the donor dopant Sn in ITO may also form Sn-O bonds, reducing the concentration of Sn^{4+}. Lower concentration of Sn^{4+} results in higher ITO resistivity [87]. Therefore, in contrast to the degradation in N_2 ambient caused by the out-diffusion of oxygen, the degradation in air at high temperature is attributed to the absorption of excessive oxygen.

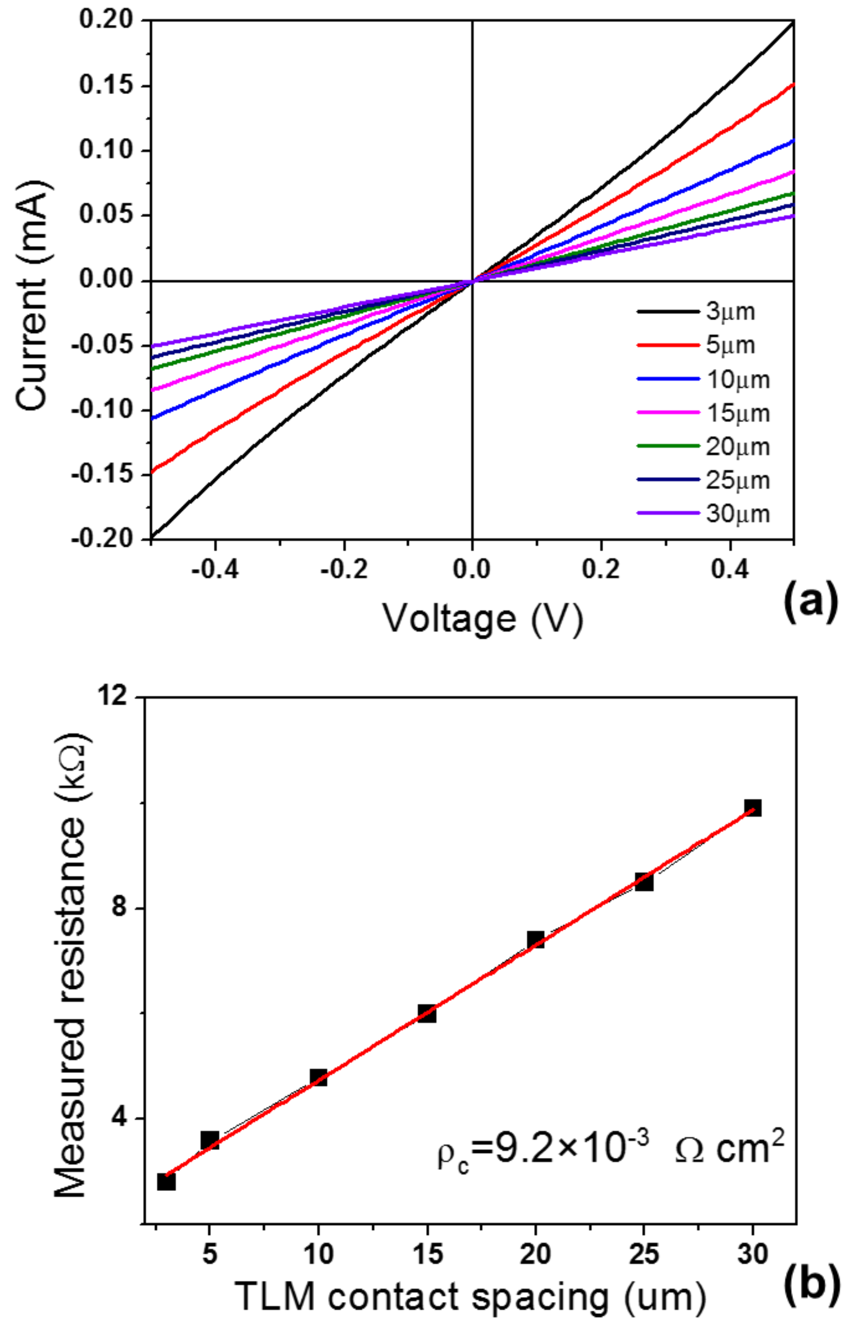

Fig. 46 (a) I-V characteristics of the ITO to p-GaN contact after thermal stress at 450 °C in air for 8h, measured on TLM A, and (b) plot of measured resistance versus TLM contact spacing.

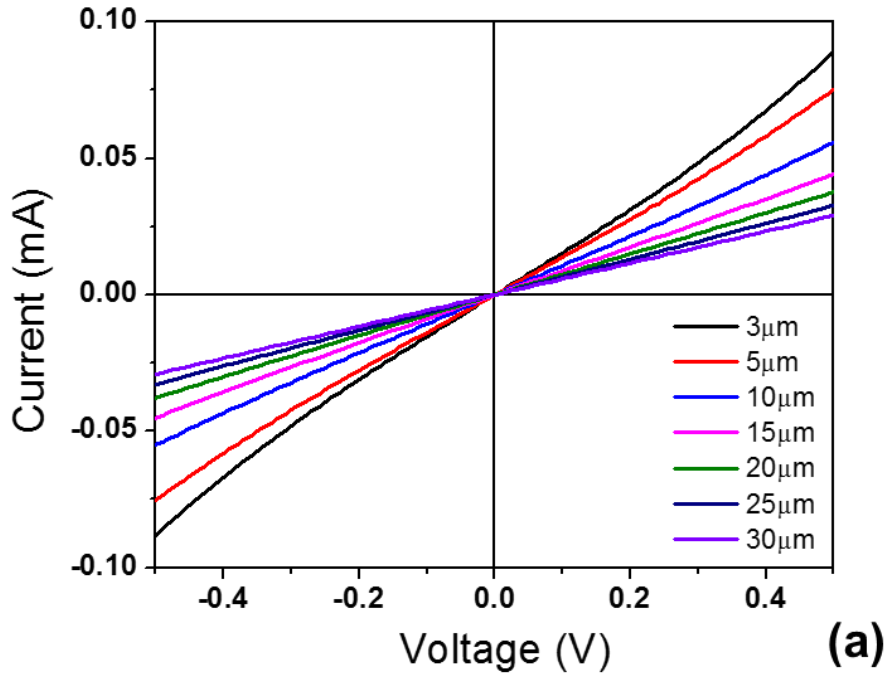

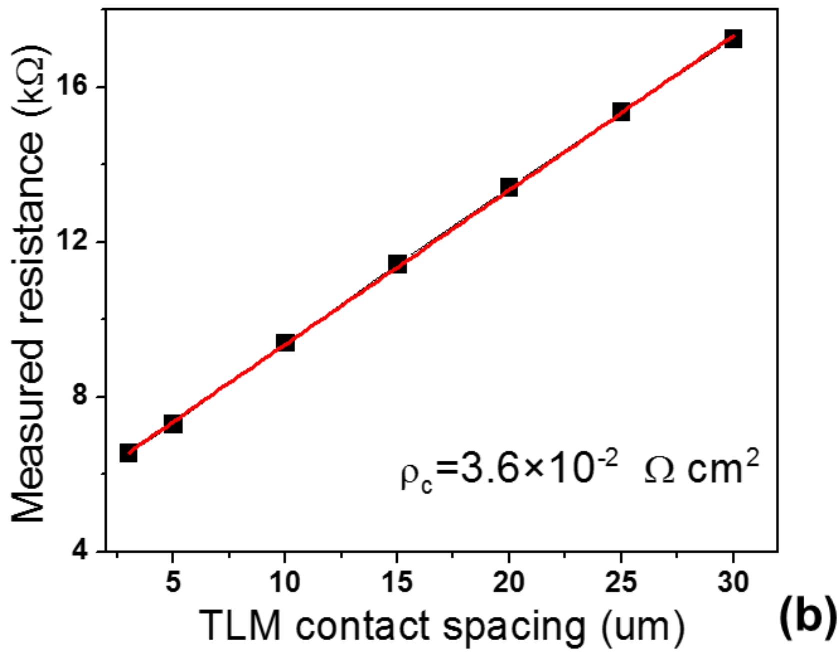

Fig. 47 (a) I-V characteristics of the ITO to p-GaN contact after thermal stress at 500 °C in air for 8h, measured on TLM A, and (b) plot of measured resistance versus TLM contact spacing.

5.3 Summary

In this chapter, two types of contacts for p-GaN have been extensively studied, viz. annealed Ni/Au contact and annealed ITO contact.

The annealed Ni/Au contacts, measuring an initial ρ_c ~2×10^{-3} $\Omega\cdot cm^2$ at room temperature retained its ohmic behavior at all temperatures from 25 °C to 390 °C. It showed superior ohmic behavior at elevated temperatures. Both contact resistivity and the sheet resistance of p-GaN reduced by one order of magnitude at 390 °C, and expected to reduce further at 450 °C, due to the increased hole concentration at high temperature. The contact showed very good stability at 450 °C in air with no degradation observed after 48 hours. TEM study showed that the formation of Au/p-GaN epitaxial structure after annealing allowed for the low contact resistivity and good stability at high temperature as well. Our studies suggested that the observed degradation at higher temperature is possibly caused by the oxidation of GaN surface. The TEM study confirmed that there was a layer of Ga_2O_3 formed on the interface between metal and GaN after the contact being subjected to 700 °C in air for 4 hours. Therefore, the annealed Ni/Au contacts is good for stable operation at temperatures up to 450 °C in air.

The annealed ITO contact with ρ_c ~1×10^{-2} $\Omega\cdot cm^2$, is stable up to 300 °C in N_2. Degradation in ITO contacts at higher temperature is probably caused by the out-diffusion of oxygen from ITO, resulting in the decrease of ITO work function. For up to 450 °C the contact was observed to be stable in air. The degradation in air at higher temperature in air is likely due to the absorption of excessive oxygen in the ITO film, reducing the conductivity of the contact.

Chapter 6

LONG TERM RELIABILITY AT HIGH TEMPERATURE

6.1 Arrhenius Model for Accelerated Life Testing

In order to produce and continually improve the reliability of electronic devices, it is necessary to find a way of predicting the lifetime of a device. The estimation of devices lifetime at a designated temperature is important to both manufacturers and users. Lifetime testing is a useful method for achieving three goals, namely, selecting durable devices, estimating the median lifetime of the device, and finding the optimal condition for operation. For example, we would like to know how long would the contacts last before significant degradation happens at 450°C operation. The answer to this question can be answered through statistical analysis of actual lifetime data. However, the lifetimes could be thousands of hours or even longer, so it is generally not practical to test the devices at normal operation conditions. Some methods must be utilized in order to obtain the failure characteristics in a relatively reasonable amount of time. The most prevalent lifetime prediction method used extensively in the semiconductor industry involves testing the devices at an elevated temperature, also called accelerated life testing (ALT). This accelerated test allows the ability to create in a short period of time the same failure modes that would take much longer to occur under normal operating conditions.

One of the most common model used to analyze device lifetime is the Arrhenius model which uses temperature and activation energy (E_a) to predict mean time before failure (MTBF), defined as lifetime. The following equations shows how the Arrhenius model can be expressed to show activation energy when lifetime and temperature are known.

$$t_f = A\,exp\left(\frac{E_a}{kT}\right), \quad (6.1)$$

where, t_f is the lifetime (h); A is a scaling factor; E_a is the activation energy (eV) for the specific failure mechanism at temperature T; k is Boltzmann's constant. Equation 6.1 could be derived as,

$$\ln t_f = E_a\left(\frac{1}{kT}\right) + \ln A \quad (6.2)$$

Equation 6.2 shows that there is linear relation between $ln\ t_f$ and $1/kT$. By measuring the lifetime at high temperatures and plotting the $ln\ t_f$ vs $1/kT$, we can extract the value of E_a and A, and then we are able to estimate the lifetime at any temperature.

It must be mentioned that the Arrhenius equation is applicable only if a single mechanism is contributing to the failure of a device, because the activation energy E_a is corresponding to one specific failure mechanism. If there is more than one failure mechanism involved, E_a would change with temperature instead of being a constant and the plot of $ln\ t_f$ vs $1/kT$ would display a change in slope as well. In other words, the lifetime prediction based on Arrhenius mode is reasonable only if the plot of $ln\ t_f$ vs $1/kT$ displays a constant slope. Although the absolute accuracy of the predicted lifetime remains questionable, this method still provide useful information in estimating the reliability of a device qualitatively, especially when comparing two devices under the same accelerating conditions.

The metal-semiconductor contacts exhibit a wear-out failure mode by showing a slow degradation in resistivity even at room temperature. We have noticed that the contact resistivity of an alloyed Ti/Al/Ni/Au to n-GaN contact increased from 6×10^{-7} $\Omega\cdot cm^2$, measured after the sample was prepared, to 6×10^{-6} $\Omega\cdot cm^2$ after the sample being

stored at room temperature for two months. The contact degradation at high temperature is much faster, so the lifetime is much shorter according to equation 6.1. The lifetime of those contacts will play an important role when designing the high temperature InGaN solar cell. In this study, the lifetime of a contact at certain temperature, also called mean time before failure (MTBF), was defined as the time after which ρ_c has increased by a factor of 10 compared with the initial value. While this can be a stringent condition for MTBF (where the voltage drop at the leads may be negligible to disrupt the solar cell operation) this study assumed such a criterion to evaluate the method of ALT based on Arrhenius model.

6.2 Accelerated Life Testing of the Annealed Ni/Au to p-GaN Contact

We applied the ALT to the annealed Ni/Au to p-GaN contact, which had an initial $\rho_c \sim 2\times10^{-3}\ \Omega\cdot cm^2$. Accord to the definition, the time after which the ρ_c increases to $2\times10^{-2}\ \Omega\cdot cm^2$ is the lifetime at a specified temperature. To predict the lifetime at 450 °C in air, ALT was conducted at higher temperatures up to 525 °C in air, assuming that the degradation mechanisms are the same in the temperature range between 450 °C and 525 °C in air.

Three samples with TLM test structures, A, B, and C, were put in the furnace with ambient air for thermal stress at 475 °C, 500 °C, and 525 °C, respectively. The contact samples were taken out and cooled down to room temperature every after few hours and the contact resistivity was monitored by TLM measurements at room temperature. Table 1 shows the values of ρ_c for the three samples as a function of time under thermal stress at different temperatures. The increase of ρ_c as a function of time under thermal stress is shown in Fig. 48, depicting linear increase of ρ_c at all the

temperatures. By doing a linear fit of ρ_c vs time under thermal stress, the lifetime of the contact at each temperature can be extracted. The extracted lifetime at 475 °C, 500 °C, and 525 °C in air are 69, 24, and 9 hours, respectively.

Table 1 Values of ρ_c for contact sample A, B, and C as a function of time under the thermal stress at 475 °C, 500 °C, and 525 °C, respectively, in air.

A(475 °C)		B(500 °C)		C (525 °C)	
Hours	ρ_c ($\Omega\cdot cm^2$)	Hours	ρ_c ($\Omega\cdot cm^2$)	Hours	ρ_c ($\Omega\cdot cm^2$)
0	2.3E-03	0	1.6E-03	0	1.7E-03
4	4.0E-03	2	3.0E-03	2	5.1E-03
8	5.3E-03	4	4.2E-03	4	8.2E-03
12	6.1E-03	6	5.4E-03	6	1.1E-02
16	7.0E-03	8	6.5E-03	10	1.9E-02

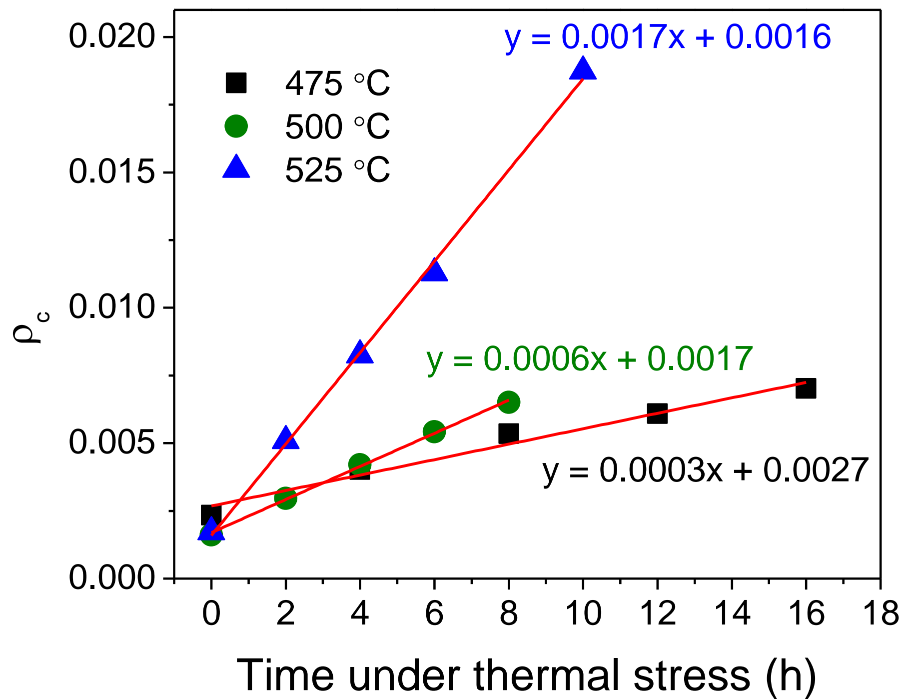

Fig. 48 Increase of ρ_c as a function of time under thermal stress at 475 °C, 500 °C, and 525 °C, respectively, in air.

With three values of temperature and the corresponding values of lifetime, ln (t_f) vs 1/kT can be plotted, shown in Fig. 49. The linear relation between ln (t_f) and 1/kT indicates that there is a single degradation mechanism in this temperature range, and thus the Arrhenius equation is applicable. The activation energy, E_a ~2eV, and the scaling factor, A ~7.2e-13 h, were extracted by linear fitting of the Arrhenius plot. The scaling factor A, in equation 6.1, is different from that in the conventionally defined equation, $k_{rc} = A \exp\left(\frac{-E_a}{kT}\right)$, where k_{rc} is the rate coefficient of the reaction.

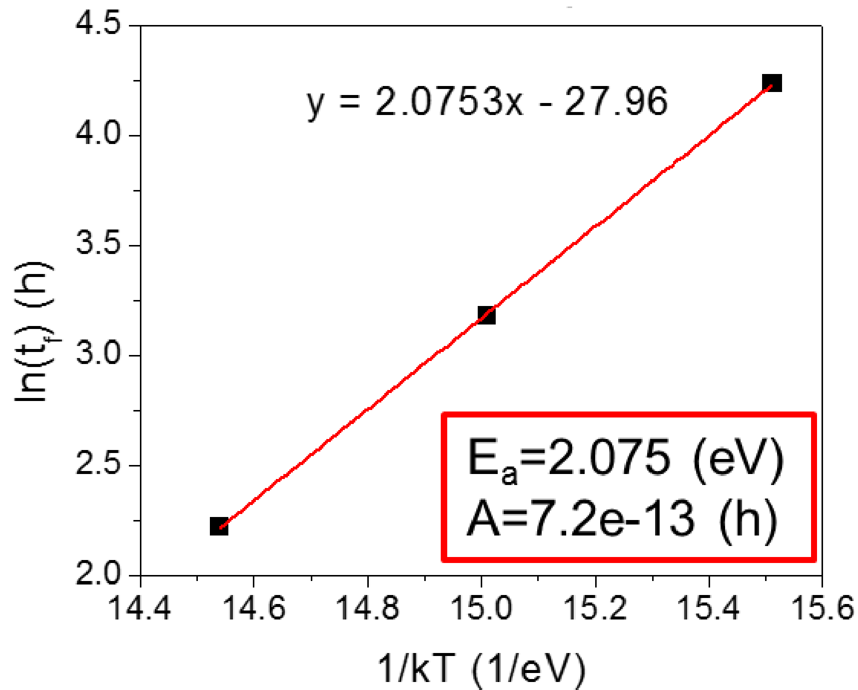

Fig. 49 Arrhenius plot of ln (t_f) vs 1/kT in air.

With the values of E_a and A, the contact lifetime can be estimated by equation 6.1. Fig. 50 shows the estimated lifetime versus temperature according to Arrhenius model. The lifetime of the annealed Ni/Au to p-GaN contacts is 1.3×10^6 h at 300 °C, 4.4×10^4 h at 350 °C, 2473 h at 400 °C, 208 h at 450 °C, respectively. The contact lifetime drops rapidly as the operating temperature increases.

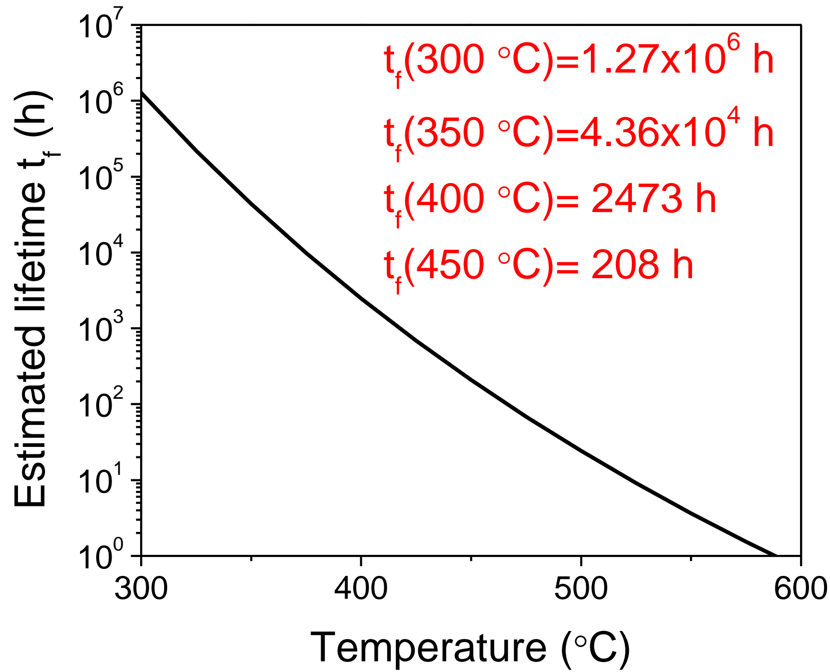

Fig. 50 Estimated lifetime in air versus temperature according to Arrhenius model.

In chapter 5, we claimed that the degradation of Ni/Au contact in air is probably due to oxidation of p-GaN surface at high temperature in the oxidizing ambient. To achieve a contrasting study and proved our hypothesis similar ALT was performed in N_2 ambient. The contact degradation in N_2 was accelerated by subjecting another set of annealed Ni/Au to p-GaN contact samples, with the same initial $\rho_c \sim 2\times10^{-3}\ \Omega\cdot cm^2$, to thermal stress at 500°C, 529°C, and 554°C, respectively. ρ_c showed much slower increase in N_2 compared with that in air. The extracted lifetime at 500°C, 529°C, and 554°C were 235, 65, and 24 hours, respectively. E_a and A were extracted as described earlier from the plot of ln (t_f) vs $1/kT$. $E_a = 2.33$ eV while $A=1.52\times10^{-13}$ h. The higher activation energy for the degradation in N_2 compared with that in air indicates the contact is more stable in N_2 ambient. The predicted lifetime at 450 °C in N_2 ambient is 2,628 hours, 12 times the lifetime in air at the same temperature. The comparison of contact lifetime (hours) in air

and in N_2 at temperatures from 300 °C to 500 °C, is shown in Table 2, demonstrating that the contact lifetime is much longer in N_2 than that in air at high temperatures.

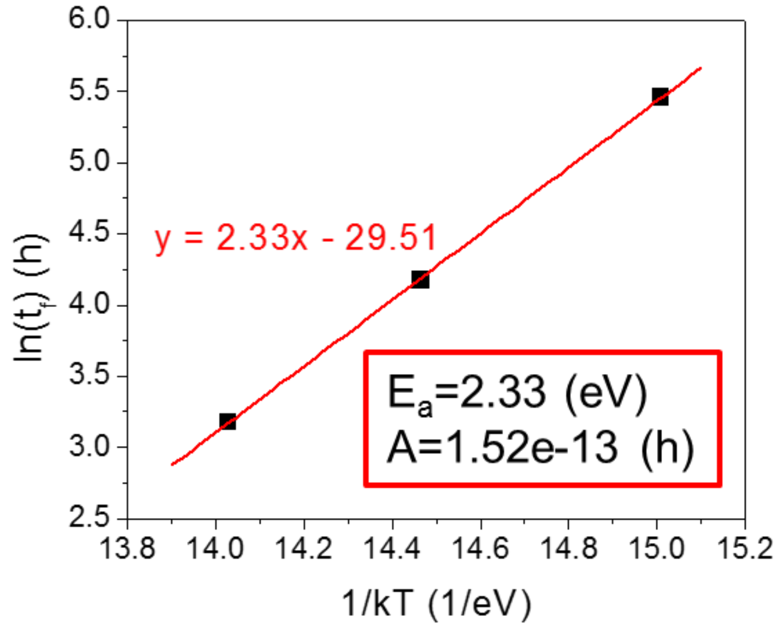

Fig. 51 Arrhenius plot of $ln\ (t_f)$ vs $1/kT$ in N_2.

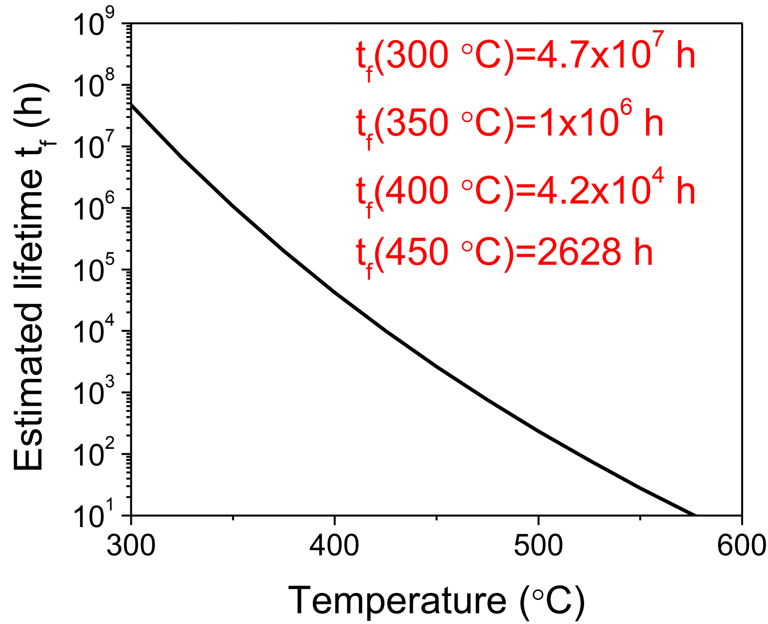

Fig. 52 Estimated lifetime in N_2 versus temperature according to Arrhenius model.

Table 2 Comparison of contact lifetime (hours) in air and in N_2 at temperatures from 300 °C to 500 °C.

Temperature (°C)	300	350	400	450	500
In air	1.3×10^6	4.4×10^4	2,473	208	24
In N_2	4.7×10^7	1×10^6	4.2×10^4	2,628	234

6.3 Summary

In this chapter, the accelerated life testing using Arrhenius mode has been employed to evaluate the reliability of the ohmic contact to GaN at high temperature. We have accomplished a quantitative analysis of lifetime for the annealed Ni/Au to p-GaN contacts at high temperature in air and N_2 ambient, respectively. At 450 °C, the lifetime of the contact in N_2 ambient is 2,628 hours, which is 12 times the lifetime in air at the same temperature. The comparison of the contact lifetime in air and N_2 indicates that the annealed Ni/Au contact is much more stable in non-oxidizing ambient. This result is consistent with the conclusions made in chapter 5 claiming that oxidation of p-GaN surface is responsible for the contact degradation at high temperature in air.

Chapter 7

CONCLUSION AND FUTURE WORK

7.1 Conclusion

In an effort to develop ohmic contacts with low resistivity and high stability for GaN high temperature electronics, especially the GaN-based high temperature solar cell, we have investigated the high temperature performance and thermal stability of two different ohmic contact schemes to n-GaN including alloyed Ti/Al/Ni/Au contacts and non-alloyed Al/Au contacts, and two ohmic contacts to p-GaN including annealed Ni/Au contacts and ITO contacts.

For the n-GaN contacts, temperature dependent measurements showed that ρ_c didn't change with ambient temperature while the sheet resistance of n-GaN increased with ambient temperature. Both the alloyed Ti/Al/Ni/Au contacts and the non-alloyed Al/Au contacts are stable for operating at temperatures up to 600 °C for at least 4 hours in air with low contact resistivity in the order of ~10^{-6} Ω•cm^2. The formation of TiN during alloying is believed to be responsible for the low resistivity and high stability of the alloyed Ti/Al/Ni/Au contacts, while the formation of Al-O-Au complex on the interface plays an important role in reducing the contact resistivity of the Al/Au contacts and maintaining the same at high temperatures.

The p-GaN contacts showed superior ohmic behavior at elevated temperatures. Temperature dependent measurements showed that both ρ_c and sheet resistance of p-GaN decreased by a factor of 10 as the ambient temperature increased from room temperature to 390 °C, and expected to be reduced further at 450 °C due to the increased hole concentration at high temperature. The annealed Ni/Au contacts, with ρ_c ~2×10^{-3} Ω cm^2

at room temperature, showed very good stability at temperatures up to 450 °C in air. The formation of faultless Au/p-GaN epitaxial lattice structure is believed to responsible for the low resistivity and high stability of the Ni/Au contacts. Evidences collected during this study suggest that the degradation of contacts at higher temperature is caused by the oxidation of p-GaN surface. ITO contact to p-GaN, with a ρ_c ~1×10^{-2} Ω cm^2 at room temperature, is stable at 450 °C in air but it is not stable at 450 °C in N_2 ambient due to the out-diffusion of oxygen, resulting in the increase of carrier concentration in ITO and the decrease of work function of ITO. The ITO contact, however, degrades at 500 °C in air, most likely due to the absorption of excessive oxygen which reduces the conductivity of ITO.

We also developed a method using ALT to quantitatively evaluate the contact stability at high temperature. The annealed Ni/Au to p-GaN contact showed a lifetime of 2,628 hours at 450 °C in N_2, which is 12 times the lifetime at 450 °C in air. The ALT showed that the annealed Ni/Au contact was more stable for operating in N_2 ambient.

In summary, we have developed stable ohmic contacts needed for the high temperature GaN-based solar cell operating at 450 °C in both oxidizing and non-oxidizing ambient. The temperature limit of each contact metallization scheme was studied and possible degradation mechanism was discussed. The impressive results discussed in this thesis demonstrate excellent performance of the ohmic contacts to GaN at high temperature, making GaN a material of choice for high temperature applications.

7.2 Future Work

The results and discussions in this dissertation point to several interesting directions for future work:

One should further analyze the interfacial layer on the Al/Au to n-GaN contacts to understand the mechanism of reducing contact resistivity by high temperature thermal stress. Our results in chapter 4 indicated that the formation of Al-O-Au complex was responsible for the reduction in contact resistivity, which needs further investigation and explanation. This finding will not only help us predict the long term stability of the Al/Au to n-GaN contact, but also provide a way of achieving very low contact resistivity without high temperature annealing.

A major direction to follow this work will be to test the Ni/Au to p-GaN contacts in a pure non-oxidizing ambient, e.g. N_2 and Ar. We concluded the contact degradation at temperatures above 450 °C was due to oxidation on the interface. Effect of other non-oxidizing ambient or baths will help understand the thermodynamics better. Studying the humidity effect on contact degradation at high temperature is extremely important. Humidity plays an important role on contact degradation. With thorough consideration of temperature, ambient, and humidity effects, we will be able to estimate the lifetime of the high temperature InGaN solar cell more accurately.

Other than studying on ALT and degradation mechanism, one should keep in mind that the ultimate benefit of these studies won't be accomplished until one develops stable contacts to GaN for temperatures relevant to the high temperature applications. For example, 600 °C is mentioned to be the sweet spot for hybrid solar towers where the efficiency of the molten salt is at its peak around 570°C. Although we have developed stable contacts to n-GaN for 600 °C operation, but the contacts to p-GaN discussed in this dissertation are not stable for operation above 450 °C. Alternative metal combinations

and contact preparation methods need to be investigated to develop stable ohmic contact to p-GaN for such applications.

The intrinsic GaN device (here the InGaN solar cell) has the capability to support high temperature operations even up to 800 ºC, but one needs to verify how the cells survive or fail at high temperatures during the operation. Therefore testing the stability of the InGaN solar cell at high temperatures and predict the lifetime using accelerated life testing will be a useful next step. The lifespan of a modern solar panel could be 30 years for normal operation, but it would be much shorter at high temperature. It is very important to know the lifespan so that we can calculate the costs and earnings of the high temperature InGaN solar cell.

Space exploration applications rely on extreme temperature operation but for a significantly shorter duration compared to commercial solar cells. This study is an important addition to understand what roles GaN devices can play in space exploration technology. The devices need not be limited to solar cells only. Power electronics, high frequency electronics, UV detectors and sensors- all of these major fields thriving on GaN's superior material qualities will be benefited from high temperature contact technologies.

REFERENCES

[1] P. G. Neudeck, R. S. Okojie, and L.-Y. Chen, "High-temperature electronics - a role for wide bandgap semiconductors?," *Proc. IEEE*, vol. 90, no. 6, pp. 1065–1076, Jun. 2002.

[2] H. A. Mantooth, M. M. Mojarradi, and R. W. Johnson, "Emerging capabilities in electronics technologies for extreme environments, Part I: High temperature electronics," *IEEE Power Electron. Soc. Newsl.*, vol. 18, no. 1, pp. 9–14, 2006.

[3] R. W. Johnson, J. L. Evans, P. Jacobsen, J. R. Thompson, and M. Christopher, "The changing automotive environment: high-temperature electronics," *IEEE Trans. Electron. Packag. Manuf.*, vol. 27, no. 3, pp. 164–176, Jul. 2004.

[4] W. J. Pulliam, P. M. Russler, and R. S. Fielder, "High-temperature high-bandwidth fiber optic MEMS pressure-sensor technology for turbine engine component testing," in *Environmental and Industrial Sensing, International Society for Optics and Photonics, 2002.* pp. 229–238, 2002.

[5] T. George, K.-A. Son, R. A. Powers, L. Y. Del Castillo, and R. Okojie, "Harsh environment microtechnologies for NASA and terrestrial applications," in *IEEE Sensors*, *2005.* pp. 1253–1258, 2005.

[6] J. C. Zolper, "A review of junction field effect transistors for high-temperature and high-power electronics," *Solid-State Electron.*, vol. 42, no. 12, pp. 2153–2156, Dec. 1998.

[7] T. P. Chow, N. Ramungul, and M. Ghezzo, "Wide Bandgap Semiconductor Power Devices," in *MRS Proceedings*, *1997*, vol. 483, p. 89, 1997.

[8] J. Wu, W. Walukiewicz, K. M. Yu, J. W. A. Iii, E. E. Haller, H. Lu, and W. J. Schaff, "Small band gap bowing in In1−xGaxN alloys," *Appl. Phys. Lett.*, vol. 80, no. 25, pp. 4741–4743, Jun. 2002.

[9] X. Cai, S. Zeng, and B. Zhang, "Fabrication and characterization of InGaN p-i-n homojunction solar cell," *Appl. Phys. Lett.*, vol. 95, no. 17, p. 173504, Oct. 2009.

[10] X. Zheng, R.-H. Horng, D.-S. Wuu, M.-T. Chu, W.-Y. Liao, M.-H. Wu, R.-M. Lin, and Y.-C. Lu, "High-quality InGaN∕GaN heterojunctions and their photovoltaic effects," *Appl. Phys. Lett.*, vol. 93, no. 26, p. 261108, Dec. 2008.

[11] H. M. Branz, W. Regan, K. J. Gerst, J. B. Borak, and E. A. Santori, "Hybrid solar converters for maximum exergy and inexpensive dispatchable electricity," *Energy Environ. Sci.*, vol. 8, no. 11, pp. 3083–3091, Oct. 2015.

[12] A. Luque and A. Martí, "Limiting efficiency of coupled thermal and photovoltaic converters," *Sol. Energy Mater. Sol. Cells*, vol. 58, no. 2, pp. 147–165, Jun. 1999.

[13] Y. Yang, W. Yang, W. Tang, and C. Sun, "High-temperature solar cell for concentrated solar-power hybrid systems," *Appl. Phys. Lett.*, vol. 103, no. 8, p. 083902, Aug. 2013.

[14] O. Jani, I. Ferguson, C. Honsberg, and S. Kurtz, "Design and characterization of GaN/InGaN solar cells," *Appl. Phys. Lett.*, vol. 91, no. 13, p. 132117, Sep. 2007.

[15] L. Kassamakova-Kolaklieva, R. Kakanakov, V. Cimalla, N. Hristeva, G. Lepoeva, N. I. Kuznetsov, and K. Zekentes, "Pd-Based Ohmic Contacts to LPE 4H-SiC with Improved Thermal Stability," *Mater. Sci. Forum*, vol. 433–436, pp. 713–716, 2003.

[16] R. Kakanakov, L. Kasamakova-Kolaklieva, N. Hristeva, G. Lepoeva, J. B. Gomes, I. Avramova, and T. Marinova, "High temperature and high power stability investigation of Al-based ohmic contacts to p-type 4H-SiC," in *27th International Spring Seminar on Electronics Technology: Meeting the Challenges of Electronics Technology Progress, 2004*, vol. 3, pp. 543–546, 2004.

[17] L. Kolaklieva, R. Kakanakov, G. Lepoeva, J. B. Gomes, and T. Marinova, "Au/Ti/Al contacts to SiC for power applications: electrical, chemical and thermal properties," in *24th International Conference on Microelectronics, 2004*, vol. 2, pp. 421–424, 2004.

[18] R. S. Okojie, D. Lukco, Y. L. Chen, and D. J. Spry, "Reliability assessment of Ti/TaSi2/Pt ohmic contacts on SiC after 1000 h at 600 °C," *J. Appl. Phys.*, vol. 91, no. 10, pp. 6553–6559, May 2002.

[19] R. Maboudian, C. Carraro, D. G. Senesky, and C. S. Roper, "Advances in silicon carbide science and technology at the micro- and nanoscales," *J. Vac. Sci. Technol. A*, vol. 31, no. 5, p. 050805, Sep. 2013.

[20] P. Hacke, T. Detchprohm, K. Hiramatsu, and N. Sawaki, "Schottky barrier on n-type GaN grown by hydride vapor phase epitaxy," *Appl. Phys. Lett.*, vol. 63, no. 19, pp. 2676–2678, Nov. 1993.

[21] J. D. Guo, F. M. Pan, M. S. Feng, R. J. Guo, P. F. Chou, and C. Y. Chang, "Schottky contact and the thermal stability of Ni on n-type GaN," *J. Appl. Phys.*, vol. 80, no. 3, pp. 1623–1627, Aug. 1996.

[22] S. C. Binari, H. B. Dietrich, G. Kelner, L. B. Rowland, K. Doverspike, and D. K. Gaskill, "Electrical characterisation of Ti Schottky barriers can n-type GaN," *Electron. Lett.*, vol. 30, no. 11, pp. 909–911, May 1994.

[23] A. C. Schmitz, A. T. Ping, M. A. Khan, Q. Chen, J. W. Yang, and I. Adesida, "Schottky barrier properties of various metals on n-type GaN," *Semicond. Sci. Technol.*, vol. 11, no. 10, p. 1464, 1996.

[24] J. D. Guo, M. S. Feng, R. J. Guo, F. M. Pan, and C. Y. Chang, "Study of Schottky barriers on n-type GaN grown by low-pressure metalorganic chemical vapor deposition," *Appl. Phys. Lett.*, vol. 67, no. 18, pp. 2657–2659, Oct. 1995.

[25] T. Mori, T. Kozawa, T. Ohwaki, Y. Taga, S. Nagai, S. Yamasaki, S. Asami, N. Shibata, and M. Koike, "Schottky barriers and contact resistances on p-type GaN," *Appl. Phys. Lett.*, vol. 69, no. 23, pp. 3537–3539, Dec. 1996.

[26] Y.-F. Wu, W.-N. Jiang, B. P. Keller, S. Keller, D. Kapolnek, S. P. Denbaars, U. K. Mishra, and B. Wilson, "Low resistance ohmic contact to n-GaN with a separate layer method," *Solid-State Electron.*, vol. 41, no. 2, pp. 165–168, Feb. 1997.

[27] B. P. Luther, S. E. Mohney, T. N. Jackson, M. A. Khan, Q. Chen, and J. W. Yang, "Investigation of the mechanism for Ohmic contact formation in Al and Ti/Al contacts to n-type GaN," *Appl. Phys. Lett.*, vol. 70, no. 1, pp. 57–59, Jan. 1997.

[28] M. E. Lin, Z. Ma, F. Y. Huang, Z. F. Fan, L. H. Allen, and H. Morkoç, "Low resistance ohmic contacts on wide band-gap GaN," *Appl. Phys. Lett.*, vol. 64, no. 8, pp. 1003–1005, Feb. 1994.

[29] A. Motayed, R. Bathe, M. C. Wood, O. S. Diouf, R. D. Vispute, and S. N. Mohammad, "Electrical, thermal, and microstructural characteristics of Ti/Al/Ti/Au multilayer Ohmic contacts to n-type GaN," *J. Appl. Phys.*, vol. 93, no. 2, pp. 1087–1094, Jan. 2003.

[30] S. Ruvimov, Z. Liliental-Weber, J. Washburn, K. J. Duxstad, E. E. Haller, Z.-F. Fan, S. N. Mohammad, W. Kim, A. E. Botchkarev, and H. Morkoç, "Microstructure of Ti/Al and Ti/Al/Ni/Au Ohmic contacts for n-GaN," *Appl. Phys. Lett.*, vol. 69, no. 11, pp. 1556–1558, Sep. 1996.

[31] B. P. Luther, J. M. DeLucca, S. E. Mohney, and R. F. K. Jr, "Analysis of a thin AlN interfacial layer in Ti/Al and Pd/Al ohmic contacts to n-type GaN," *Appl. Phys. Lett.*, vol. 71, no. 26, pp. 3859–3861, Dec. 1997.

[32] Z. Fan, S. N. Mohammad, W. Kim, Ö. Aktas, A. E. Botchkarev, and H. Morkoç, "Very low resistance multilayer Ohmic contact to n-GaN," *Appl. Phys. Lett.*, vol. 68, no. 12, pp. 1672–1674, Mar. 1996.

[33] N. A. Papanicolaou, M. V. Rao, J. Mittereder, and W. T. Anderson, "Reliable Ti/Al and Ti/Al/Ni/Au ohmic contacts to n-type GaN formed by vacuum annealing," *J. Vac. Sci. Technol. B*, vol. 19, no. 1, pp. 261–267, Jan. 2001.

[34] A. N. Bright, P. J. Thomas, M. Weyland, D. M. Tricker, C. J. Humphreys, and R. Davies, "Correlation of contact resistance with microstructure for Au/Ni/Al/Ti/AlGaN/GaN ohmic contacts using transmission electron microscopy," *J. Appl. Phys.*, vol. 89, no. 6, pp. 3143–3150, Mar. 2001.

[35] C.-T. Lee and H.-W. Kao, “Long-term thermal stability of Ti/Al/Pt/Au Ohmic contacts to n-type GaN,” *Appl. Phys. Lett.*, vol. 76, no. 17, pp. 2364–2366, Apr. 2000.

[36] Q. Z. Liu and S. S. Lau, “A review of the metal–GaN contact technology,” *Solid-State Electron.*, vol. 42, no. 5, pp. 677–691, May 1998.

[37] E. F. Chor, D. Zhang, H. Gong, G. L. Chen, and T. Y. F. Liew, “Electrical characterization and metallurgical analysis of Pd-containing multilayer contacts on GaN,” *J. Appl. Phys.*, vol. 90, no. 3, pp. 1242–1249, Aug. 2001.

[38] V. Kumar, L. Zhou, D. Selvanathan, and I. Adesida, “Thermally-stable low-resistance Ti/Al/Mo/Au multilayer ohmic contacts on n–GaN,” *J. Appl. Phys.*, vol. 92, no. 3, pp. 1712–1714, Aug. 2002.

[39] S. N. Mohammad, “Contact mechanisms and design principles for alloyed ohmic contacts to n-GaN,” *J. Appl. Phys.*, vol. 95, no. 12, pp. 7940–7953, Jun. 2004.

[40] Z. X. Qin, Z. Z. Chen, Y. Z. Tong, X. M. Ding, X. D. Hu, T. J. Yu, and G. Y. Zhang, “Study of Ti/Au, Ti/Al/Au, and Ti/Al/Ni/Au ohmic contacts to n-GaN,” *Appl. Phys. A*, vol. 78, no. 5, pp. 729–731, Jan. 2003.

[41] M. Hou and D. G. Senesky, “Operation of ohmic Ti/Al/Pt/Au multilayer contacts to GaN at 600 °C in air,” *Appl. Phys. Lett.*, vol. 105, no. 8, p. 081905, Aug. 2014.

[42] F. Iucolano, F. Roccaforte, A. Alberti, C. Bongiorno, S. D. Franco, and V. Raineri, “Temperature dependence of the specific resistance in Ti/Al/Ni/Au contacts on n-type GaN,” *J. Appl. Phys.*, vol. 100, no. 12, p. 123706, Dec. 2006.

[43] W. Götz, N. M. Johnson, J. Walker, D. P. Bour, and R. A. Street, “Activation of acceptors in Mg-doped GaN grown by metalorganic chemical vapor deposition,” *Appl. Phys. Lett.*, vol. 68, no. 5, pp. 667–669, Jan. 1996.

[44] J. K. Sheu, Y. K. Su, G. C. Chi, P. L. Koh, M. J. Jou, C. M. Chang, C. C. Liu, and W. C. Hung, “High-transparency Ni/Au ohmic contact to p-type GaN,” *Appl. Phys. Lett.*, vol. 74, no. 16, pp. 2340–2342, Apr. 1999.

[45] J.-K. Ho, C.-S. Jong, C. C. Chiu, C.-N. Huang, C.-Y. Chen, and K.-K. Shih, “Low-resistance ohmic contacts to p-type GaN,” *Appl. Phys. Lett.*, vol. 74, no. 9, pp. 1275–1277, Mar. 1999.

[46] J.-K. Ho, C.-S. Jong, C. C. Chiu, C.-N. Huang, K.-K. Shih, L.-C. Chen, F.-R. Chen, and J.-J. Kai, “Low-resistance ohmic contacts to p-type GaN achieved by the oxidation of Ni/Au films,” *J. Appl. Phys.*, vol. 86, no. 8, pp. 4491–4497, Oct. 1999.

[47] L.-C. Chen, J.-K. Ho, C.-S. Jong, C. C. Chiu, K.-K. Shih, F.-R. Chen, J.-J. Kai, and L. Chang, "Oxidized Ni/Pt and Ni/Au ohmic contacts to p-type GaN," *Appl. Phys. Lett.*, vol. 76, no. 25, pp. 3703–3705, Jun. 2000.

[48] S. Zhao, Y. Shi, H. Li, and Q. He, "The improvement of low-resistance and high-transmission ohmic contact to p-GaN by Zn+ implantation," *Nucl. Instrum. Methods Phys. Res. Sect. B Beam Interact. Mater. At.*, vol. 268, no. 9, pp. 1435–1439, May 2010.

[49] H. Omiya, F. A. Ponce, H. Marui, S. Tanaka, and T. Mukai, "Atomic arrangement at the Au/p-GaN interface in low-resistance contacts," *Appl. Phys. Lett.*, vol. 85, no. 25, pp. 6143–6145, Dec. 2004.

[50] J. K. Sheu, Y. K. Su, G. C. Chi, W. C. Chen, C. Y. Chen, C. N. Huang, J. M. Hong, Y. C. Yu, C. W. Wang, and E. K. Lin, "The effect of thermal annealing on the Ni/Au contact of p-type GaN," *J. Appl. Phys.*, vol. 83, no. 6, pp. 3172–3175, Mar. 1998.

[51] C.-S. Lee, Y.-J. Lin, and C.-T. Lee, "Investigation of oxidation mechanism for ohmic formation in Ni/Au contacts to p-type GaN layers," *Appl. Phys. Lett.*, vol. 79, no. 23, pp. 3815–3817, Dec. 2001.

[52] H. W. Jang, S. Y. Kim, and J.-L. Lee, "Mechanism for Ohmic contact formation of oxidized Ni/Au on p-type GaN," *J. Appl. Phys.*, vol. 94, no. 3, pp. 1748–1752, Aug. 2003.

[53] C. Y. Hu, Z. B. Ding, Z. X. Qin, Z. Z. Chen, K. Xu, Z. J. Yang, B. Shen, S. D. Yao, and G. Y. Zhang, "Ohmic contact mechanism of Ni/Au contact to p-type GaN studied by Rutherford backscattering spectrometry," *J. Cryst. Growth*, vol. 298, pp. 808–810, Jan. 2007.

[54] J. Smalc-Koziorowska, S. Grzanka, E. Litwin-Staszewska, R. Piotrzkowski, G. Nowak, M. Leszczynski, P. Perlin, E. Talik, J. Kozubowski, and S. Krukowski, "Ni–Au contacts to p-type GaN – Structure and properties," *Solid-State Electron.*, vol. 54, no. 7, pp. 701–709, Jul. 2010.

[55] G. Greco, P. Prystawko, M. Leszczyński, R. L. Nigro, V. Raineri, and F. Roccaforte, "Electro-structural evolution and Schottky barrier height in annealed Au/Ni contacts onto p-GaN," *J. Appl. Phys.*, vol. 110, no. 12, p. 123703, Dec. 2011.

[56] X. J. Li, D. G. Zhao, D. S. Jiang, Z. S. Liu, P. Chen, J. J. Zhu, L. C. Le, J. Yang, X. G. He, S. M. Zhang, B. S. Zhang, J. P. Liu, and H. Yang, "The significant effect of the thickness of Ni film on the performance of the Ni/Au Ohmic contact to p-GaN," *J. Appl. Phys.*, vol. 116, no. 16, p. 163708, Oct. 2014.

[57] Y. Koide, T. Maeda, T. Kawakami, S. Fujita, T. Uemura, N. Shibata, and M. Murakami, "Effects of annealing in an oxygen ambient on electrical properties of

ohmic contacts to p-type GaN," *J. Electron. Mater.*, vol. 28, no. 3, pp. 341–346, Mar. 1999.

[58] T. Maeda, Y. Koide, and M. Murakami, "Effects of NiO on electrical properties of NiAu-based ohmic contacts for p-type GaN," *Appl. Phys. Lett.*, vol. 75, no. 26, pp. 4145–4147, Dec. 1999.

[59] H. Ishikawa, S. Kobayashi, Y. Koide, S. Yamasaki, S. Nagai, J. Umezaki, M. Koike, and M. Murakami, "Effects of surface treatments and metal work functions on electrical properties at p-GaN/metal interfaces," *J. Appl. Phys.*, vol. 81, no. 3, pp. 1315–1322, Feb. 1997.

[60] G. K. Reeves and H. B. Harrison, "Obtaining the specific contact resistance from transmission line model measurements," *IEEE Electron Device Lett.*, vol. 3, no. 5, pp. 111–113, May 1982.

[61] D. K. Schroder, *Semiconductor Material and Device Characterization*. John Wiley & Sons, 2006.

[62] D. S. Stone, K. B. Yoder, and W. D. Sproul, "Hardness and elastic modulus of TiN based on continuous indentation technique and new correlation," *J. Vac. Sci. Technol. A*, vol. 9, no. 4, pp. 2543–2547, Jul. 1991.

[63] H. O. Pierson, *Handbook of Refractory Carbides & Nitrides: Properties, Characteristics, Processing and Apps.* Elsevier Science, 2013.

[64] S. Nakamura, M. Senoh, and T. Mukai, "High-power InGaN/GaN double-heterostructure violet light emitting diodes," *Appl. Phys. Lett.*, vol. 62, no. 19, pp. 2390–2392, May 1993.

[65] D. Steigerwald, S. Rudaz, H. Liu, R. S. Kern, W. Götz, and R. Fletcher, "III–V Nitride semiconductors for high-performance blue and green light-emitting devices," *JOM*, vol. 49, no. 9, pp. 18–23, Sep. 1997.

[66] D. Sawdai, D. Pavlidis, and D. Cui, "Enhanced transmission line model structures for accurate resistance evaluation of small-size contacts and for more reliable fabrication," *IEEE Trans. Electron Devices*, vol. 46, no. 7, pp. 1302–1311, Jul. 1999.

[67] I. Daumiller, C. Kirchner, M. Kamp, K. J. Ebeling, and E. Kohn, "Evaluation of the temperature stability of AlGaN/GaN heterostructure FETs," *IEEE Electron Device Lett.*, vol. 20, no. 9, pp. 448–450, Sep. 1999.

[68] L. L. Smith, R. F. Davis, M. J. Kim, R. W. Carpenter, and Y. Huang, "Microstructure, electrical properties, and thermal stability of Au-based ohmic contacts to p-GaN," *J. Mater. Res.*, vol. 12, no. 09, pp. 2249–2254, Sep. 1997.

[69] G. Kaune, M. A. Ruderer, E. Metwalli, W. Wang, S. Couet, K. Schlage, R. Röhlsberger, S. V. Roth, and P. Müller-Buschbaum, "In Situ GISAXS Study of Gold Film Growth on Conducting Polymer Films," *ACS Appl. Mater. Interfaces*, vol. 1, no. 2, pp. 353–360, Feb. 2009.

[70] T. Hossain, D. Wei, N. Nepal, N. Y. Garces, J. K. Hite, H. M. Meyer, C. R. Eddy, T. Baker, A. Mayo, J. Schmitt, and J. H. Edgar, "Insulating gallium oxide layer produced by thermal oxidation of gallium-polar GaN," *Phys. Status Solidi C*, vol. 11, no. 3–4, pp. 565–568, Feb. 2014.

[71] H. S. Oon and K. Y. Cheong, "Recent development of gallium oxide thin film on GaN," *Mater. Sci. Semicond. Process.*, vol. 16, no. 5, pp. 1217–1231, Oct. 2013.

[72] S. D. Wolter, S. E. Mohney, H. Venugopalan, A. E. Wickenden, and D. D. Koleske, "Kinetic Study of the Oxidation of Gallium Nitride in Dry Air," *J. Electrochem. Soc.*, vol. 145, no. 2, pp. 629–632, Feb. 1998.

[73] S. D. Wolter, B. P. Luther, D. L. Waltemyer, C. Önneby, S. E. Mohney, and R. J. Molnar, "X-ray photoelectron spectroscopy and x-ray diffraction study of the thermal oxide on gallium nitride," *Appl. Phys. Lett.*, vol. 70, no. 16, pp. 2156–2158, Apr. 1997.

[74] S. Ishibashi, Y. Higuchi, Y. Ota, and K. Nakamura, "Low resistivity indium–tin oxide transparent conductive films. II. Effect of sputtering voltage on electrical property of films," *J. Vac. Sci. Technol. A*, vol. 8, no. 3, pp. 1403–1406, May 1990.

[75] T. Ishida, H. Kobayashi, and Y. Nakato, "Structures and properties of electron-beam-evaporated indium tin oxide films as studied by x-ray photoelectron spectroscopy and work-function measurements," *J. Appl. Phys.*, vol. 73, no. 9, pp. 4344–4350, May 1993.

[76] H. Kim, C. M. Gilmore, A. Piqué, J. S. Horwitz, H. Mattoussi, H. Murata, Z. H. Kafafi, and D. B. Chrisey, "Electrical, optical, and structural properties of indium–tin–oxide thin films for organic light-emitting devices," *J. Appl. Phys.*, vol. 86, no. 11, pp. 6451–6461, Dec. 1999.

[77] Y. Choi and H. Kim, "Surface Fermi level pinning and carrier transport of indium-tin-oxide Ohmic contact to p-type GaN," *J. Alloys Compd.*, vol. 533, pp. 15–18, Aug. 2012.

[78] J. K. Kim, S. Chhajed, M. F. Schubert, E. F. Schubert, A. J. Fischer, M. H. Crawford, J. Cho, H. Kim, and C. Sone, "Light-Extraction Enhancement of GaInN Light-Emitting Diodes by Graded-Refractive-Index Indium Tin Oxide Anti-Reflection Contact," *Adv. Mater.*, vol. 20, no. 4, pp. 801–804, Feb. 2008.

[79] D. W. Kim, Y. J. Sung, J. W. Park, and G. Y. Yeom, "A study of transparent indium tin oxide (ITO) contact to p-GaN," *Thin Solid Films*, vol. 398–399, pp. 87–92, Nov. 2001.

[80] T. Margalith, O. Buchinsky, D. A. Cohen, A. C. Abare, M. Hansen, S. P. DenBaars, and L. A. Coldren, "Indium tin oxide contacts to gallium nitride optoelectronic devices," *Appl. Phys. Lett.*, vol. 74, no. 26, pp. 3930–3932, Jun. 1999.

[81] D. C. Paine, T. Whitson, D. Janiac, R. Beresford, C. O. Yang, and B. Lewis, "A study of low temperature crystallization of amorphous thin film indium–tin–oxide," *J. Appl. Phys.*, vol. 85, no. 12, pp. 8445–8450, Jun. 1999.

[82] V. S. Reddy, K. Das, A. Dhar, and S. K. Ray, "The effect of substrate temperature on the properties of ITO thin films for OLED applications," *Semicond. Sci. Technol.*, vol. 21, no. 12, p. 1747, 2006.

[83] W.-L. Hsu, Y.-H. Pai, F.-S. Meng, C.-W. Liu, and G.-R. Lin, "Nanograin crystalline transformation enhanced UV transparency of annealing refined indium tin oxide film," *Appl. Phys. Lett.*, vol. 94, no. 23, p. 231906, Jun. 2009.

[84] T. Minami, "Transparent conducting oxide semiconductors for transparent electrodes," *Semicond. Sci. Technol.*, vol. 20, no. 4, pp. S35–S44, Mar. 2005.

[85] T. Minami, "New n-Type Transparent Conducting Oxides," *MRS Bull.*, vol. 25, no. 08, pp. 38–44, Aug. 2000.

[86] T. Minami, "Transparent and conductive multicomponent oxide films prepared by magnetron sputtering," *J. Vac. Sci. Technol. A*, vol. 17, no. 4, pp. 1765–1772, Jul. 1999.

[87] M. Yamaguchi, A. Ide-Ektessabi, H. Nomura, and N. Yasui, "Characteristics of indium tin oxide thin films prepared using electron beam evaporation," *Thin Solid Films*, vol. 447–448, pp. 115–118, Jan. 2004.